SOME ASPECTS OF THE CHIRAL POTTS MODEL AND THE ISING MODEL

By

BAI-QI JIN

Bachelor of Science
Zhejiang University
Hangzhou, P. R. China
1990

Master Of Science
Institute of High Energy Physics
Beijing, P. R. China
1996

Submitted to the Faculty of the
Graduate College of the
Oklahoma State University
in partial fulfillment of
the requirements for
the Degree of
DOCTOR OF PHILOSOPHY
August, 2001

SOME ASPECTS OF THE CHIRAL POTTS MODEL
AND THE ISING MODEL

Thesis Approved:

Thesis Advisor

Dean of the Graduate College

ACKNOWLEDGMENTS

I wish to express my deepest gratitude to Prof. Helen Au-Yang and my advisor Prof. Jacques H. H. Perk for their constructive guidance, constant encouragement, kindness and great patience. Without their guidance and collaboration, I would not have been able to finish this work. Their critical reading and precious suggestions greatly enhanced the writing of this thesis.

Many thanks are also due to Prof. Robert Hauenstein for his valuable comments on this thesis and suggestions on the use of LaTeX.

I also would like to express my sincere appreciation to Prof. Paul Westhaus for his assistance during these years of my study at Oklahoma State University.

My appreciation extends to my other committee members Prof. Xin-Cheng Xie and Prof. Birne Binegar, whose encouragement has also also been invaluable.

Moreover, I wish to express my thanks to Lin Zhi Biao and the office staff in the Physics Department for their help in various ways.

Finally, I thank the Physics Department for providing the opportunity for my graduate study and part of my financial support. I also thank the National Science Foundation for further financial support under Grants Nos. PHY 95-07769, PHY 97-22159, and PHY 97-24788.

TABLE OF CONTENTS

Chapter Page

1. INTRODUCTION 1

1.1. CELL SPIN MODELS 2
1.1.1. THE ANNNI MODEL 5
1.1.2. THE 3-STATE CHIRAL POTTS MODEL 6
1.2. FERMION THEORY 8
1.3. PREVIOUS STUDIES OF THE 3-STATE CHIRAL POTTS MODEL 12

2. MEAN FIELD STUDY OF THE PHASE DIAGRAM OF THE 3-STATE CHIRAL POTTS MODEL (I) 14

2.1. INTRODUCTION 14
2.2. NOTATIONS AND WELL-KNOWN RESULTS 15
2.3. FREE ENERGY CALCULATION BY THE MEAN-FIELD TRANSFER MATRIX METHOD 17
2.4. NUMERICAL RESULTS ON THE PHASE DIAGRAM 26
2.5. SUMMARY 39

3. MEAN FIELD STUDY OF THE PHASE DIAGRAM OF THE 3-STATE CHIRAL POTTS MODEL (II) 41

3.1. INTRODUCTION 41
3.2. CAM THEORY 42
3.3. WEISS-TYPE AND BETHE-TYPE APPROXIMATION 43
3.3.1. WEISS-TYPE APPROXIMATION 46
3.3.2. BETHE-TYPE APPROXIMATION 47
3.4. NEW EXTRAPOLATION METHOD 49
3.5. CAM ANALYSIS 53
3.5.1. CAM TEST FOR $\Delta = 0$ 56
3.5.2. CAM ANALYSIS FOR GENERAL Δ 60
3.6. WAVEVECTOR ANALYSIS 63
3.7. SUMMARY 66

Chapter Page

3.8. DISCUSSION OF RELATED WORKS 67

4. SCALING LIMIT FOR THE TWO-POINT CORRELATION FUNCTION IN THE Z-INVARIANT ISING MODEL 75

4.1. Z-INVARIANT ISING MODEL 75
4.2. SCALING LIMIT 78
4.3. PAINLEVÉ EQUATIONS 82

5. FIBONACCI ISING MODEL 84

5.1. INTRODUCTION 84
5.2. ONE-DIMENSIONAL FIBONACCI ISING MODEL 85
5.3. Z-INVARIANT FIBONACCI ISING MODEL 90
5.4. EFFECTIVE CONNECTED PAIR CORRELATION FUNCTION IN THE SCALING LIMIT 91
5.5. WAVEVECTOR DEPENDENT SUSCEPTIBILITY OF THE FIBONACCI ISING MODEL IN THE SCALING LIMIT 94
5.6. CONCLUSIONS 96

6. FREE ENERGY OF THE INTEGRABLE CHIRAL POTTS MODEL 98

6.1. INTRODUCTION 98
6.2. THE LARGEST EIGENVALUE 102
6.3. ROTATIONS AND SYMMETRIES 111
6.4. CONCLUSION 116

BIBLIOGRAPHY 118

APPENDICES 124

APPENDIX A—DIFFERENCE SEQUENCE 125

APPENDIX B—SIMPLIFIED FORMALISM FOR A SPECIAL CASE 127

APPENDIX C—MAIN FORTRAN PROCEDURE FOR CHAPTER 2 129

APPENDIX D—MAIN FORTRAN PROCEDURE FOR CHAPTER 3 148

LIST OF TABLES

Table Page

2.1. Table of f_{MF} for various mean-field solutions and temperatures where $K_n = K_t$, $\Delta = 0.30$, and $N = 2$. Two items are empty meaning that no corresponding solution for the mean-field equations in our scheme exists. The approximated free energy for the modulated solution is the lowest one resulting from all modulated solutions we considered. 28

2.2. Table of f_{MF}, $\boldsymbol{\eta}$ and $\mathbf{m}_{\mathrm{c}}$ for $\Delta = 0$. $f_{\mathrm{MF}}(N)$ is the approximated free energy, $\boldsymbol{\eta}(N)$ is the ordered solution and $\mathbf{m}_{\mathrm{c}}(N)$ is the magnetization on the central row with this ordered solution at $K_n = K_t = 1/T_{\mathrm{c}}$, $\Delta = 0$ with strip width N. At this point, the approximated free energies given by the disordered solution and the ordered solution are equal. 30

2.3. Table of Δ_L^l. The Δ_L^l in the second row are obtained with m_i taking any value of 0, 1 and 2, but the Δ_L^l in the third row are obtained with m_i taking only values 0 or 2. $K_n = K_t$ and $N = 1$ in both cases. . 37

3.1. Table of T_{b}, T_{w} and T_{n} for the square lattice Ising model. Critical temperature $T_{\mathrm{b}}(N)$ is obtained by the Bethe-type approximation and $T_{\mathrm{w}}(N)$ by the Weiss-type approximation where N is the width of the finite strip. $T_{\mathrm{n}}(N)$ is obtained by Eq. (3.38) with $\delta N = 2$. The exact value $T_{\mathrm{c}}^* = 2.269$. 52

3.2. Table of T_{b}, T_{w} and T_{n} for the model with $\Delta = 0$ and $K_n = K_t$. Critical temperature $T_{\mathrm{b}}(N)$ is obtained by Bethe-type approximation, $T_{\mathrm{w}}(N)$ by Weiss-type approximation, where N is the width of the finite strip, and $T_{\mathrm{n}}(N)$ is obtained by (3.38) with $\delta N = 2$. The exact value $T_{\mathrm{c}}^* = 1.4925$. 52

3.3. Table of T_{b}, T_{w} and T_{n} for the model with $\Delta = 0$ and $K_n = 10K_t$. Critical temperature $T_{\mathrm{b}}(N)$ is obtained by Bethe-type approximation, $T_{\mathrm{w}}(N)$ by Weiss-type approximation, where N is the width of the finite strip, and $T_{\mathrm{n}}(N)$ is obtained by (3.38) with $\delta N = 2$. The exact value $T_{\mathrm{c}}^* = 6.0899$. 52

Table Page

3.4. Table of $T_{\rm b}$, $T_{\rm w}$ and $T_{\rm n}$ for the model with $\Delta = 0$ and $K_n = 100K_t$. Critical temperature $T_{\rm b}(N)$ is obtained by Bethe-type approximation, $T_{\rm w}(N)$ by Weiss-type approximation, where N is the width of the finite strip, and $T_{\rm n}(N)$ is obtained by (3.38) with $\delta N = 2$. The exact value $T_{\rm c}^* = 35.2947$. 53

3.5. Table of $T_{\rm b}$, $T_{\rm w}$ and $T_{\rm n}$ for the model with $\Delta = 1/2$ and $K_n = K_t$. Critical temperature $T_{\rm b}(N)$ is obtained by Bethe-type approximation, $T_{\rm n}(N)$ by Weiss-type approximation, where N is the width of the finite strip, and $T_{\rm n}(N)$ is obtained by (3.38) with $\delta N = 2$..... 54

3.6. Table of $T_{\rm b}$, $T_{\rm w}$ and $T_{\rm n}$ for the model with $\Delta = 1/2$ and $K_n = 10K_t$. Critical temperature $T_{\rm b}(N)$ is obtained by Bethe-type approximation, $T_{\rm w}(N)$ by Weiss-type approximation, where N is the width of the finite strip, and $T_{\rm n}(N)$ is obtained by (3.38) with $\delta N = 2$. 54

3.7. Table of $T_{\rm b}$, $T_{\rm w}$ and $T_{\rm n}$ for the model with $\Delta = 1/2$ and $K_n = 100K_t$. Critical temperature $T_{\rm b}(N)$ is obtained by Bethe-type approximation, $T_{\rm w}(N)$ by Weiss-type approximation, where N is the width of the finite strip, and $T_{\rm n}(N)$ is obtained by (3.38) with $\delta N = 2$. 54

3.8. Table of $\hat{q}_{\rm b}$, $\hat{q}_{\rm w}$ and $\hat{q}_{\rm n}$ for $\Delta = 0.05$ and $K_n = 10K_t$. The reduced critical wavevector $\hat{q}_{\rm b}(N)$ is obtained by Bethe-type approximation and $\hat{q}_{\rm w}(N)$ by Weiss-type approximation, where N is the width of the finite strip. Here, $\hat{q}_{\rm c}(N)$ is obtained by (3.38) with $\delta N = 2$..... 64

3.9. Table of $\hat{q}_{\rm b}$, $\hat{q}_{\rm w}$ and $\hat{q}_{\rm n}$ for $\Delta = 0.05$ and $K_n = 100K_t$. The reduced critical wavevector $\hat{q}_{\rm b}(N)$ is obtained by Bethe-type approximation and $\hat{q}_{\rm w}(N)$ by Weiss-type approximation, where N is the width of the finite strip. Here, $\hat{q}_{\rm c}(N)$ is obtained by (3.38) with $\delta N = 2$..... 65

6.1. Free energy of integrable chiral Potts model for different regions. 115

LIST OF FIGURES

Figure Page

1.1. Commensurate $c(2 \times 2)$ structure of Xe adsorbed on Cu(110). 4

1.2. (3×1) commensurate structure on a rectangular substrate. 7

2.1. Exact vertical interactions within one row approximated by effective field interactions. 24

2.2. f_{MF} versus $(\eta_1, 0)$, with $\Delta = 0$, $K_n = K_t$ and different temperatures..... 24

2.3. f_{MF} versus $(\eta_1, 0)$, with $\Delta = 0$, $K_n = K_t$ and temperatures near the critical one T_{c}. 30

2.4. The mean-field transfer matrix phase diagram with strip width $N = 1$. The approximate value of $\Delta_L > 0.30$. To obtain the phase diagram, we considered mean-field solutions with $l \leq 12$. 32

2.5. The mean-field transfer matrix phase diagram with width $N = 2$. The approximate value of $\Delta_L \approx 0.29$. We considered mean-field solutions with $l \leq 12$. 33

2.6. The mean-field transfer matrix phase diagram with width $N = 3$. The approximate value of $\Delta_L \leq 0.28$. We considered mean-field solutions with $l \leq 12$. 34

2.7. Systematic improvement of the approximated critical point T_{c} versus $1/N$, where N is the width of the strip, $\circ$ denotes approximated mean-field transfer matrix results and T_{c}^* the exact 3-state Potts result. 35

2.8. Δ versus T_{c}. The solid line is derived from the free-fermion approximation which should be a better approximation for Δ close to $1/2$..... 37

2.9. $\Delta_L^l(N)$ versus l with $K_n = K_t$ and strip width N. Local minima are 0.3143 at $l = 4$, 8, 12 for $N = 1$, 0.2883 at $l = 5$, 10, 15 for $N = 2$, 0.2770 at $l = 6$ for $N = 3$, and 0.2709 at $l = 7$ for $N = 4$..... 38

Figure Page

2.10. $\Delta_L^l(N)$ versus l with $K_n = 10K_t$ and strip width N. The minima are 0.2258 at $l = 14$ or 15 for $N = 1$ and 0.2156 at $l = 16$ for $N = 2$.... 40

3.1. Critical temperature shift t_c versus $1/N$ for Potts model, where $t_c = (T_c - T_c^*)/T_c^*$ and N is the width of strip in Weiss-type MFTM method. 57

3.2. Critical temperature shift t_c versus $1/N$ for Potts model, where $t_c = (T_c - T_c^*)/T_c^*$ and N is the width of strip in Bethe-type MFTM method. 58

3.3. Power-law fits of the CAM for the case $K_n = K_t$ and $\Delta = 0$. 59

3.4. Power-law fits of the CAM for the case $K_n = 10K_t$ and $\Delta = 0$. 59

3.5. Power-law fits of the CAM for the case $K_n = 100K_t$ and $\Delta = 0$. 62

3.6. Power-law fits of the CAM for the case of $K_n = 100K_t$, $\Delta = 0.15$ and $T_c^* = 31$..... 62

3.7. Power-law fits of the CAM for the case of $K_n = 100K_t$, $\Delta = 0.45$ and $T_c^* = 7.94$. 65

3.8. Exponential fits of the CAM for the case of $K_n = 100K_t$, $\Delta = 0.15$ and $T_c^* = 30.90$ with $\sigma = 0.14$..... 70

3.9. Exponential fits of the CAM for the case of $K_n = 100K_t$, $\Delta = 0.45$ and $T_c^* = 7.76$ with $\sigma = 0.35$. 71

3.10. Exponential fits of the CAM for the case of $K_n = 100K_t$, $\Delta = 0.15$ and $T_c^* = 30.56$ with $\sigma = 0.5$. 72

3.11. Reduced wavevector $\hat{q}_c$ versus Δ with $N = 5$ based on Weiss approximation. As K_n/K_t increases, $\hat{q}_c$ decreases for fixed Δ. 73

3.12. Reduced wavevector $\hat{q}_w$ versus Δ with $K_n = 10K_t$ based on Weiss approximation. As N increases, $\hat{q}_c$ decreases for fixed Δ. 74

4.1. The lattice of a two-dimensional Z-invariant Ising model is represented by solid lines, the rapidity lines on the medial graph are represented by oriented dashed lines. These lines carry rapidity variables u_i and v_j. The position of the spins are indicated by small black circles, the positions of the dual spins by white circles. 76

Figure Page

4.2. (a) The horizontal coupling K_{ij} and (b) the vertical coupling $\bar{K}_{ij}$. 80

4.3. Part of an Ising model and its dual on a general planar graph: Indicated are two neighbor pairs of spins indicated by small black circles with their reduced interaction constants K_i (drawn lines). Also indicated are their corresponding two pairs of dual spins indicated by white circles with their reduced interaction constants K_i^* (dashed lines). Note that are both $(\mathrm{x}_1, \mathrm{x}_1^*, \mathrm{y}_1, \mathrm{y}_1^*)$ and $(\mathrm{x}_2, \mathrm{x}_2^*, \mathrm{y}_2, \mathrm{y}_2^*)$ are arranged clockwise. 80

5.1. Reduced wavevector dependent susceptibility $k_{\mathrm{B}}T\chi(q)$ for the one-dimensional Ising chain. The four cases are: (a) the uniform ferromagnetic case; (b) the $4:1$ Fibonacci case; (c) the $2^{26}:1$ Fibonacci case; and (d) the mixed-sign $1:1$ Fibonacci case. See text. 87

6.1. Boltzmann weights $W_{\mathrm{pq}}(a-b)$ and $\overline{W}_{\mathrm{pq}}(a-b)$ for the two types of edge interaction between the spins a and b. 117

CHAPTER 1

INTRODUCTION

Phase transitions are interesting natural phenomena, common in our daily experience. The most common is the transition of water into ice. There are lots of substances other than water which undergo phase transitions under certain conditions. Indeed, phase transitions are central to life on earth and understanding them is one of the main objects of physics research.

Under ordinary circumstances, phase transitions of water are first-order with latent heat absorbed or released, involving radical structure changes in the system. However, there are other kinds of phase transitions, where the structures change continuously during phase transitions. For example, when the temperature T increases, certain magnetic materials will change from a ferromagnetic phase to a paramagnetic phase at Curie temperature T_{c}. In the paramagnetic phase ($T > T_{\mathrm{c}}$), the material is not magnetized in the absence of an applied magnetic field. If a weak field $\mathbf{B}$ is applied, the magnetic moment per unit volume $\mathbf{m}$ is proportional to the applied field: $\mathbf{m} = \mu\mathbf{B}$ with μ a positive constant. In the ferromagnetic phase ($T < T_{\mathrm{c}}$), the material is magnetized even when no field is applied (spontaneous magnetization), and this magnetization swings almost instantaneously to align with $\mathbf{B}$ when an external field $\mathbf{B}$ is applied, large enough to overcome the effects of hysteresis. Consequently, $\mathbf{m}$ is no longer linearly related to $\mathbf{B}$.

The Ising model which has become a well-known model now has been invented originally to understand these magnetic phenomena. They are called order-disorder transitions. There exist many models that describe this kind of phase transitions other than the Ising model. Comparing with the order-disorder phase transitions, another kind of phase transition, the so called commensurate-incommensurate (C-IC) transitions, which shall be described in detail later, are not fully understood, although they

occur in systems as diverse as ferroelectrics,[1,2] magnetic systems,[3,4] physisorbates,[5] structural polytypes,[6] lipid bilayers,[7] etc. They are associated with the onset of spatially modulated phases and have been extensively studied both experimentally and theoretically since the eighties.[8–17]

Scaling theory is well known and has led to attempts to classify phase transitions into different universality classes and to determine the scaling properties of these universality classes. From this point of view, C-IC transitions are of particular interest because the scaling properties of some of these transitions are still elusive in two-dimensional systems. Consequently, a great deal of theoretical and experimental research has been done to study C-IC transitions in two-dimensional systems. The basic understanding of such transitions mainly comes from the domain wall theory or more specifically, the fermion theory (see den Nijs[18] for full review). Other than the fermion theory[19–24] which is valid for uniaxial systems where only one type of domain walls exists, the ANNNI (Axial-Next-Nearest-Neighbor Ising) model[25] and the 3-state chiral Potts model[26,27] are used to study such transitions because these two models are the simplest but still can exhibit highly nontrivial physics.

In this chapter, we shall first compare experiments and models, then give some basic understanding of the theory. Following M. den Nijs,[18] we shall build the cell spin models based on a few specific examples in physisorption. We then shall use these to describe C-IC transitions and how the different models such as the ANNNI model, the 3-state chiral Potts model and the fermion theory are used for the different experimental situations.

1.1 CELL SPIN MODELS

Adsorbed monolayers can be modelled as two-dimensional systems of interacting particles subject to a periodic external substrate field. In the modelling, the grand canonical ensemble will be used.

In the domain wall theory of C-IC transitions, domain walls, instead of the monolayer particles, are the basic fluctuating variables. All degrees of freedom at length scales smaller than the wall width are integrated out, and the grand canonical

ensemble for adsorbed particles is replaced by a grand canonical ensemble for domain walls.

Let us consider a specific physisorption experiment, more specifically xenon monolayer physisorbed on the (110) face of copper.[17]

A xenon monolayer physisorbed on the (110) face of copper orders into the c(2×2) structure shown in Fig. 1.1. The absorption sites form a rectangular array. Because the diameter of the Xe atoms is too large for nearest-neighbor occupation, in the ground state the Xe atoms occupy only one of the two (checker-board) sublattices, resulting in the commensurate (C) phase. Obviously, because of symmetry, there are two phases with the same energy. One phase is generated by displacing the other phase by lattice vector $\mathbf{a}_n$ or $\mathbf{a}_t$. If the Xe atoms occupy only one of the two sublattices in certain region, the configuration in this region is called a commensurate (C) patch and this region a commensurate (C) domain. Hence there are two kinds of C patches and C domains. In diffraction experiments such as LEED (low-energy electron diffraction) and synchrotron X-ray diffraction, the Bragg peaks are locked in certain positions when the monolayer is in the C phase. As the temperature and atom density increase, both C domains appear in the monolayer and different C domains are separated by domain walls. Apparently there is excess energy called interfacial tension due to the appearance of these domain walls and domain walls carry excess density as well. When the ratio of the average distance between absorption sites of xenon and the lattice spacing of copper is an irrational number, the phases are called incommensurate (IC) phases. In IC phases, the Xe atom density is between the density of the C phase and the onset of second layer formation. The diffraction peaks move continuously with density and temperature.

Having the above experiment in mind, let us now describe the general procedures available to obtain cell spin models for adsorbed monolayers. In the domain wall theory, domain walls carry additional energy and the thermodynamic properties are determined by the fluctuation of domain walls. There are many different domain walls. Since different domain walls have different excess energies, the possibility for each domain wall to appear is different. However, it is not necessary to consider all

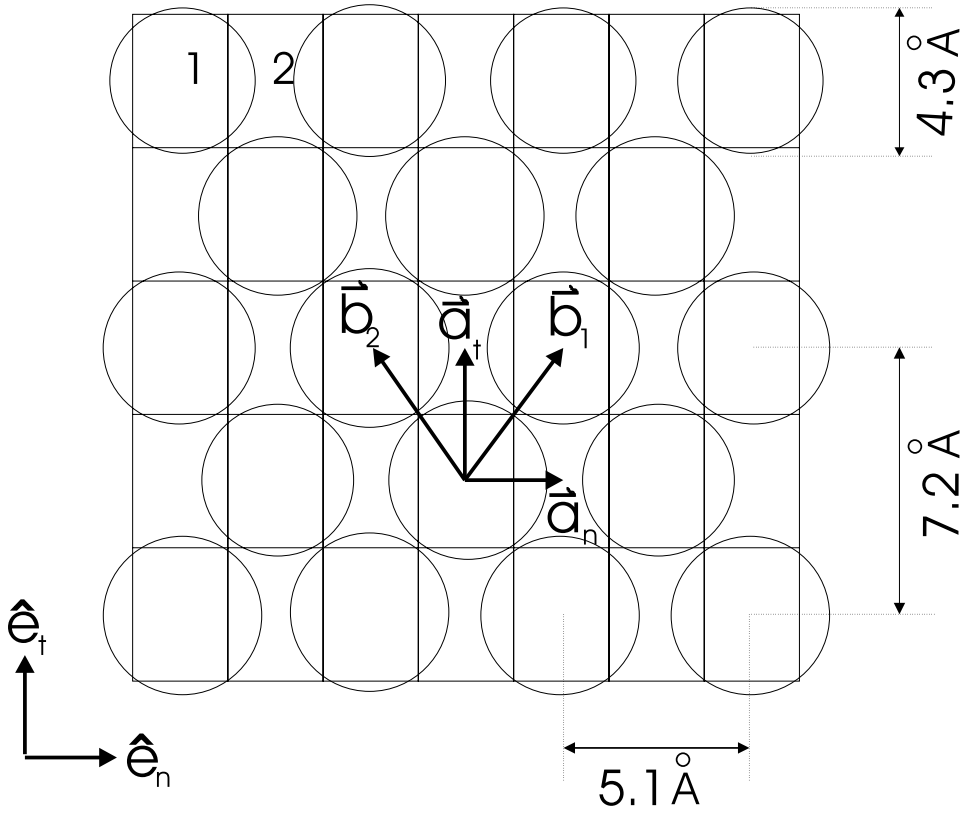

Figure 1.1. Commensurate $c(2 \times 2)$ structure of Xe adsorbed on Cu(110).

kinds of domain walls and their fine structures. The wall widths, the rigidities of walls at small length-scales, and the preferred wall directions can be taken into account by introducing a lattice cut-off with lattice constants comparable to the typical domain wall width. In the resulting lattice model (cell spin model), the domain walls are along the bonds of a lattice. The symmetry of the lattice of the cell spin model reflects the preferred wall directions imposed by the substrate. Typically it will have the same symmetry as the substrate. Clearly, each face can be associated with a cell spin variable to describe the possible C patch. A cell spin configuration does not uniquely describe a domain wall configuration since the widths of the domain walls are undetermined in cell spin configurations. However, the term Bloch walls is used to represent the whole class of domain walls that are possible between two C patches. Consequently, a cell spin configuration can uniquely describe a Bloch wall configuration. Formally, the reduction of the domain wall lattice model to the cell spin model involves the summing over all other degrees of freedom of domain wall configurations which contribute to the same Bloch wall configuration. This can be done trivially only in some special cases. In specific local regions of chemical potential and temperature, the excess energy for certain domain walls becomes much lower. Practically, instead of averaging, we can select the domain wall with lowest excess energy for each set of domain walls with the same Bloch wall.

Following the general procedure described above, we use specific examples to derive the ANNNI model and the 3-state chiral Potts model.

1.1.1 THE ANNNI MODEL

For a xenon monolayer physisorbed on the (110) face of copper as shown in Fig. 1.1, the adsorption sites of the substrate form a rectangular array with basis vectors $\mathbf{a}_n = a_n\hat{\mathbf{e}}_n$ and $\mathbf{a}_t = a_t\hat{\mathbf{e}}_t$. The C ground state has basis vectors $\mathbf{b}_1 = \mathbf{a}_n + \mathbf{a}_t$ and $\mathbf{b}_2 = \mathbf{a}_t - \mathbf{a}_n$. In each cell, the two possible choices of C patches can be represented by Ising spins $S(\mathbf{r}) = \pm 1$. The monolayer prefers to compress in the direction $\hat{\mathbf{e}}_n$ with the domain walls parallel to the direction $\hat{\mathbf{e}}_t$. The Hamiltonian for this system can

be written as

$$H = \sum_{n,t}\Big\{\frac{1}{2}(E_n-\mu)[1-S(n,t)S(n+1,t)]+\frac{1}{2}E_t[1-S(n,t)S(n,t+1)] + \frac{1}{4}L[1-S(n-1,t)S(n,t)][1-S(n,t)S(n+1,t)]\Big\} \quad (1.1)$$

where the nearest-neighbor interaction in the $\hat{\mathbf{e}}_n$ direction, $E_n - \mu$, represents the energy and chemical potential contributions of a compressed domain wall in the uniaxial direction $\hat{\mathbf{e}}_n$. The nearest-neighbor coupling constant E_t represents the energy contribution of a shear wall in the $\hat{\mathbf{e}}_t$ direction. Domain walls in the direction $\hat{\mathbf{e}}_n$ at nearest-neighbor vertical bonds repel each other for $L > 0$. Other domain wall interactions are neglected. Because the cell spin configuration doesn't uniquely determine the state of the monolayer, these parameters should be the thermo-average of all states with the same cell spin configuration. It is more common to write the Hamiltonian of the ANNNI model as following:[28–30]

$$H = -\sum_{n,t}\{E'_nS(n,t)S(n+1,t)+E'_tS(n,t)S(n,t+1) + E'_{nn}S(n-1,t)S(n+1,t)\}. \quad (1.2)$$

1.1.2 THE 3-STATE CHIRAL POTTS MODEL

The 3-state chiral Potts model applies to uniaxial systems with three competing C ground states. For example, H chemisorbed on Fe(110) includes a C (3×6)H6 phase with such a symmetry.[31] For simplicity, it is generally assumed that the underlying symmetry is the simpler 3×1 structure shown in Fig. 1.2.

The absorption sites form a rectangular array with basis vectors $\mathbf{a}_n = a_n\hat{\mathbf{e}}_n$ and $\mathbf{a}_t = a_t\hat{\mathbf{e}}_t$. The C ground state has basis vectors $\mathbf{b}_n = 3\mathbf{a}_n$ and $\mathbf{b}_t = \mathbf{a}_t$. Hence in each cell, there are three kinds of adsorption sites, corresponding to three competing C patches. The monolayer prefers to compress in the $\hat{\mathbf{e}}_n$ direction with domain walls parallel to the $\hat{\mathbf{e}}_t$ direction. The three types of C patches can be represented by the discrete angle variables $\theta = 0, \pm2\pi/3$ of the 3-state Potts model. The cell spin model then contains two types of Bloch walls with $\theta(\mathbf{r}') - \theta(\mathbf{r}) = \pm2\pi/3$ in the Potts model language, in which they are called clockwise and anticlockwise walls. For the

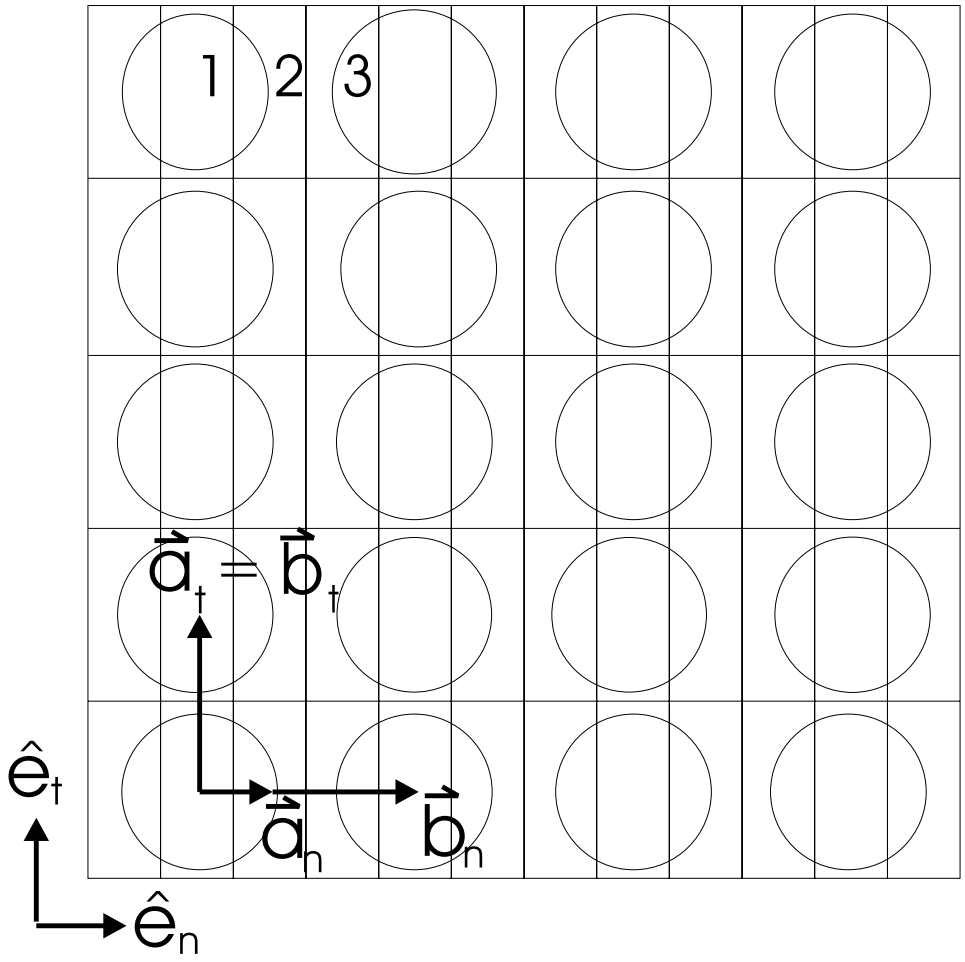

Figure 1.2. (3×1) commensurate structure on a rectangular substrate.

$\hat{\mathbf{e}}_n$ direction, anticlockwise (ACW) and clockwise (CW) walls generally have different excess energy. But for the $\hat{\mathbf{e}}_t$ direction, no Bloch wall exists and the excess energy in cell spin model is due to shear. We denote the excess energy for an anticlockwise Bloch wall ($\theta(n,t) - \theta(n+1,t) \pmod{2\pi} = 2\pi/3$) by $E_{\rm AC}$, the excess energy for a clockwise Bloch wall ($\theta(n,t) - \theta(n+1,t) \pmod{2\pi} = -2\pi/3$) by $E_{\rm C}$ and the shear energy by $E_{\rm S}$. If $\theta(n,t) - \theta(n+1,t) = 0$, no Bloch wall exists locally. Since generally $E_{\rm AC} \neq E_{\rm C}$, chirality is present in this effective model.

Conventionally, we can introduce E_n, E_t and Δ to express $E_{\rm AC}$, $E_{\rm C}$ and $E_{\rm S}$ by

$$E_{\rm AC} = E_n \cos\left(\frac{2\pi}{3}\Delta\right) - E_n \cos\left(\frac{2\pi}{3}(1+\Delta)\right),$$
$$E_{\rm C} = E_n \cos\left(\frac{2\pi}{3}\Delta\right) - E_n \cos\left(\frac{2\pi}{3}(-1+\Delta)\right),$$
$$E_{\rm S} = E_t - E_t \cos\left(\frac{2\pi}{3}\right) = \frac{3}{2}E_t.$$

Hence, the Hamiltonian for the 3-state chiral Potts model[26,27] can be written as

$$H = -\sum_{n,t}\left\{E_n \cos\left(\theta(n,t) - \theta(n+1,t) + \frac{2}{3}\pi\Delta\right) + E_t \cos\left(\theta(n,t) - \theta(n,t+1)\right)\right\}. \tag{1.3}$$

1.2 FERMION THEORY

It is well known that for every D-dimensional problem in statistical mechanics, there is a corresponding $D-1$ dimensional quantum field theory. The correspondence can be constructed by the path integral formalism. Just as the two-dimensional Ising model is equivalent to a free fermion theory, the two-dimensional ANNNI model can be transformed into an interacting fermion theory with the Hamiltonian[32]

$$\begin{aligned} H &= \sum_n \{(E_n - \mu)\sigma^+(n)\sigma^-(n) + L\sigma^+(n)\sigma^-(n)\sigma^+(n+1)\sigma^-(n+1) \\ &\quad -\frac{1}{2}t[\sigma^+(n)\sigma^-(n+1) + \sigma^-(n)\sigma^+(n+1) \\ &\quad +\sigma^+(n)\sigma^+(n+1) + \sigma^-(n)\sigma^-(n+1)]\} \end{aligned} \tag{1.4}$$

This is just a special case of a more general fermion theory, where $\sigma^{\pm}$ are standard Pauli matrices. The generic form of the fermion theory's Hamiltonian is

$$H = \sum_n \{m_0\sigma^+(n)\sigma^-(n)$$

$$
\begin{aligned}
&+L\sigma^+(n)\sigma^-(n)\sigma^+(n+1)\sigma^-(n+1)\\
&-L_2t^2\sigma^-(n)\sigma^+(n)\sigma^-(n+1)\sigma^+(n+1)\\
&-\frac{1}{2}t[\sigma^+(n)\sigma^-(n+1)+\sigma^-(n)\sigma^+(n+1)]\\
&-\frac{1}{2}t^{p-1}u_p[D_p^+(n)+D_p^-(n)]\},
\end{aligned}
\tag{1.5}
$$

where the $D_p^{\pm}$ are dislocation operators

$$
D_p^+(n) = \sigma^+(n)\sigma^+(n+1)\sigma^+(n+2)\ldots\sigma^+(n+p-1), \tag{1.6}
$$

$$
D_p^-(n) = \sigma^-(n)\sigma^-(n+1)\sigma^-(n+2)\ldots\sigma^-(n+p-1). \tag{1.7}
$$

The value of p is 2 in the ANNNI model.

When we restrict ourselves to regions in any phase diagram where one type of domain wall is significantly more abundant than any other type of wall, only one kind of wall need be considered and the critical properties of the monolayer can be described by a one-dimensional fermion quantum field theory. As we have mentioned earlier, only one type of domain wall exists in the ANNNI model and this model is essentially a special case of the fermion theory with $p = 2$.[32] Let Q denote the wavenumber of the oscillation in the domain wall density or the pitch of quasi-particles in fermion language. The formalism of the fermion theory is suitable for the study of the region around $Q = 0$, but the formulation as a spin model, i.e. the ANNNI model, is more suitable for the study of the region around $Q = \frac{1}{2}$ (with period equal two lattice spacings) in fermion language. In the 3-state chiral Potts model with large chirality and low temperature where the energy of ACW walls becomes much larger than the energy of CW walls, the system can be approximated by a $p = 3$ fermion field theory as well.[26] The fermion theory is the most developed theory for C-IC transitions and it provides us basic understanding of C-IC transitions.

In the fermion description, there are four types of phases: C solids (commensurate ordered phases), SIC floating solids (striped incommensurate phases), C fluids (commensurate disordered phases) and SIC fluids (striped incommensurate disordered phases). The different phases are distinguished by their difference in the fermion density correlation functions. The solid phase has long-range-order with nonvanishing

order parameters, whereas the fluid phase has short-range-order with vanishing order parameter. The correlation functions decay exponentially with possible oscillatory envelopes with pitch Q. If the period, which is Q^{-1}, of this oscillation is commensurate with the lattice spacing, the system is called commensurate, otherwise it is called incommensurate. The peaks in the diffraction pattern, which are intimately related to the density correlations through Fourier transform, are therefore locked in certain positions for the commensurate phase, but shift as function of density and temperature in the incommensurate phase. The SIC floating solid phase is more often called modulated phase because the correlation functions decay algebraically with infinite correlation length. It is therefore not strictly a solid phase but a critical phase. So there are totally six types of possible transitions between these four types of phases. The fermion theory predicts the nature of four of the six possible types of phase transitions. In uniaxial systems, the phase transitions from SIC floating solids into C solids are Pokrovsky–Talapov (PT) transitions.[19] The melting of the SIC floating solids into the SIC fluids are Kosterlitz–Thouless (KT) transitions.[33,34] From the results of the antiferromagnetic Ising model, it is known that the correlations decay exponentially below the disorder temperature T_{D} but with an oscillatory envelope above T_{D}. However, T_{D} is not a singular point in any of the physical quantities. Therefore there is no phase transition at T_{D}. We have no evidence that C fluids and IC fluids are different phases. Similarly, we have assumed these are different phases to see if there is a different type of phase transition. The phase boundaries between SIC fluids and C fluids are probably not sharply defined in general. The C melting transitions, direct transitions between C solids and C fluids, are also well understood. This leaves only two other types of phase transitions, direct transitions between SIC floating solids and C fluids, and direct transitions between C solids and SIC fluids. Both are absent from the solved part of the fermion theory (local structure of phase diagram around the $Q = 0$ C solids), but might appear in general context (for example it is believed that there is possible chiral melting around $Q = 1/2$ C solids).

Lifshitz points are defined as kind of triple points where the uniformly ordered, modulated ordered and disordered phase meet. So, in the global phase diagram, a

Lifshitz point may appear with the direct melting of a solid into an IC fluid. Although there are no models or experimental systems for which we are sure that there is a Lifshitz point, it is believed to exist. Experimentally, they have been suggested to occur in various systems including liquid crystals,[35,36] ferroelectrics[37] and magnets.[38,39] Theoretically, the ANNNI model[25] and the 3-state chiral Potts model have been thought as good candidates for the study of chiral melting and Lifshitz points. Chiral melting is named for the case of a direct transition from C solids into SIC fluids. There is no evidence, not even the slightest hint, that the other possibility, a direct transition from an IC floating solid into a C fluid, can ever be realized.

Theoretical study has only been concentrated on the direct transitions from C solids into IC fluids. Because an IC fluid is characterized by two length-scales: the correlation length ξ and the inverse of pitch Q, the C-IC transition is a transition in which the lock-in of Q and the divergence of the correlation length take place simultaneously. Let us denote the lock-in pitch for commensurate solids by Q_0, then both $1/(Q-Q_0)$ and ξ diverge simultaneously when the system reaches the critical point. Den Nijs argued that there are three kinds of possible behaviors for C-IC transitions.[18]

(i) When $1/(Q-Q_0)$ diverges faster than ξ, the C-IC melting transition will remain in the same universality class as the C melting transition.

(ii) When $1/(Q-Q_0)$ diverges slower than ξ, the C-IC melting transition should be KT-like or first-order.

(iii) When $1/(Q-Q_0)$ diverges at the same rate as ξ, i.e. $1/(Q-Q_0) \sim \xi$, the nature of the transition might change in a fundamental way.

Among (i-iii), (iii) is the most interesting. Huse and Fisher realized this and called the effect chiral melting. Unfortunately, no models or experimental systems can tell us if this type of transition is realized for sure. The ANNNI model and the 3-state chiral Potts model have served as model candidates to study chiral melting behavior since then.

1.3 PREVIOUS STUDIES OF THE 3-STATE CHIRAL POTTS MODEL

The 3-state chiral Potts model has attracted much attention as it is a natural extension of the fermion theory and a possible realization of chiral melting.[26,27,40,41] In this section, we give a brief review of the understanding of the possible phase diagram of this model.

The model contains two types of walls: clockwise and anticlockwise domain walls. At $\Delta = 0$ they cost equal amounts of energy, but when $0 < \Delta \leq 1/2$ the anticlockwise domain walls cost more energy than clockwise domain walls. When $\Delta = 0$, the model is reduced to the 3-state Potts model. When $\Delta = 1/2$, the model becomes a model with antiferromagnetic horizontal interaction and ferromagnetic vertical interaction that has been studied by Kinzel et al.[42]

The general model was originally introduced and studied by Ostlund and Huse.[26,27] Ostlund used free fermion analysis to show that there are IC phases in this model. This makes the model interesting for the study of C-IC phase transitions.

Although there is one integrable line available,[43] unfortunately this integrable line is located in the region of C solids except for the Potts point. It cannot provide information on the phase boundary. Since the model could not be solved exactly and there is no known analytical method applicable to the case with general chirality Δ, numerical study is very important for the understanding of this model. It has been studied by finite-size scaling in the transfer matrix formalism,[44,45] Monte-Carlo simulations,[46] Monte-Carlo renormalization group[47] and series expansions in the quantum Hamiltonian formalism,[48–50] and finite size scaling in the quantum Hamiltonian formalism.[51–53]

These numerical calculations help to fill the gap in the phase diagram left by the analytical results, i.e. the fermion theory which describes the phase diagram around $\Delta = 1/2$ and the chiral cross-over results at $\Delta = 0$. Around $\Delta = 1/2$ the fermion theory predicts PT transitions from SIC floating solids into C solids, and KT melting transitions from the SIC floating solids into the SIC fluids. At $\Delta = 0$, the exact values of the critical dimension x_{CH} of the chiral operator have been determined at the C

melting transition in the Potts model but it leaves several possible melting scenarios about the phase transition for small Δ.[54]

In spite of all these efforts, it is still not clear which scenario is realized in this model. It has been a long time mystery if there is a Lifshitz point in the phase diagram, i.e. whether the floating phase extends up to $\Delta = 0$. Haldane et al.[40] and Schulz[41] argued against the idea of a Lifshitz point at finite chirality, while Howes,[48] Huse et al.,[10] Selke[46] and Duxbury et al.[44] are for it. Even among the authors who agree on the existence of a Lifshitz point at finite Δ, there is no agreement on the nature of the transitions from C solids into SIC fluids. According to Howes, the transition is in the Potts universality class. Huse and Fisher[10] proposed that it should be in a new chiral universality class and their conjecture is supported by the numerical work of Duxbury et al.[44] but is questioned by the work of Vescan et al.[53]

Meanwhile, as a result of the fermion theory, the IC floating solids should bear the characteristics of Kosterlitz–Thouless (KT) phases.[33,34] In particular, the wavevector-dependent susceptibility should satisfy $\chi_q(T) \simeq \exp(a(1 - T/T_c)^{-1/2})$, when T is above but close to T_c, at which the transition from the IC fluid into the IC floating solid takes place. Here $\chi_q(T)$ is defined in (3.51). The last assertion depends on the assumption that the dislocation density of the domain wall array is still low even at the melting temperature. This has never been checked in an independent calculation.

In Chapters 2 and 3, the existence of Lifshitz point will be investigated and the phase transition nature of the melting of incommensurate floating solids in this model will be focused on to give a reasonable explanation of previous results.

CHAPTER 2

MEAN FIELD STUDY OF THE PHASE DIAGRAM OF THE 3-STATE CHIRAL POTTS MODEL (I)

2.1 INTRODUCTION

Since the chiral Potts model exhibits such rich and complicated behaviors as mentioned in the last chapter, no one method has been able to fully reveal its phase diagram. The existence of a Lifshitz point and the nature of the related phase transitions are still unclear. To get a reliable understanding of this model, further study by different methods is necessary.

It is well known that mean field theory is the simplest tool for the study of critical phenomena. In simple mean field theory, all interactions are replaced by effective fields. Therefore, in this theory only long-range order parameters are included, while short-range correlations due to local interactions are completely ignored. In an improved mean field theory, instead of replacing all interactions with effective fields, a cluster is considered while replacing interactions along the boundary of this cluster by effective fields and keeping the interactions within the cluster exact. Hence, part of the short-range correlations are successfully included in this kind of mean field theory. Although the phase diagram can be systematically improved by considering larger and larger clusters, any mean field theory will only give classical critical exponents.

Several years ago, Suzuki introduced the coherent anomaly method (CAM),[55] which is a systematic procedure to include more and more interactions exactly in the effective field approximation such that CAM series can be obtained. These series are then used to extrapolate to the critical behavior of the original system. This

method has been successfully applied in various models.[56] The mean-field transfer matrix (MFTM) method was introduced by him as one possible way to construct a CAM series.[57] The MFTM method retains the intuitive spirit of mean field theory by separating the whole system into several different decoupled strips with effective fields on their boundaries and treating interactions within them exactly.

By systematically treating wider and wider strips, i.e. more and more interactions are treated exactly, one should get better and better approximations to the exact phase diagram of the original physical system. From these successive approximations, one can obtain an extrapolation to the exact results. Meanwhile, it has been found that the MFTM method in its simplest form (i.e. an infinite chain with effective fields on the boundaries) can qualitatively improve the simple mean field results.[58]

In this chapter, the approximate free energy is calculated by the MFTM method. We compare approximate free energies for different mean-field solutions to determine the possible phase diagram of the 3-state chiral Potts model. From the systematic improvement of the mean-field approximation, the resulting mean-field phase diagram should become closer and closer to the exact one. Possible CAM behavior will be analyzed in the next chapter.

In Section 2.2, we review some basic knowledge of the model. In Section 2.3, we describe the approximate free energy resulting from the Gibbs-Bogoliubov inequality and the MFTM method. Numerical results will be presented in Section 2.4. Finally, a brief summary is given in Section 2.5.

2.2 NOTATIONS AND WELL-KNOWN RESULTS

In the last chapter, we have introduced the cell spin model. The Hamiltonian for this model reads

$$H = -\sum_{n,t} \left\{ E_n \cos\left(\theta(n,t) - \theta(n+1,t) + \frac{2}{3}\pi\Delta\right) + E_t \cos\left(\theta(n,t) - \theta(n,t+1)\right)\right\} \tag{2.1}$$

where (n,t) represents a lattice site of a two-dimensional square lattice, and $\theta(n,t)$ is the spin variable on the lattice site (n,t) taking values 0, $2\pi/3$ or $4\pi/3$. This model is a special case (Ostlund–Huse case) of the more general chiral Potts model.

For later convenience, we change some notations and write the model as

$$-\beta H(\{n_{i,j}\},\Delta) = \sum_{i,j}\left[K_n \cos\frac{2}{3}\pi(n_{i,j}-n_{i,j+1}+\Delta) + K_t \cos\frac{2}{3}\pi(n_{i,j}-n_{i+1,j})\right] \quad (2.2)$$

where $\beta = 1/k_{\mathrm{B}}T$, $K_n = \beta E_n$ and $K_t = \beta E_t$. We may not write out arguments explicitly for $H(\{n_{i,j}\},\Delta)$ if it will not cause confusion.

There are some useful symmetry relations in this model. For example, if

$$\Delta' = \Delta + 1/2, \quad n'_{i,j} = n_{i,j} - j \pmod 3 \quad (2.3)$$

then

$$H(\{n'_{i,j}\},\Delta') = -H(\{n_{i,j}\},\Delta), \quad (2.4)$$

and if

$$\Delta' = \Delta + 1, \quad n'_{i,j} = n_{i,j} + j \pmod 3 \quad (2.5)$$

or if

$$\Delta' = -\Delta, \quad n'_{i,j} = -n_{i,j} \pmod 3 \quad (2.6)$$

then

$$H(\{n'_{i,j}\},\Delta') = H(\{n_{i,j}\},\Delta). \quad (2.7)$$

The second relation also indicates that if

$$\Delta' = 1 - \Delta, \quad n'_{i,j} = -n_{i,j} + j \pmod 3 \quad (2.8)$$

then

$$H(\{n'_{i,j}\},\Delta') = H(\{n_{i,j}\},\Delta). \quad (2.9)$$

Hence, we only need to examine the region with $0 \le \Delta \le 1/2$ in this model.

Particularly, when $\Delta = 1/2$, the model becomes a model with antiferromagnetic horizontal interactions and ferromagnetic vertical interactions studied by Kinzel et al.[42] and its spin correlation is exactly known when $T = 0$.[26] When $\Delta = 0$ and $K_t =$

$K_n = K$, the model becomes the 3-state Potts model. For the 3-state ferromagnetic Potts model, the critical point K_c, critical exponents α, β, μ, and ν have been obtained as $K_c = 2\ln(\sqrt{3}+1)/3$, $\alpha = 1/3$, $\beta = 1/9$, $\mu = \nu = 5/6$.

In this model with $0 \leq \Delta < 1/2$, the order parameter $\langle\sigma\rangle = \langle\exp(2\pi i n_{i,j}/3)\rangle \neq 0$ for C solids which means pitch $Q = 0$. For IC floating solids or IC fluids, we would expect that the pair correlation decays exponentially with an oscillatory envelope along the chiral direction and with a continuously varying oscillation frequency ($Q \neq 0$). To distinguish IC floating solids and IC fluids, we have to see correlation lengths along the chiral direction and the non-chiral direction respectively. For IC floating solids, the correlation length is infinite in one direction at least but for IC fluids, both correlation lengths are finite. From now on, we change some of the terminology used in Chapter 1. Since we only need study the region $0 \leq \Delta \leq 1/2$, the pitch Q of C solids in this region is 0. Meanwhile, in our method, we are not able to distinguish IC fluids and C fluids. Hence we use ordered phases to denote C solids, disordered phases to denote C or IC fluids. Without confusion, incommensurate phases or modulated phases are used to denote IC floating solids.

2.3 FREE ENERGY CALCULATION BY THE MEAN-FIELD TRANSFER MATRIX METHOD

The approximated free energy is obtained by the use of the Gibbs-Bogoliubov inequality

$$F < F_{\mathrm{MF}} = \min(F_0 + \langle H - H_0\rangle), \tag{2.10}$$

where F is the exact free energy of the original system and H is the original Hamiltonian. H_0 is a trial Hamiltonian and F_0 is the exact free energy of the system defined by H_0. $\langle\cdots\rangle$ means average carried out in the ensemble defined by H_0 and this convention will be used throughout this chapter. For boundary spins, it is more convenient to introduce the vector notation

$$\mathbf{S}_{i,j} = \left(\cos\frac{2\pi}{3}n_{i,j},\ \ \sin\frac{2\pi}{3}n_{i,j}\right). \tag{2.11}$$

H and H_0 are defined as follows:

$$-\beta H = \sum_{i,j}\left[K_n\cos\frac{2\pi}{3}(n_{i,j}-n_{i,j+1}+\Delta)+K_t\cos\frac{2\pi}{3}(n_{i,j}-n_{i+1,j})\right], \quad (2.12)$$

$$\begin{aligned}-\beta H_0 &= \sum_{i,j}K_n\cos\frac{2\pi}{3}(n_{i,j}-n_{i,j+1}+\Delta)\\ &+\sum_{p=0}^{N_s-1}\sum_{k=pN}^{(p+1)N-2}\sum_j K_t\cos\frac{2\pi}{3}(n_{k,j}-n_{k+1,j})\\ &+\sum_{p,p'=0}^{N_s-1}\sum_{k=0}^{L-1}K_t\boldsymbol{\eta}_k\cdot(\mathbf{S}_{pN-1,p'L+k}+\mathbf{S}_{pN,p'L+k}),\end{aligned} \quad (2.13)$$

where $0 \le i \le N_sN-1$, $0 \le j \le N_sL-1$, periodic boundary conditions are imposed on both directions and $\beta = 1/k_{\rm B}T$. The trial Hamiltonian H_0 consists of N_s independent strips of width N and length N_sL with effective boundary fields $\{\boldsymbol{\eta}_j=(\eta_{j1},\eta_{j2})\}$ having period L to replace the exact interactions between strips.* In Fig. 2.1, we show how to replace the exact vertical interactions in the original model by effective field interactions within one row.

To find a good approximation for the free energy, we use (2.10) to find the minimum conditions which $\{\boldsymbol{\eta}_j\}$ should satisfy. Let

$$\begin{aligned}F(\{\boldsymbol{\eta}_j\}) &= F_0+\langle H-H_0\rangle\\ &= -\beta^{-1}\ln Z_0+\langle H-H_0\rangle,\end{aligned} \quad (2.14)$$

where

$$Z_0=\sum_{\{n_{i,j}\}}\exp(-\beta H_0), \quad \langle H-H_0\rangle=\sum_{\{n_{i,j}\}}(H-H_0)\exp(-\beta H_0)/Z_0. \quad (2.15)$$

Then the effective fields $\{\boldsymbol{\eta}_j\}$ should satisfy

$$\frac{\partial F(\{\boldsymbol{\eta}_j\})}{\partial\boldsymbol{\eta}_i}=0 \quad (2.16)$$

for any i to make $F(\{\boldsymbol{\eta}_j\})$ minimal and therefore the best possible approximated free energy for this given trial Hamiltonian. Eq. (2.16) can be calculated as follows:

$$\frac{\partial F(\{\boldsymbol{\eta}_j\})}{\partial\boldsymbol{\eta}_i} = \beta\left(\langle\frac{\partial H_0}{\partial\boldsymbol{\eta}_i}\rangle\langle H-H_0\rangle-\langle\frac{\partial H_0}{\partial\boldsymbol{\eta}_i}(H-H_0)\rangle\right) \quad (2.17)$$

*We could have chosen the length to be $N_s'L$ with N_s' independent of N_s. But in the thermodynamic limit $N_s', N_s \to \infty$, we can limit ourselves to the case $N_s'=N_s$ without loss of generality.

with

$$\begin{aligned} H - H_0 &= -\sum_{p,p'=0}^{N_s-1}\sum_{k=0}^{L-1} K_t\beta^{-1}[\mathbf{S}_{pN,p'L+k}\cdot\mathbf{S}_{pN-1,p'L+k} \\ &\quad -\boldsymbol{\eta}_k\cdot(\mathbf{S}_{pN,p'L+k}+\mathbf{S}_{pN-1,p'L+k})] \\ \frac{\partial H_0}{\partial\boldsymbol{\eta}_k} &= -K_t\beta^{-1}\sum_{p,p'=0}^{N_s-1}(\mathbf{S}_{pN-1,p'L+k}+\mathbf{S}_{pN,p'L+k}). \end{aligned} \tag{2.18}$$

Since there is no interaction between the different strips in H_0, we find

$$\langle\mathbf{S}_{pN,j}\mathbf{S}_{pN-1,i}\rangle = \langle\mathbf{S}_{pN,j}\rangle\langle\mathbf{S}_{pN-1,i}\rangle,$$
$$\langle\mathbf{S}_{pN,j}\cdot\mathbf{S}_{pN-1,j}\mathbf{S}_{p'N,i}\rangle - \langle\mathbf{S}_{pN,j}\cdot\mathbf{S}_{pN-1,j}\rangle\langle\mathbf{S}_{p'N,i}\rangle = 0 \quad \text{if } p'\neq p, p-1,$$
$$\langle\mathbf{S}_{pN,j}\cdot\mathbf{S}_{pN-1,j}\mathbf{S}_{p'N-1,i}\rangle - \langle\mathbf{S}_{pN,j}\cdot\mathbf{S}_{pN-1,j}\rangle\langle\mathbf{S}_{p'N-1,i}\rangle = 0 \quad \text{if } p'\neq p, p+1.$$

By periodicity of the trial Hamiltonian H_0 along both directions and reflection symmetry, we have

$$\langle\mathbf{S}_{pN,j}\rangle = \langle\mathbf{S}_{pN-1,j}\rangle = \langle\mathbf{S}_{p'N,j}\rangle = \langle\mathbf{S}_{p'N,j+L}\rangle,$$
$$\langle\mathbf{S}_{pN,j}\mathbf{S}_{(p+1)N-1,i}\rangle = \langle\mathbf{S}_{(p+1)N-1,j}\mathbf{S}_{pN,i}\rangle = \langle\mathbf{S}_{(p'+1)N-1,j}\mathbf{S}_{p'N,i}\rangle$$

for arbitrary p, p'. Hence explicitly substituting (2.18) into (2.17) and using the above relations to simplify it, we have

$$\frac{\partial F(\{\boldsymbol{\eta}_j\})}{\partial\boldsymbol{\eta}_i} = -\sum_{p=0}^{N_s-1}\sum_{k=0}^{L-1}\frac{2N_s^2K_t^2}{\beta}(\langle\mathbf{S}_{0,k}\rangle-\boldsymbol{\eta}_k)\cdot\langle\mathbf{S}_{0,k}\{\mathbf{S}_{0,pL+i}+\mathbf{S}_{N-1,pL+i}\}\rangle^{(\mathrm{c})}, \tag{2.19}$$

where we have used the connected correlation function

$$\langle\mathbf{S}_{i,j}\mathbf{S}_{k,l}\rangle^{(\mathrm{c})} \equiv \langle\mathbf{S}_{i,j}\mathbf{S}_{k,l}\rangle - \langle\mathbf{S}_{i,j}\rangle\langle\mathbf{S}_{k,l}\rangle. \tag{2.20}$$

From (2.19), we immediately get the necessary conditions for $F(\{\boldsymbol{\eta}_j\})$ to be minimal as

$$\boldsymbol{\eta}_j = \langle\mathbf{S}_{0,j}\rangle \equiv \mathbf{m}_j. \tag{2.21}$$

Since H_0 contains N_s identical independent strips, we can write Z_0 defined in (2.15) as

$$Z_0 = z_0^{N_s}, \tag{2.22}$$

where z_0 is the partition function defined on one strip. It is convenient for us to introduce the site-dependent column transfer matrix for one strip

$$\begin{aligned} T(\boldsymbol{\eta}_j)_{\{n_i\},\{n_i'\}} &= \exp\Big[\sum_{i=0}^{N-1} K_n \cos\frac{2\pi}{3}(n_i - n_i' + \Delta) \\ &\quad + \sum_{i=0}^{N-2} K_t \cos\frac{2\pi}{3}(n_i - n_{i+1}) + K_t \boldsymbol{\eta}_j \cdot (\mathbf{S}_0 + \mathbf{S}_{N-1})\Big] \end{aligned} \tag{2.23}$$

and boundary-spin operator matrix $\mathbf{M}$

$$\mathbf{M}_{\{n_j\},\{n_j'\}} = \mathbf{S}_0 \prod_{j=0}^{N-1} \delta(n_j, n_j'), \tag{2.24}$$

where

$$\mathbf{S}_i = \left(\cos\frac{2\pi}{3}n_i,\ \ \sin\frac{2\pi}{3}n_i\right),$$

and $\{n_i\}$ is a short-hand notation for $\{n_0,\, n_1,\, \cdots,\, n_{N-1}\}$, which is the column spin configuration within one strip along the non-chiral direction, and $\boldsymbol{\eta}_j$ is the effective boundary field. Hence z_0 can be given as

$$z_0 = \mathrm{Tr}\left(\left\{\prod_{j=0}^{L-1} T(\boldsymbol{\eta}_j)\right\}^{N_s}\right). \tag{2.25}$$

and $\mathbf{m}_j$ can be calculated by

$$\mathbf{m}_j = \mathrm{Tr}\left(\left\{\prod_{j=0}^{L-1} T(\boldsymbol{\eta}_j)\right\}^{N_s-1} T(\boldsymbol{\eta}_0)T(\boldsymbol{\eta}_1)\cdots\mathbf{M}T(\boldsymbol{\eta}_j)\cdots T(\boldsymbol{\eta}_{L-1})\right)/z_0. \tag{2.26}$$

If we define

$$\tau^i = \prod_{k=i}^{L-1} T(\boldsymbol{\eta}_k) \prod_{k=0}^{i-1} T(\boldsymbol{\eta}_k), \tag{2.27}$$

then we have

$$z_0 = \mathrm{Tr}\Big((\tau^i)^{N_s}\Big), \tag{2.28}$$

where i can take any value of $0, 1, \cdots, L-1$, and

$$\begin{aligned} \mathbf{m}_j &= \mathrm{Tr}\Big((\tau^0)^{N_s-1} T(\boldsymbol{\eta}_0)T(\boldsymbol{\eta}_1)\cdots\mathbf{M}T(\boldsymbol{\eta}_j)\cdots T(\boldsymbol{\eta}_{L-1})\Big)/z_0 \\ &= \mathrm{Tr}\Big((\tau^j)^{N_s}\mathbf{M}\Big)/z_0, \quad j = 0, 1, \cdots, L-1. \end{aligned} \tag{2.29}$$

Consequently, in thermodynamic limit $N_s \to \infty$, ignoring the exponentially small terms in the trace, we find that z_0 and $\mathbf{m}_j$ are given in terms of the largest eigenvalue of τ^j and its corresponding eigenvector. Hence, we get

$$z_0 = \left(\lambda^0\right)^{N_s} \tag{2.30}$$

and

$$\mathbf{m}_j = (\lambda^0)^{-1}\langle\lambda^0|T(\boldsymbol{\eta}_0)T(\boldsymbol{\eta}_1)\cdots\mathbf{M}T(\boldsymbol{\eta}_j)\cdots T(\boldsymbol{\eta}_{L-1})|\lambda^0\rangle, \tag{2.31}$$

where $|\lambda^0\rangle$ and $\langle\lambda^0|$ are the right and left eigenvectors of τ^0 respectively (with $\langle\lambda^0|\lambda^0\rangle = 1$), corresponding to the largest eigenvalue $\lambda^0 = \lambda^0(\{\boldsymbol{\eta}_j\})$. Therefore, from (2.14) and (2.18), we can write the approximated free energy per site as

$$f_{\mathrm{MF}} = -\frac{1}{NL\beta}\ln\lambda^0(\{\boldsymbol{\eta}_j\}) + \frac{K_t}{NL\beta}\sum_{j=0}^{L-1}(2\boldsymbol{\eta}_j\cdot\mathbf{m}_j - \mathbf{m}_j\cdot\mathbf{m}_j) \tag{2.32}$$

and the effective boundary fields are determined by the equations

$$\boldsymbol{\eta}_j = \mathbf{m}_j, \quad \text{where } j = 0, 1, \cdots, L-1. \tag{2.33}$$

It is easy to see that the effective fields in our trial Hamiltonian are essentially the thermal average of boundary spins from (2.33) and our study is essentially a mean-field theory. Since (2.33) only gives a necessary but not a sufficient condition for f_{MF} to be minimal, any solution to the mean-field equations (2.33) only gives an extremum of the approximated free energy (2.32) in the phase space and could be is metastable or unstable. The thermodynamically stable phase is the one that gives the absolute minimum free energy for all different solutions with all possible L. Therefore, to find the best approximation to the true free energy of the system requires obtaining all solutions for all L.

Clearly it is impossible to do that, namely to obtain all the solutions for all L and we have to put a restriction $L \leq L_{\max}$. Meanwhile, since the largest eigenvalue λ^0 and its corresponding eigenvector are functions of $\{\boldsymbol{\eta}_j\}$ with $0 \leq j \leq L-1$, the mean-field equations (2.33) and (2.31) are systems of transcendental equations in L unknowns, such that their solutions can only be calculated numerically and may admit many many different solutions. In this calculation, we limit our solutions to

those which can be obtained by direct iteration.* That is, the boundary fields are obtained iteratively as

$$\boldsymbol{\eta}'_j = \mathbf{m}_j(\{\boldsymbol{\eta}_i\}), \quad \boldsymbol{\eta}''_j = \mathbf{m}_j(\{\boldsymbol{\eta}'_i\}), \ \cdots, \ \boldsymbol{\eta}_j^{(n)} = \mathbf{m}_j(\{\boldsymbol{\eta}_i^{(n-1)}\}). \tag{2.34}$$

Since H_0 depends on the effective fields $\{\boldsymbol{\eta}_i\}$ and $\mathbf{m}_j = \langle \mathbf{S}_{0,j} \rangle = \langle \mathbf{S}_{N-1,j} \rangle$, $\mathbf{m}_j$ will depend on $\{\boldsymbol{\eta}_i\}$ and we write the dependence explicitly in the above equations. If we have the initial set of $\{\boldsymbol{\eta}_i\}$ for the trial Hamiltonian H_0, we can calculate $\{\boldsymbol{\eta}'_j\}$ according to (2.34) and then use the results as effective fields to obtain $\{\boldsymbol{\eta}''_j\}$. This process can be continued until the difference between $\{\boldsymbol{\eta}_j^{(n)}\}$ and $\{\boldsymbol{\eta}_j^{(n-1)}\}$ becomes negligible, hence we get the approximated solutions to the mean-field equations. Obviously, the convergence of these solutions fully depends on the given initial conditions, and it is very important to choose the right initial conditions in order to obtain a fast convergent result. We make this choice according to the physical situation.

For $0 \leq \Delta \leq 1/2$, we expect that the average magnetization of the system is translationally invariant—the same for all sites (Q=0), and is identically zero when it is in the disordered state, nonvanishing when it is in the C ordered state. In the modulated phase, it is aperiodic or approximately periodic with $L > 1$. Hence we may expect three types of solution to the mean-field equations (2.33), i.e. the disordered solution with ($\boldsymbol{\eta} = \mathbf{0}$), the ordered solution with ($\boldsymbol{\eta} \neq \mathbf{0}$) which can be obtained by setting $L = 1$ in the mean-field equations (2.33) and modulated solutions with unequal boundary magnetizations ($L > 1$).

Let us first discuss the ordered and the disordered solutions, which is equivalent to discussing the solutions to the mean-field equation (2.33) with $L = 1$. It can be shown that the boundary magnetization $\mathbf{m} = 0$ if $\boldsymbol{\eta} = \mathbf{0}$. Therefore, the disordered solution is always present and its corresponding approximated free energy is always a local extremum in the phase space. To obtain the ordered solution by iteration, we set the initial value $\boldsymbol{\eta} = (1, 0)$. For $L = 1$, the mean-field equation (2.33) has only one variable $\boldsymbol{\eta}$, and can be solved directly. The extrema of $f_{\rm MF}$ can be obtained with

*We have verified by Maple and Fortran that this procedure gives the desired solution for small $N = 1, 2, 3, 4$, as is discussed below.

high accuracy for $N \leq 4$, and the results are used to understand the validity and the accuracy of our iterative procedure.

The free energy $f_{\rm MF}$ in (2.32) is plotted versus the magnitude η of the boundary field $\boldsymbol{\eta}$ for three different temperature regions in Fig. 2.2 for $\Delta = 0$. We find $f_{\rm MF}(\boldsymbol{\eta})$ is an extremum for $\boldsymbol{\eta} = \mathbf{0}$, as expected. It is a minimum at high temperature as shown by the bottom line and is the only minimum. The top line is the low-temperature behavior which has a maximum at $\eta = 0$, and a minimum at η near 1. But for intermediate temperatures, near the transition temperature $T_{\rm c}$ it is represented by the middle line (enlarged in Fig. 2.3), which has two local minima. Above $T_{\rm c}$, the minimum at $\eta = 0$ has a lower value and below $T_{\rm c}$ a higher value. At $T_{\rm c}$ the two minima have the same value: Thus the initial condition $\boldsymbol{\eta} = (1, 0)$, would converge to the local minimum near $\eta = 1$, and we call it the ordered solution which may or may not be the true minimum. It is also easy to see from Fig. 2.3 that the phase transition at $T_{\rm c}$ is of first order (with discontinuity in the derivative of the free energy). For $\Delta \neq 0$, these features for $L = 1$ remain the same. In our iteration scheme, we are only able to get the solution with the larger value of $\boldsymbol{\eta}$. However, the solution, which is missed in our iteration scheme, always gives a higher approximated free energy than the solution obtained by our iteration scheme. Because $f_{\rm MF}(\boldsymbol{\eta})$ is bounded below and increases for $\boldsymbol{\eta}$ large enough, the iteration scheme always converges to a minimum.

Now let us discuss how to get modulated solutions. Obviously, to obtain a modulated solution by iteration, we have to choose non-uniform $\{\boldsymbol{\eta}_i\}$ as initial conditions. Here we choose the initial values of $\{\boldsymbol{\eta}_i\}$ with period L to be

$$\boldsymbol{\eta}_i = \left(\cos\frac{2\pi}{3}n_i, \sin\frac{2\pi}{3}n_i\right) \quad \text{with } i = 0, 1, \cdots, L-1,$$

where $\{n_0, n_1, \cdots, n_{L-1}\}$ can be any row spin configuration. Since not all initial non-uniform values for $\{\boldsymbol{\eta}_i\}$ lead to modulated solutions (some may converge to the ordered solution or the disordered solution and some may not converge at all) and not all modulated solutions give local minima (some of them may be maxima) of the approximated free energy, we have to include as many initial conditions as possible. On the other hand, there are many different initial conditions leading to modulated solutions with equal or nearly equal approximated free energies which means we

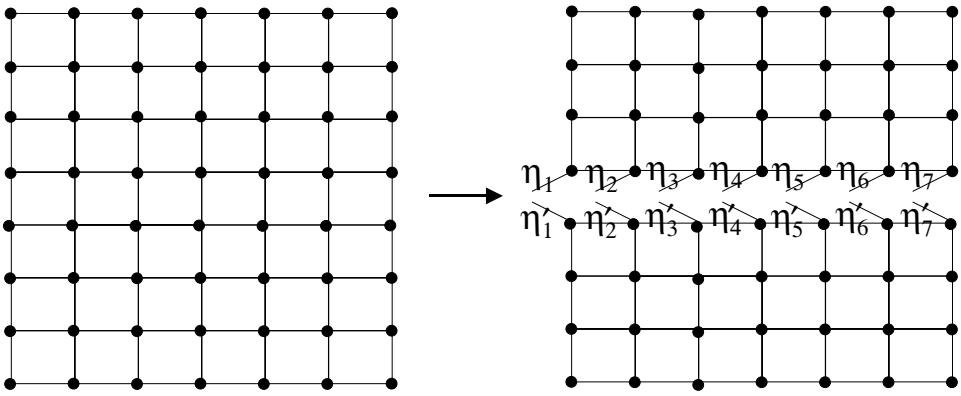

Figure 2.1. Exact vertical interactions within one row approximated by effective field interactions.

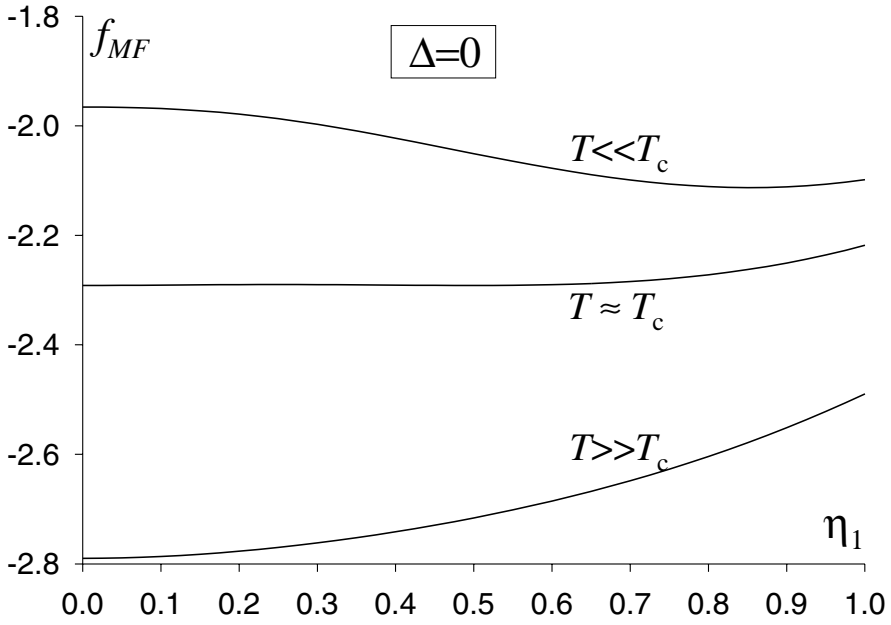

Figure 2.2. f_{MF} versus $(\eta_1, 0)$, with $\Delta = 0$, $K_n = K_t$ and different temperatures.

can ignore their difference when we determine the phase diagram. It should not be necessary to include all possible different configurations with the same period. Indeed, we find that instead of the spin configuration $\{n_i\}$, it is more economical for us to put restrictions on the initial values of $\{\boldsymbol{\eta}_i\}$ through the difference sequence $\{m_i\}$, which is defined in Appendix A.

If we put all independent difference sequences with length $l \leq l_{\max}$ as possible initial conditions for $\{\boldsymbol{\eta}_i\}$, it shall be shown in Appendix A that this set of initial conditions not only includes all possible initial conditions for $\{\boldsymbol{\eta}_i\}$ determined by all different spin configurations with period $L \leq l_{\max}$, but it also includes a small fraction of the spin configurations with period L in the range $l_{\max} < L \leq 3l_{\max}$. Although the periods for the two cases ($P \equiv n_0 - n_l = 0$ or $P \neq 0$) are different, they take approximately equal calculation time as shown in Appendix B. Since the m_i in difference sequence $\{m_i\}$ is the difference of successive spins along the chiral direction, and is related to the excess energy of the spin configuration, we may reduce further the number of possible initial conditions by restricting $m_i = 0$ or 2, as $m_i = 0$ or 2 gives a lower edge interaction than $m_i = 1$.

The approximated free energies for the disordered and ordered solutions can be obtained without much effort. To determine if the system is in a modulated phase, we only need to find a modulated solution giving a lower approximated free energy than the free energies given by the ordered and disordered solutions. However, to be sure that the system is not in a modulated phase, we have to find all the modulated solutions with all possible L. Hence, because only part of the modulated solutions is considered, the incommensurate phase region in our approximated phase diagram is possibly smaller than the one in the exact phase diagram, with exact in the sense that we obtain all possible modulated solutions and compare their free energies. The validity of the restriction of $l \leq l_{\max}$ is checked below in Figs. 2.9 and 2.10, and the validity of the restriction of $m_i \neq 1$ is checked in Table 2.3.

2.4 NUMERICAL RESULTS ON THE PHASE DIAGRAM

Before presenting our numerical results, we would like to mention that since K_t and K_n are proportional to $1/T$ and we are only concerned about the relative values of approximated free energies and temperatures, we can set $E_t = k_{\rm B} = 1$, giving in $T = 1/K_t$, in Chapters 2 and 3 without loss of generality. In our numerical calculation, the maximum number of iterations used to solve the mean-field equations is 3000 and typically the solutions are obtained after hundreds of times of iteration.

We first establish the global phase diagram of the model by comparing the approximated free energies for different solutions of (2.33), and then compare our results with the well-established results to check the validity of this method. To obtain the phase diagram, we have to find the upper-temperature limit and the lower-temperature limit of the modulate phase for fixed Δ in the phase diagram.

To determine the phase boundaries, we first locate a temperature T_e at which the approximated free energy for the ordered solution and the approximated free energy for the disordered solution are equal. The reason for searching for $T_{\rm e}$ is that if there are modulated phases for this fixed Δ, then the system at $T_{\rm e}$ must be in the modulate phase. This can be shown as follows: Let us denote the approximated free energy by $f_{\rm o}$ for the ordered solution, $f_{\rm d}$ for the disordered solution and $f_{\rm m}$ for the lowest approximated free energy resulting from all modulated solutions. Then on the phase boundary between the ordered phase and modulated phase, we have $f_{\rm o} = f_{\rm m}$. Hence, near the phase boundary, which separates the ordered phase from the modulated phase, we can expect in the ordered phase $f_{\rm o} < f_{\rm m} < f_{\rm d}$, and in the modulated phase we have $f_{\rm m} < f_{\rm o} < f_{\rm d}$. Similarly, near the phase boundary which separates the disordered phase from the modulated phase, in the modulated phase we have $f_{\rm m} < f_{\rm d} < f_{\rm o}$. Therefore, we can conclude that $f_{\rm d} = f_{\rm o}$ must happen somewhere within the modulated phase region. To search for $T_{\rm e}$, we first take a temperature $T_{\rm d}$ with $T_{\rm d}$ high enough so that the approximated free energy for the disordered solution is lower than the one for the ordered solution. Then we take another temperature $T_{\rm o}$ with $T_{\rm o}$ low enough so that the approximated free energy for

the ordered solution is lower than the one for the disordered solution. After taking these two initial temperatures, we use a bisecting method by checking the system at temperature $(T_{\rm d}+T_{\rm o})/2$. If the approximated free energy for the disordered solution is lower than the one for the ordered solution at temperature $(T_{\rm d}+T_{\rm o})/2$, we set this temperature as the new $T_{\rm d}$, otherwise we choose it as the new $T_{\rm o}$. We can repeat this process until the difference of $T_{\rm d}$ and $T_{\rm o}$ vanishes within our numerical accuracy, resulting in the point with $T_{\rm e}=(T_{\rm d}+T_{\rm o})/2$.

After the temperature $T_{\rm e}$ is located, we can use this temperature to locate the upper-temperature limit $T_{\rm h}$ and the lower-temperature limit $T_{\rm l}$, which are estimates of the boundaries of the modulated phases. In the following, we show how to search for the upper-temperature limit for fixed Δ. We first check if the system at temperature $T_{\rm e}$ is in the modulated phase. If the system is not in the modulated phase, this means that no modulated phase exists for this Δ, and that there are ordered phases for temperatures lower than $T_{\rm e}$ and disordered phases for temperatures higher than $T_{\rm e}$. If the system is in a modulated phase, we set $T_{\rm m}=T_{\rm e}$ and find a temperature $T_{\rm h}$ with $T_{\rm h}$ high enough so that the corresponding system is in the disordered phase. Then we check the phase of the system with temperature $(T_{\rm m}+T_{\rm h})/2$. If it is in the modulated phase, we set this temperature as the new $T_{\rm m}$, otherwise we set it as the new $T_{\rm h}$. We can repeat this bisecting procedure until the difference between $T_{\rm h}$ and $T_{\rm m}$ is within the required accuracy for the upper-temperature limit of the modulated phase. Similarly, we can get the lower-temperature limit of the modulated phase for fixed Δ.

The initial values $\{\boldsymbol{\eta}_i\}$ that we use are given by all possible difference sequences $\{m_1,m_2,\cdots,m_l\}$ with $l\le 12$ and $m_i=0$ or 2, representing different spin configurations. The accuracy used in this part of the calculation is 10^{-11} for free energies, 10^{-6} for effective fields and 10^{-3} for critical temperatures. In Table 2.1, we present the approximated free energies of the disordered solution, the ordered solution, and the lowest one resulting from all modulated solutions for various T at $\Delta=0.30$ with $K_n=K_t$ and width $N=2$. In this table, there are significant differences between the free energies of the disordered solution, the ordered solution, and the lowest one

T	Disordered	Ordered	Modulated
1.57244	-1.98083	-1.98165	
1.57457	-1.98279	-1.98312	-1.98312
1.57670	-1.98476	-1.98460	-1.98495
1.57883	-1.98672	-1.98610	-1.98680
1.58096	-1.98869	-1.98762	

TABLE 2.1. Table of $f_{\rm MF}$ for various mean-field solutions and temperatures where $K_n = K_t$, $\Delta = 0.30$, and $N = 2$. Two items are empty meaning that no corresponding solution for the mean-field equations in our scheme exists. The approximated free energy for the modulated solution is the lowest one resulting from all modulated solutions we considered.

resulting from all modulated solutions when the temperature T is away from a critical one $T_{\rm c} = T_{\rm h}$ or $T_{\rm l}$ with $|T - T_{\rm c}| > 10^{-3}$.

For a slightly smaller value of $\Delta = \Delta_L$, we find evidence for the existence of a Lifshitz point in the case of a strip with width $N = 2$ in a periodic effective boundary field. At $K_n = K_t = 0.627354$ and $\Delta = 0.288313$ we find a modulated solution* with

$$f_{\rm MF} = -2.0022416, \tag{2.35}$$

$$\left\{ \begin{array}{c} \boldsymbol{\eta}_0 \\ \boldsymbol{\eta}_1 \\ \boldsymbol{\eta}_2 \\ \boldsymbol{\eta}_3 \\ \boldsymbol{\eta}_4 \end{array} \right\} = \left\{ \begin{array}{ll} (0.036778, & -0.007183) \\ (0.036778, & 0.007183) \\ (0.029948, & 0.020518) \\ (0.017780, & 0.030796) \\ (0.002795, & 0.036195), \end{array} \right\}, \tag{2.36}$$

*Since this modulated solution is close to the form $\boldsymbol{\eta}_j = A(\cos(jq+\alpha), \sin(jq+\alpha))$, we may expect that the modulated solution, which gives the lowest free energy, is close to $\boldsymbol{\eta}_j = A(\cos(jq+\alpha), \sin(jq+\alpha))$ with suitable q. Hence, in our calculation, we also put the initial condition $\boldsymbol{\eta}_j = (\cos(2\pi kj/L), \sin(2\pi kj/L))$ with $k = 0, 1, \cdots, L-1$ and L being the period of $\{\boldsymbol{\eta}_i\}$. (However, since translational invariance has been broken within the mean-field transfer matrix method, we may not expect the solution to be exactly of this form. Further group-theoretical analysis may clarify the situation.) We also calculated Δ_L with L up to 250 and confirmed the accuracy for Δ_L achieved in Figs. 2.9 and 2.10.

and $\boldsymbol{\eta}_{i+5} = \mathbf{R}\boldsymbol{\eta}_i$ where $\mathbf{R}$ is defined in (B.2) with $P = 1$. This modulated solution above has almost the same free energy as the disordered solution with $\boldsymbol{\eta}_i = \mathbf{0}$ and the ordered solution with $\boldsymbol{\eta}_i = (0.556284, 0)$. However, to our numerical accuracy, this modulated solution is significantly different from the disordered solution and the ordered solution. This also indicates that the transition from the disordered phase into the modulated phase for $\Delta \neq 0$ is first order in a finite-width mean-field system just as the transition from the disordered phase into the ordered phase for $\Delta = 0$. Meanwhile, (2.36) and Table 2.1 also show that we need not worry about the floating-point errors when we determine the phase of a system.

As reviewed by Wu,[59] simple mean-field theory predicts a first-order phase transition in the 3-state Potts model which is equivalent to the $\Delta = 0$ 3-state chiral Potts model. Our finite-width MFTM theory also predicts a first-order phase transition for $\Delta = 0$. There are ordered and disordered solutions which give equal free energies at the critical point in the MFTM method. The disordered solution is trivial and the ordered solutions with different strip width N are presented in Table 2.2. These numbers have been compared with the results obtained by solving the mean-field equation directly using Maple for $N \leq 4$, and have been found to be quite accurate. From Table 2.2, we can see that the two solutions for $\boldsymbol{\eta}$ will not merge when $N \to \infty$. Hence, the effective fields $\boldsymbol{\eta}$ have a jump as the temperature crosses the critical point. In the simple mean-field theory, this effective field can be explained as magnetization and therefore the result indicates a first-order phase transition.[59] This effective field $\boldsymbol{\eta}$ is not related to the bulk magnetization but to the boundary magnetization in the MFTM method; it nevertheless also leads to a non-vanishing bulk magnetization and a jump of the specific heat at a critical point in any finite-width mean-field system. From Table 2.2, it also can be seen that the bulk magnetization $\mathbf{m}_c$, which is the spin average of the central row of the strip, decreases as N increases. When $N \to \infty$, this effective field $\boldsymbol{\eta}$ should give an infinitely small effect on the bulk magnetization $\mathbf{m}_c$ and the specific heat. Hence, the extrapolation of the MFTM method would be able to give the correct nature of the phase transition, i.e. a continuous phase transition. This should also be true for cases with $\Delta \neq 0$.

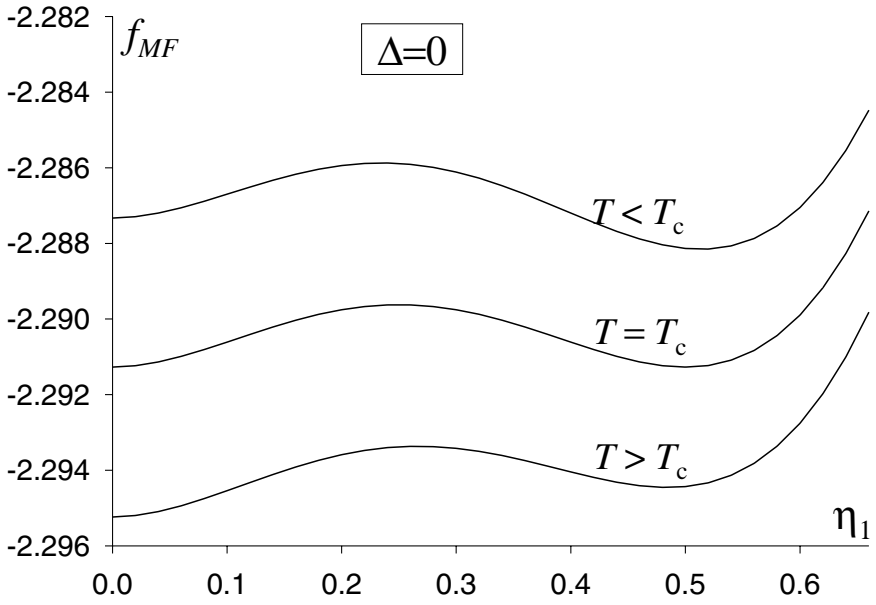

Figure 2.3. f_{MF} versus $(\eta_1, 0)$, with $\Delta = 0$, $K_n = K_t$ and temperatures near the critical one T_{c}.

N	$1/T_{\mathrm{c}}$	f_{MF}	$\boldsymbol{\eta}$	$\mathbf{m}_{\mathrm{c}}$
1	0.50966	-2.29128	$(0.500000, 0)$	$(0.500000, 0)$
2	0.55266	-2.22560	$(0.495022, 0)$	$(0.495022, 0)$
3	0.57291	-2.19947	$(0.495454, 0)$	$(0.464888, 0)$
4	0.58511	-2.18501	$(0.497653, 0)$	$(0.450472, 0)$
5	0.59336	-2.17579	$(0.500329, 0)$	$(0.423631, 0)$
6	0.59934	-2.16941	$(0.502935, 0)$	$(0.406160, 0)$
7	0.60386	-2.16478	$(0.505231, 0)$	$(0.380529, 0)$

TABLE 2.2. Table of f_{MF}, $\boldsymbol{\eta}$ and $\mathbf{m}_{\mathrm{c}}$ for $\Delta = 0$. $f_{\mathrm{MF}}(N)$ is the approximated free energy, $\boldsymbol{\eta}(N)$ is the ordered solution and $\mathbf{m}_{\mathrm{c}}(N)$ is the magnetization on the central row with this ordered solution at $K_n = K_t = 1/T_{\mathrm{c}}$, $\Delta = 0$ with strip width N. At this point, the approximated free energies given by the disordered solution and the ordered solution are equal.

The global phase diagrams with $K_n = K_t$ are shown in Fig. 2.4 for $N = 1$, in Fig. 2.5 for $N = 2$, and in Fig. 2.6 for $N = 3$. We find approximately $\Delta_L > 0.30$ for $N = 1$, $\Delta_L \approx 0.29$ for $N = 2$ and $\Delta_L \leq 0.28$ for $N = 3$. In order to check the applicability of the MFTM method, we compare the result for the critical point at the Potts point $\Delta = 0$ in Fig. 2.7 and the result for the C-IC transition line with a well-known result[26] which was obtained by free-fermion approximation for Δ near $1/2$ in Fig. 2.8. From Figs. 2.7 and 2.8, we see that the convergence is slow but the phase diagram is really systematically improved. From the phase diagram obtained in Figs. 2.6, 2.7, and 2.8, the global structure of the phase diagram agrees with the well-established results. This gives us more confidence that the results for the free energy obtained by the mean-field transfer matrix method will be reliable.

One of the main motivations for the current study is the question of the existence of Lifshitz point Δ_L at finite chirality. Therefore, higher accuracy for Δ_L is desired. For later purposes, it is necessary to explain more clearly the approximation for Δ_L we made. From now on, we use Δ_L to denote the exact Lifshitz point for the original thermodynamic system, $\Delta_L^{\infty}(N)$ to denote the exact Lifshitz point of the mean-field transfer matrix system for a strip of width N (in a sense, we consider all the possible modulated solutions with all possible l), and $\Delta_L^{l}(N)$ to denote the approximate Lifshitz point in which we only consider the modulated solutions with initial values of $\{\boldsymbol{\eta}_i\}$ represented by the independent set of difference sequences of length l, although in principle it should be better to include all the solutions with length of difference sequence less than l. We would expect that $\min_{\ell \leq l} \Delta_L^{\ell}(N)$ will approach $\Delta_L^{\infty}(N)$ when $l \to \infty$ for fixed width N of the mean-field transfer matrix system and that $\Delta_L^{\infty}(N)$ will approach Δ_L when the width N of the strip goes to infinity. Since no closed form for the solutions of the mean-field transfer matrix equation exists, it is impossible to determine $\Delta_L^{\infty}(N)$ directly. We use $\Delta_L^{l}(N)$ for suitable l as a good approximation to $\Delta_L^{\infty}(N)$.

We shall now concentrate on the calculation of Δ_L since the information about Δ_L is still crude in our early calculation. Because the approximated free energies of the ordered solution, the disordered solution and certain modulated solutions (which

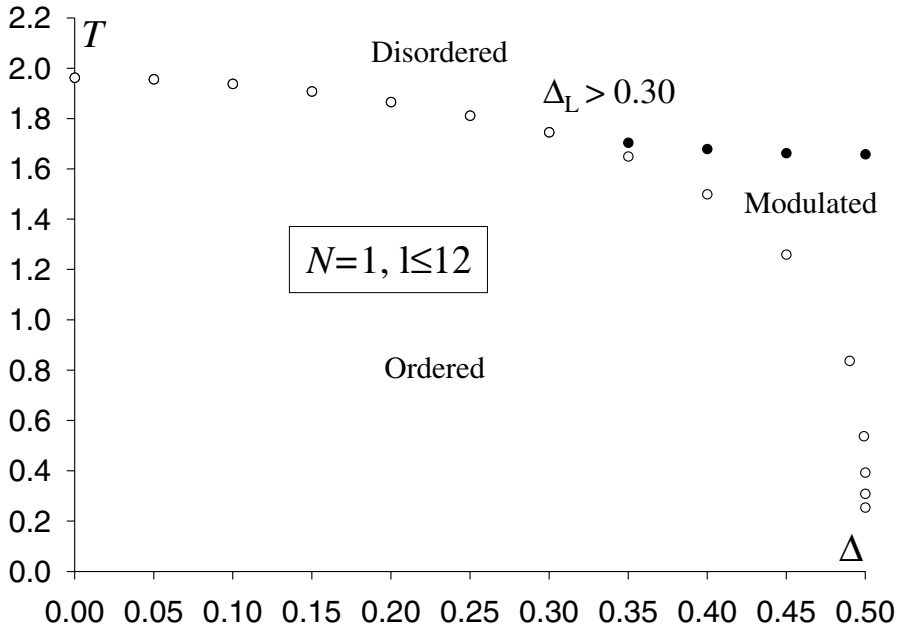

Figure 2.4. The mean-field transfer matrix phase diagram with strip width $N = 1$. The approximate value of $\Delta_L > 0.30$. To obtain the phase diagram, we considered mean-field solutions with $l \leq 12$.

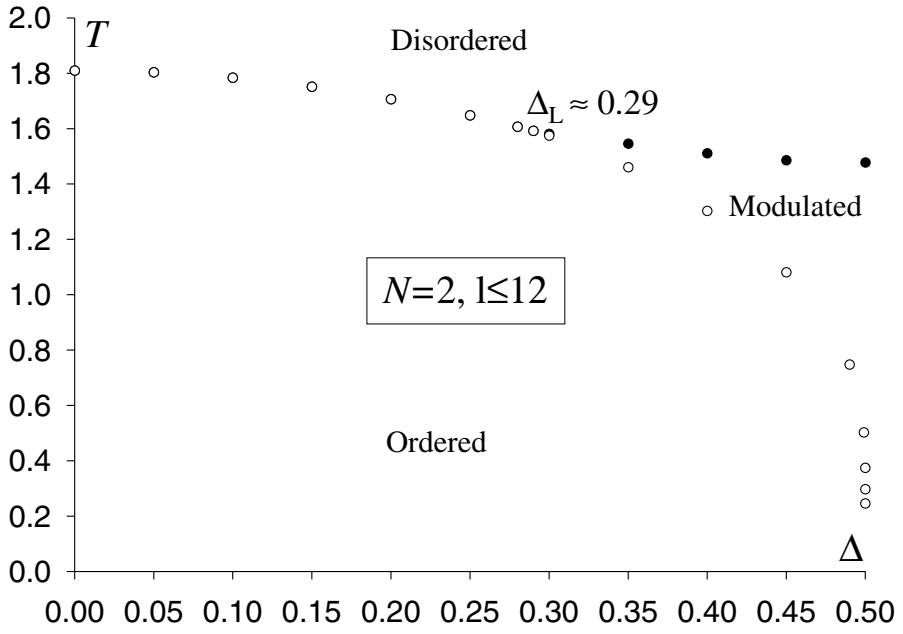

Figure 2.5. The mean-field transfer matrix phase diagram with width $N = 2$. The approximate value of $\Delta_L \approx 0.29$. We considered mean-field solutions with $l \leq 12$.

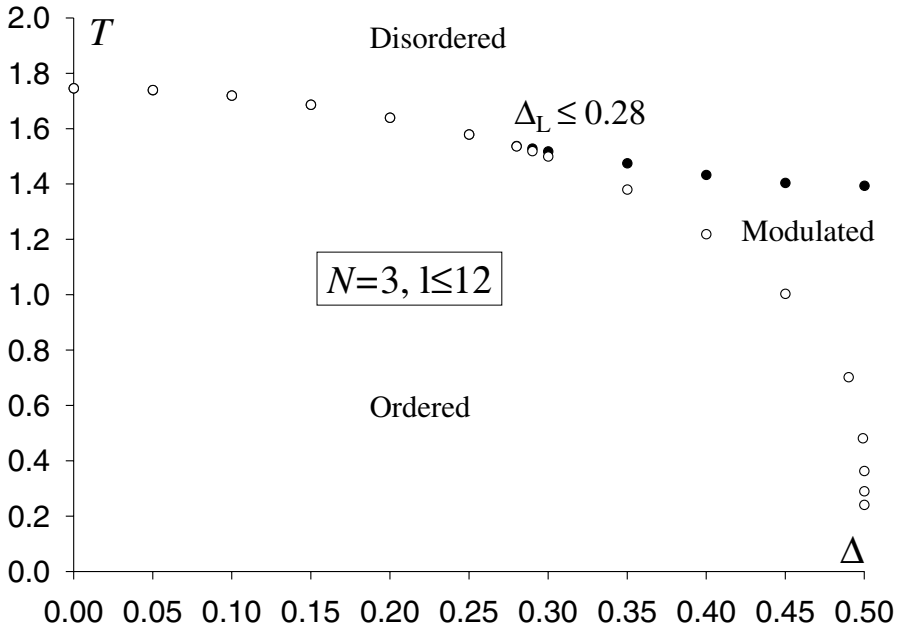

Figure 2.6. The mean-field transfer matrix phase diagram with width $N = 3$. The approximate value of $\Delta_L \leq 0.28$. We considered mean-field solutions with $l \leq 12$.

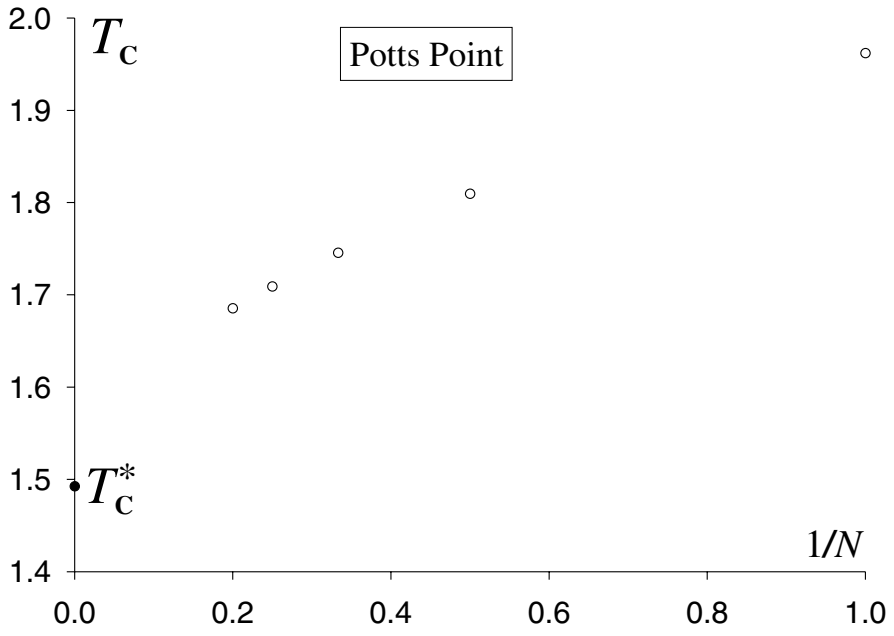

Figure 2.7. Systematic improvement of the approximated critical point T_c versus $1/N$, where N is the width of the strip, $\circ$ denotes approximated mean-field transfer matrix results and T_c^* the exact 3-state Potts result.

give the lowest approximated free energy among all possible modulated solutions) are equal at the Lifshitz point, we only need to calculate the approximated free energy with modulated solutions along the line (Δ,$T_{\rm e}$) on which the approximated free energies of the ordered solution and the disordered solution are equal to obtain higher accuracy for $\Delta_L^l(N)$. This greatly reduces the calculation time. Hence, we can spend more time to increase the accuracy for $\Delta_L^l(N)$ up to 10^{-4} making larger N and l possible (up to 16 for l where l is the length of difference sequence which determines the initial value of $\{\boldsymbol{\eta}_i\}$). The limiting $\Delta_L^\infty(N)$ should be the minimum among the set $\{\Delta_L^l(N)\}$ with l taking all positive integer values.

In the following, we show how to use a bisecting procedure to get $\Delta_L^l(N)$. We first take $\Delta_{\rm min} = 0$ and $\Delta_{\rm max} = 0.5$, then check if point ($\Delta_{\rm m}$,$T_{\rm e}$) with $\Delta_{\rm m} = (\Delta_{\rm min} + \Delta_{\rm max})/2$ is in the modulated phase. If point ($\Delta_{\rm m}$,$T_{\rm e}$) is in the modulated phase, we set new $\Delta_{\rm max} = \Delta_{\rm m}$ otherwise $\Delta_{\rm min} = \Delta_{\rm m}$. We repeat the above procedure until the difference between $\Delta_{\rm max}$ and $\Delta_{\rm min}$ is negligible. The results are shown in Figs. 2.9 and 2.10. From Figs. 2.9 and 2.10, we find that $\Delta_L^l(N)$ is oscillating with l and that the local minima shown in Fig. 2.9 are very close. If this is the case for arbitrary l, then we can conclude that the first local minimum of $\Delta_L^l(N)$ is good enough to be an approximation for $\Delta_L^\infty(N)$. We also find that the l which gives the first minimum of $\Delta_L^l(N)$ increases and $\Delta_L^l(N)$ decreases when N increases. We obtain $\Delta_L^\infty(1) \approx 0.3143$, $\Delta_L^\infty(2) \approx 0.2883$, $\Delta_L^\infty(3) \approx 0.2770$ and $\Delta_L^\infty(4) \approx 0.2709$ when $K_n = K_t$. When $K_n = 10K_t$, we get $\Delta_L^\infty(1) \approx 0.2258$ and $\Delta_L^\infty(2) \leq 0.2156$. This coincides with our intuition that larger K_n/K_t leads to faster convergence. We can roughly explain it as follows: Since larger K_n/K_t effectively reduces the correlation length λ_t in the non-chiral direction at the approximated critical temperature, this will increase the scaled variable N/λ_t in finite-size scaling theory.

Finally, we come back to the validity of the restriction of $m_i = 0$ or 2 in the difference sequence $m_1 m_2 \cdots m_l$ by comparing $\Delta_L^l(1)$ obtained by m_i taking all possible values (0,1 and 2) with $\Delta_L^l(1)$ obtained by only taking $m_i = 0$ or 2. From Table 2.3, we see that the difference is very small within our error bars and thus can be neglected. This is assumed to be the general case for larger l and wider strips.

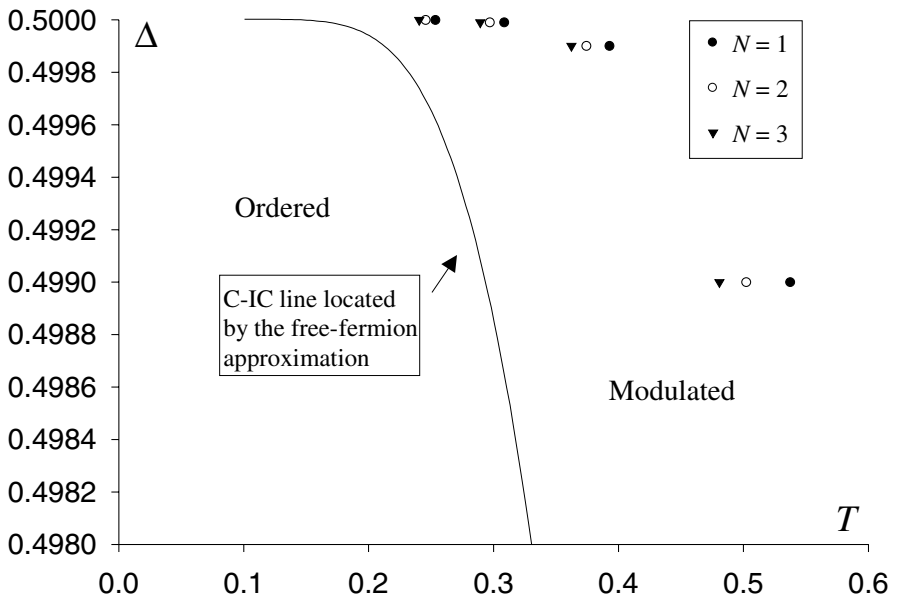

Figure 2.8. Δ versus $T_{\rm c}$. The solid line is derived from the free-fermion approximation which should be a better approximation for Δ close to 1/2.

l	4	5	6	7	8	9	10
$\Delta_L^l(1)$	0.3143	0.3163	0.3179	0.3172	0.3142	0.3152	0.3164
$\Delta_L^l(1)$	0.3143	0.3164	0.3180	0.3173	0.3143	0.3152	0.3164

TABLE 2.3. Table of Δ_L^l. The Δ_L^l in the second row are obtained with m_i taking any value of 0, 1 and 2, but the Δ_L^l in the third row are obtained with m_i taking only values 0 or 2. $K_n = K_t$ and $N = 1$ in both cases.

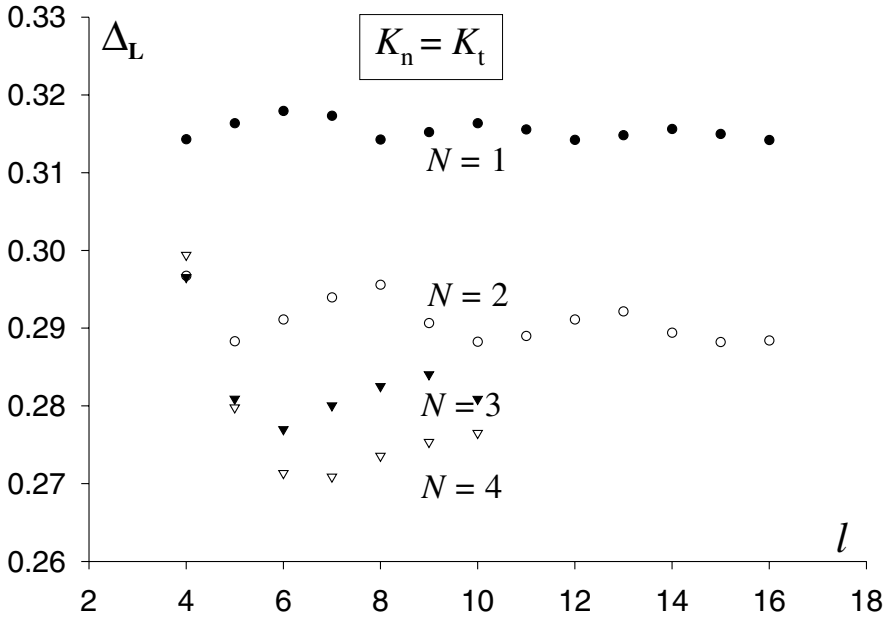

Figure 2.9. $\Delta_L^l(N)$ versus l with $K_n = K_t$ and strip width N. Local minima are 0.3143 at $l = 4$, 8, 12 for $N = 1$, 0.2883 at $l = 5$, 10, 15 for $N = 2$, 0.2770 at $l = 6$ for $N = 3$, and 0.2709 at $l = 7$ for $N = 4$.

From the above, we can safely claim that the Lifshitz point located by the MFTM method is systematically moving to the left when the width N becomes larger. It is conceivable that the Lifshitz point is located at $\Delta = 0$ when width $N \to \infty$ as suggested by Haldane et al.[40] and Schulz.[41]

2.5 SUMMARY

In this chapter, we have studied the Lifshitz point problem in the 3-state chiral Potts model. We have compared the mean-field transfer matrix free energies of different phases to find the true phase for certain points in the phase diagram. We first calculated the global phase diagram and compared it with some reliable information. The result is confirmed strikingly well. Then, we applied this method to a more subtle point of the phase diagram, i.e. the existence of a Lifshitz point Δ_L at finite chirality. We first approximated the real Lifshitz point Δ_L assuming it exists by Lifshitz point $\Delta_L^\infty(N)$ in a finite strip mean-field transfer matrix system. Unfortunately, we cannot determine the Lifshitz point $\Delta_L^\infty(N)$ in the mean-field transfer matrix system directly, which requires the determination of the whole set of solutions of non-uniform mean-field parameters $\{\boldsymbol{\eta}_i\}$ to the mean-field transfer matrix equations. These $\{\Delta_L^l(N)\}$ are used to find an approximation for $\Delta_L^\infty(N)$ where l is the index to denote certain mean-field solutions. By systematically increasing the size of the mean-field system, the $\Delta_L^\infty(N)$ are found to become smaller. We can expect that $\Delta_L^\infty(N)$ will give Δ_L when the MFTM strip becomes infinitely wide. We see that $\Delta_L^\infty(N)$ decreases with N and it is possible that there is no Lifshitz point at finite chirality ($\Delta \neq 0$).

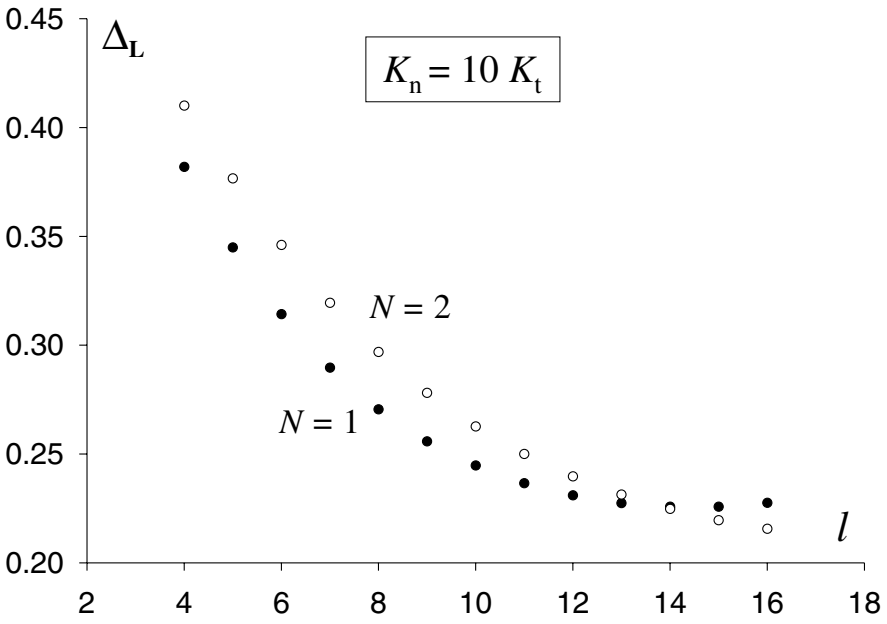

Figure 2.10. $\Delta_L^l(N)$ versus l with $K_n = 10K_t$ and strip width N. The minima are 0.2258 at $l = 14$ or 15 for $N = 1$ and 0.2156 at $l = 16$ for $N = 2$.

CHAPTER 3

MEAN FIELD STUDY OF THE PHASE DIAGRAM OF THE 3-STATE CHIRAL POTTS MODEL (II)

3.1 INTRODUCTION

In the previous chapter, we calculated mean-field transfer matrix (MFTM) free energies of various metastable states and compared these free energies to determine the approximate phase diagram of the 3-state chiral Potts model. In that calculation, we found that a Lifshitz point at finite chirality (Δ_L) is always present in the finite-strip calculation, but Δ_L becomes smaller when the width of the strip is increased. This may hint that the Lifshitz point at finite chirality is a finite-size effect as first pointed out by von Gehlen et al.[52]

In this chapter, we are going to continue our mean-field transfer matrix study of the problem of the Lifshitz point and the nature of the phase transition along the critical line between the IC floating solid phase (incommensurate) and the IC fluid phase (disorder), i.e. paramagnetic-incommensurate transitions. The coherent anomaly method (CAM)[55] will be used to analyze the critical behavior. The MFTM method[55] with Weiss-type[60] and Bethe-type[61] mean-field approximation will be used to construct the CAM series respectively.

In order to circumvent the difficulty of data analysis involving logarithmic correction, based on some reasonable assumption, we construct a new series to show that it is most likely that there is no direct transition from the IC fluid phase into the C solid phase, i.e. no Lifshitz point exists at finite chirality in this model and the phase transitions from the IC fluid phase into the IC floating solid phase are most likely of Kosterlitz–Thouless type.

The plan is as follows. In Section 3.2, the CAM theory is briefly reviewed. In Section 3.3, we describe the mean-field transfer matrix method putting mean fields on the boundary by Weiss-type and Bethe-type approximation respectively. We present a new series whose convergence is based on two other converging series in Section 3.4. In Section 3.5, we analyze the CAM series obtained by the two types of mean-field transfer matrix method. In Section 3.6, we analyze the characteristic wavevector of the correlation function at the critical point. A brief summary is given in Section 3.7.

3.2 CAM THEORY

The coherent anomaly method (CAM) has been introduced first by Suzuki in 1986.[55] It is based on the observation that as the degree of the approximation is increased, or as the approximate critical points approach the exact one, the residues of these classical singularities vary systematically and show a definite anomaly.

In this chapter we shall consider the susceptibility as an example. In the mean-field type theories, the susceptibility is always given by the Curie–Weiss form

$$\chi(T) \simeq \overline{\chi}(T_{\rm c})/(T - T_{\rm c}) \tag{3.1}$$

where $T_{\rm c}$ is the critical temperature and $\overline{\chi}(T_{\rm c})$ the amplitude of the singularity. No matter how good the mean-field type of approximation is, such an approximation can only give classical critical exponents. In CAM theory, a canonical series of approximations will be used instead. The approximating series is called canonical if the $T_{\rm c}$ of this series is convergent to the true critical point $T_{\rm c}^*$ of the original thermodynamical system. By systematically improving the approximation, such a series can be constructed. It is to be expected that $\overline{\chi}(T_{\rm c})$ encodes the information on the real susceptibility $\chi^*(T)$ of the system. Moreover, Suzuki has argued that the real susceptibility is well approximated by the envelope curve of curves defined by this set of approximations in $\chi - T$ space.

For the susceptibility to have the conventional power-law divergence, all of the $\overline{\chi}(T_{\rm c})$ should show the coherent anomalous behavior

$$\overline{\chi}(T_{\rm c}) \simeq f/(T_{\rm c} - T_{\rm c}^*)^{\psi} \qquad \text{as } T_{\rm c} \to T_{\rm c}^*. \tag{3.2}$$

The envelope curve of this set of curves will then be

$$\chi^*(T) = f\frac{(\psi+1)^{\psi+1}}{\psi^\psi}\frac{1}{(T-T_c^*)^{\psi+1}}. \tag{3.3}$$

So, the real critical exponent γ is found to be $\gamma = \psi + 1$ and the real susceptibility can be extrapolated from these mean-field results.[57] This idea has been generalized to Kosterlitz–Thouless phase transitions.[62,63] For a Kosterlitz–Thouless phase transition,[33,34] the susceptibility is expected to diverge exponentially[64,65], i.e.

$$\chi(T) \simeq \frac{f}{(T-T_c^*)^\psi}\exp\left(\frac{c}{(T-T_c^*)^\sigma}\right), \tag{3.4}$$

but the mean-field approximations still will be of the form

$$\chi^*(T) \simeq \overline{\chi}(T_c)/(T-T_c). \tag{3.5}$$

According to CAM theory, it should be expected that[62,66]

$$\overline{\chi}(T_c) \simeq \frac{f'}{(T-T_c^*)^{\psi-\sigma-1}}\exp\left(\frac{c}{(T_c-T_c^*)^\sigma}\right) \qquad \text{as } T_c \to T_c^*. \tag{3.6}$$

This has been checked for a two-dimensional ferromagnetic six-state clock model but the result is not very conclusive.[62]

For the conventional power-law divergent case, Suzuki[67] has also found that the coherent anomaly behavior of $\overline{\chi}(T_c)$ can be derived from Fisher's finite size scaling theory. See ref. 56 for a full review.

3.3 WEISS-TYPE AND BETHE-TYPE APPROXIMATION

Within an improved mean-field theory, there are two most important aspects that have to be paid serious attention to: The first one is how to treat fluctuations effectively in a finite (here finite-width strip) system and the second one is how to relate the effective fields on the boundary and the typical order parameters of the relevant finite (finite-width strip) system. These two aspects determine whether the approximate critical points obtained will be convergent to the true one and how fast the convergence will be. Currently, the two most-commonly used kinds of approximations are the Weiss approximation and the Bethe approximation. In this section,

we will show how the Weiss-type[60] and the Bethe-type[61] approximation can be applied in our case. We decouple the whole lattice into many identical strips, treat the interactions within strips exactly and put effective fields on the boundary and a small auxiliary modulated external field in the bulk to be determined by Weiss and Bethe approximation condition respectively. Although we will not give a rigorous proof of the validity of these approximations, they have been successfully applied in the Ising model and many other models.[56] Here we shall apply these approximations to the 3-state chiral Potts model.

We take the trial Hamiltonian of one strip in the disordered regime as follows:

$$\begin{aligned} -\beta H' &= -\beta H + K_t h \sum_j \sum_{i=1}^{N} \cos\Big(\frac{2\pi}{3} n_{i,j} - jq\Big) \\ &+ K_t \eta \sum_j \Big[\cos\Big(\frac{2\pi}{3} n_{1,j} - jq\Big) + \cos\Big(\frac{2\pi}{3} n_{N,j} - jq\Big)\Big] \end{aligned} \tag{3.7}$$

with

$$\begin{aligned} -\beta H &= \sum_j \Big[K_n \sum_{i=1}^{N} \cos\Big(\frac{2\pi}{3}(n_{i,j} - n_{i,j+1} + \Delta)\Big) \\ &+ K_t \sum_{i=1}^{N-1} \cos\Big(\frac{2\pi}{3}(n_{i,j} - n_{i+1,j})\Big)\Big], \end{aligned} \tag{3.8}$$

where η denotes the amplitude of the modulated effective boundary fields, h the amplitude of the auxiliary external bulk fields, and q the wavevector of the external field and modulated effective boundary fields along the chiral direction. Meanwhile, because most of the previous understanding has come from the study of the Hamiltonian limit, which corresponds to either $K_n/K_t \to 0$ or $K_n/K_t \to \infty$,[48,50–53] it is kind of natural for us to keep K_n/K_t general.

In the disordered phase and with a weak field condition, we can expect the response of the spin average to be characterized by the same wavevector q because of the symmetry of H and $H'|_{\eta=0,h=0}$ under translation. When we introduce our Weiss-type and Bethe-type mean-field approximations, the effective fields should be characterized by this wavevector q as well.

Since in all calculations below we take ensemble averages based on H' and often with both η and h being zero, we use $\langle\cdots\rangle$ to denote the statistical average with ensemble based on H' and $\langle\cdots\rangle_0$ to denote $\langle\cdots\rangle|_{\eta=0,h=0}$.

The average of a physical quantity Q can be calculated as

$$\langle Q\rangle = \sum_{\text{all states}} Q\exp(-\beta H')/\sum_{\text{all states}}\exp(-\beta H'). \tag{3.9}$$

Because here we are only interested in the critical phenomena of the system with vanishing external bulk fields, the effective bulk fields can be taken to be infinitesimal. Hence, we can make the following Taylor expansion about these fields:

$$\langle Q\rangle = \langle Q\rangle_0 + \left\langle\frac{\partial P}{\partial h}Q\right\rangle_0^{(\mathrm{c})} h + \left\langle\frac{\partial P}{\partial \eta}Q\right\rangle_0^{(\mathrm{c})}\eta + \cdots, \tag{3.10}$$

where we have used the notations $P = -\beta H'$ and $\langle AQ\rangle_0^{(\mathrm{c})} = \langle AQ\rangle_0 - \langle A\rangle_0\langle Q\rangle_0$, in which A can be $\partial P/\partial\eta$ or $\partial P/\partial h$. If Q is a spin-like quantity such as $\exp(\mathrm{i}2\pi n_{i,j}/3)$, from $\mathbb{Z}_3$ symmetry of the model, the term $\langle Q\rangle_0$ will vanish and $\langle AQ\rangle_0^{(\mathrm{c})} = \langle AQ\rangle_0$. For later notational convenience, we define quantities Q_{c}, $Q_{\partial,j}$, M_j and E_j as follows:

$$Q_{\mathrm{c}} = \begin{cases} \exp\left(\mathrm{i}\dfrac{2\pi}{3}n_{m+1,0}\right) & \text{if } N = 2m+1, \\ \dfrac{1}{2}\left[\exp\left(\mathrm{i}\dfrac{2\pi}{3}n_{m,0}\right) + \exp\left(\mathrm{i}\dfrac{2\pi}{3}n_{m+1,0}\right)\right] & \text{if } N = 2m, \end{cases} \tag{3.11}$$

$$Q_{\partial,j} = \frac{1}{2}\left[\exp\left(\mathrm{i}\frac{2\pi}{3}n_{1,j}\right) + \exp\left(\mathrm{i}\frac{2\pi}{3}n_{N,j}\right)\right], \tag{3.12}$$

$$M_j = \sum_{i=1}^{N}\exp\left(\mathrm{i}\frac{2\pi}{3}n_{i,j}\right), \tag{3.13}$$

$$E_j = K_n\sum_{i=1}^{N}\cos\left(\frac{2\pi}{3}(n_{i,j}-n_{i,j+1}+\Delta)\right) + K_t\sum_{i=1}^{N-1}\cos\left(\frac{2\pi}{3}(n_{i,j}-n_{i+1,j})\right). \tag{3.14}$$

These quantities have a direct interpretation: Q_{c} is the spin in the middle row of the 0-th column, if the number of rows N is odd; if the number of rows N is even we take the average over the two middle rows. $Q_{\partial,j}$ is the average of the two spins in the boundary rows $i = 1$ and $i = N$ of the j-th column ($j = -\infty, \cdots, \infty$). In addition,

$$P|_{h=\eta=0} = -\beta H'|_{h=\eta=0} = -\beta H = \sum_j E_j, \tag{3.15}$$

$$\left.\frac{\partial P}{\partial h}\right|_{h=\eta=0} = K_t\sum_j\frac{1}{2}\left(M_j\mathrm{e}^{-\mathrm{i}jq} + M_j^*\mathrm{e}^{\mathrm{i}jq}\right), \tag{3.16}$$

$$\left.\frac{\partial P}{\partial \eta}\right|_{h=\eta=0} = K_t\sum_j\left(Q_{\partial,j}\mathrm{e}^{-\mathrm{i}jq} + Q_{\partial,j}^*\mathrm{e}^{\mathrm{i}jq}\right). \tag{3.17}$$

This decomposition will be useful as we shall exploit the $\mathbb{Z}_3$ symmetry under the transformation $n_{i,j} \to n_{i,j} + 1$ for all i, j simultaneously in the high-temperature

disordered phase, which implies that

$$\left\langle \exp\left(\mathrm{i}\frac{2\pi}{3}n_{i,j}\right)\exp\left(\mathrm{i}\frac{2\pi}{3}n_{i',j'}\right)\right\rangle_0 = 0, \tag{3.18}$$

as the LHS would go to $\exp(\mathrm{i}4\pi/3)$ times itself.

3.3.1 WEISS-TYPE APPROXIMATION

In the Weiss-type approximation[60], we put the self-consistent condition as

$$\langle Q_\mathrm{c}\rangle = \eta. \tag{3.19}$$

From (3.10), we can rewrite this mean-field equation as

$$\left\langle Q_\mathrm{c}\frac{\partial P}{\partial h}\right\rangle_0 h = \left(1-\left\langle Q_\mathrm{c}\frac{\partial P}{\partial \eta}\right\rangle_0\right)\eta + \mathrm{O}(\eta^2). \tag{3.20}$$

The wavevector-dependent susceptibility is best approximated by the ratio of the order parameter $\langle Q_\mathrm{c}\rangle$ and the infinitesimal field h. Hence, it is given by

$$\chi_\mathrm{Weiss} = \frac{\langle Q_\mathrm{c}\rangle}{h} = \frac{\eta}{h} = \frac{\left\langle Q_\mathrm{c}\frac{\partial P}{\partial h}\right\rangle_0}{\left(1-\left\langle Q_\mathrm{c}\frac{\partial P}{\partial \eta}\right\rangle_0\right)}. \tag{3.21}$$

This wavevector-dependent susceptibility has a peak located at q_m which gives an approximation to the characteristic wavevector of the corresponding correlation function. Eq. (3.21) is valid only when the system is in the disordered phase. In the disordered phase, the peak of the wavevector-dependent susceptibility is finite, which means

$$\min_q\left(1-\left\langle Q_\mathrm{c}\frac{\partial P}{\partial \eta}\right\rangle_0\right) > 0. \tag{3.22}$$

When the system changes from the disordered phase into the incommensurate phase as the temperature is lowered, the peak of the wavevector-dependent susceptibility also changes into a divergence. Hence, the critical point that demarcates the paramagnetic-incommensurate phase transition can be located from

$$\min_q\left(1-\left\langle Q_\mathrm{c}\frac{\partial P}{\partial \eta}\right\rangle_0\right) = 0. \tag{3.23}$$

This can be written, using the $\mathbb{Z}_3$ symmetry (3.18) as

$$\min_q \left(1 - K_{\rm c} \sum_j \langle Q_{\rm c} Q^*_{\partial,j} \rangle \exp({\rm i}jq) \right) = 0 \tag{3.24}$$

where the minimum condition is over all q. The corresponding $q_{\rm m}$ will give an approximation to the wavevector $q_{\rm c}$, characteristic of the correlation function at the phase transition point. Here and in the following we write $K \equiv K_t$ and $K_{\rm c} \equiv K_{tc}$, its value at the critical point separating the disordered and modulated phases. K_n and K_t vary proportionally. Below, we shall most often fix $K_n = K_t$, $K_n = 10K_t$, or $K_n = 100K_t$.

The susceptibility near this critical point ($K < K_{\rm c}$) is

$$\chi_{\rm Weiss} = \left. \frac{\left\langle Q_{\rm c} \dfrac{\partial P}{\partial h} \right\rangle_0}{K_{\rm c} \dfrac{d}{dK} \left\langle Q_{\rm c} \dfrac{\partial P}{\partial \eta} \right\rangle_0} \right|_{K=K_{\rm c}} \frac{1}{\dfrac{K_{\rm c}}{K} - 1}. \tag{3.25}$$

The coherent anomaly amplitude is worked out as

$$\begin{aligned}
\overline{\chi}_{\rm Weiss} &= \left. \frac{\left\langle Q_{\rm c} \dfrac{\partial P}{\partial h} \right\rangle_0}{K_{\rm c} \dfrac{d}{dK} \left\langle Q_{\rm c} \dfrac{\partial P}{\partial \eta} \right\rangle_0} \right|_{K=K_{\rm c}} \\
&= \left. \frac{\left\langle Q_{\rm c} \dfrac{\partial P}{\partial h} \right\rangle_0}{1 + K_{\rm c} \left(\left\langle Q_{\rm c} \dfrac{\partial P}{\partial \eta} \dfrac{\partial P}{\partial K} \right\rangle_0 - \left\langle Q_{\rm c} \dfrac{\partial P}{\partial \eta} \right\rangle_0 \left\langle \dfrac{\partial P}{\partial K} \right\rangle_0 \right)} \right|_{K=K_{\rm c}} \\
&= \left. \frac{\displaystyle\sum_j \langle Q_{\rm c} M^*_j \rangle \exp({\rm i}jq_{\rm m})}{2 \left(\dfrac{1}{K_{\rm c}} + \displaystyle\sum_{i,j} \left(\langle Q_{\rm c} Q^*_{\partial,j} E_i \rangle - \langle Q_{\rm c} Q^*_{\partial,j} \rangle \langle E_i \rangle \right) \exp({\rm i}jq_{\rm m}) \right)} \right|_{K=K_{\rm c}},
\end{aligned} \tag{3.26}$$

where we again have used the $\mathbb{Z}_3$ symmetry (3.18), and the susceptibility can be rewritten as

$$\chi_{\rm Weiss} = \frac{\overline{\chi}_{\rm Weiss}}{\dfrac{K_{\rm c}}{K} - 1}. \tag{3.27}$$

3.3.2 BETHE-TYPE APPROXIMATION

In the Bethe-type approximation, we have to put the self-consistent condition as

$$\langle Q_{\rm c} \rangle = \langle Q_{\partial,0} \rangle. \tag{3.28}$$

The mean-field equation can now be written as

$$\begin{aligned}&\left(\left\langle Q_{\rm c}\frac{\partial P}{\partial h}\right\rangle_0-\left\langle Q_{\partial,0}\frac{\partial P}{\partial h}\right\rangle_0\right)h\\ =\;&\left(\left\langle Q_{\partial,0}\frac{\partial P}{\partial \eta}\right\rangle_0-\left\langle Q_{\rm c}\frac{\partial P}{\partial \eta}\right\rangle_0\right)\eta+{\rm O}(\eta^2)+{\rm O}(h^2),\end{aligned}\tag{3.29}$$

and the wavevector-dependent susceptibility can be given as

$$\begin{aligned}\chi_{\rm Bethe}&=\left\langle Q_{\rm c}\frac{\partial P}{\partial h}\right\rangle_0+\left\langle Q_{\rm c}\frac{\partial P}{\partial \eta}\right\rangle_0\frac{\eta}{h}\\ &=\left\langle Q_{\rm c}\frac{\partial P}{\partial h}\right\rangle_0+\left\langle Q_{\rm c}\frac{\partial P}{\partial \eta}\right\rangle_0\frac{\left(\left\langle Q_{\rm c}\frac{\partial P}{\partial h}\right\rangle_0-\left\langle Q_{\partial,0}\frac{\partial P}{\partial h}\right\rangle_0\right)}{\left(\left\langle Q_{\partial,0}\frac{\partial P}{\partial \eta}\right\rangle_0-\left\langle Q_{\rm c}\frac{\partial P}{\partial \eta}\right\rangle_0\right)}.\end{aligned}\tag{3.30}$$

Similarly as in the Weiss approximation case, the paramagnetic-incommensurate phase transition point is determined by

$$\min_q\left(\left\langle Q_{\partial,0}\frac{\partial P}{\partial \eta}\right\rangle_0-\left\langle Q_{\rm c}\frac{\partial P}{\partial \eta}\right\rangle_0\right)=0.\tag{3.31}$$

Again using the $\mathbb{Z}_3$ symmetry (3.18), this can be written as

$$\min_q\sum_j\left(\langle Q_{\partial,0}Q^*_{\partial,j}\rangle-\langle Q_{\rm c}Q^*_{\partial,j}\rangle\right)\exp({\rm i}jq)=0,\tag{3.32}$$

where the minimum condition is taking over all q, and the corresponding $q_{\rm m}$ will give the approximation of the wavevector $q_{\rm c}$ at the phase transition point. The susceptibility near $K_{\rm c}$ ($K<K_{\rm c}$) is

$$\chi_{\rm Bethe}=\left.\frac{\left\langle Q_{\rm c}\frac{\partial P}{\partial \eta}\right\rangle_0\left(\left\langle Q_{\partial,0}\frac{\partial P}{\partial h}\right\rangle_0-\left\langle Q_{\rm c}\frac{\partial P}{\partial h}\right\rangle_0\right)}{K_{\rm c}\frac{d}{dK}\left(\left\langle Q_{\rm c}\frac{\partial P}{\partial \eta}\right\rangle_0-\left\langle Q_{\partial,0}\frac{\partial P}{\partial \eta}\right\rangle_0\right)}\right|_{K=K_{\rm c}}\frac{1}{\frac{K_{\rm c}}{K}-1}.\tag{3.33}$$

The coherent anomaly coefficient is

$$\begin{aligned}\overline{\chi}_{\rm Bethe}&=\left.\frac{\left\langle Q_{\rm c}\frac{\partial P}{\partial \eta}\right\rangle_0\left(\left\langle Q_{\partial,0}\frac{\partial P}{\partial h}\right\rangle_0-\left\langle Q_{\rm c}\frac{\partial P}{\partial h}\right\rangle_0\right)}{K_{\rm c}\frac{d}{dK}\left(\left\langle Q_{\rm c}\frac{\partial P}{\partial \eta}\right\rangle_0-\left\langle Q_{\partial,0}\frac{\partial P}{\partial \eta}\right\rangle_0\right)}\right|_{K=K_{\rm c}}\\ &=\left.\frac{\left\langle Q_{\rm c}\frac{\partial P}{\partial \eta}\right\rangle_0\left(\left\langle Q_{\rm c}\frac{\partial P}{\partial h}\right\rangle_0-\left\langle Q_{\partial,0}\frac{\partial P}{\partial h}\right\rangle_0\right)\Big/K_{\rm c}}{\left\langle Q_{\rm c}\frac{\partial P}{\partial \eta}\frac{\partial P}{\partial K}\right\rangle_0-\left\langle Q_{\rm c}\frac{\partial P}{\partial \eta}\right\rangle_0\left\langle\frac{\partial P}{\partial K}\right\rangle_0-\left\langle Q_{\partial,0}\frac{\partial P}{\partial \eta}\frac{\partial P}{\partial K}\right\rangle_0+\left\langle Q_{\partial,0}\frac{\partial P}{\partial \eta}\right\rangle_0\left\langle\frac{\partial P}{\partial K}\right\rangle_0}\right|_{K=K_{\rm c}}\\ &=\left.\frac{K_{\rm c}\sum_k\langle Q_{\rm c}Q^*_{\partial,k}\rangle\exp({\rm i}kq_{\rm m})\sum_j\left(\langle Q_{\rm c}M^*_j\rangle_0-\langle Q_{\partial,0}M^*_j\rangle_0\right)\exp({\rm i}jq_{\rm m})/2}{\sum_{i,j}\left(\langle Q_{\rm c}Q^*_{\partial,j}E_i\rangle^{(c)}-\langle Q_{\partial,0}Q^*_{\partial,j}E_i\rangle^{(c)}\right)\exp({\rm i}jq_{\rm m})}\right|_{K=K_{\rm c}},\end{aligned}\tag{3.34}$$

where we have used the $\mathbb{Z}_3$ symmetry (3.18) and

$$\langle Q_{\rm c} Q^*_{\partial,j} E_i \rangle^{(c)} = \langle Q_{\rm c} Q^*_{\partial,j} E_i \rangle - \langle Q_{\rm c} Q^*_{\partial,j} \rangle \langle E_i \rangle \tag{3.35}$$

and

$$\langle Q_{\partial,0} Q^*_{\partial,j} E_i \rangle^{(c)} = \langle Q_{\partial,0} Q^*_{\partial,j} E_i \rangle - \langle Q_{\partial,0} Q^*_{\partial,j} \rangle \langle E_i \rangle, \tag{3.36}$$

and the susceptibility can be rewritten as

$$\chi_{\rm Bethe} = \frac{\overline{\chi}_{\rm Bethe}}{\dfrac{K_{\rm c}}{K} - 1}. \tag{3.37}$$

Within the Weiss approximation, we calculated numerically cases with widths $N = 2,\ 3,\ 4,\ 5,\ 6,\ 7$. But within the Bethe approximation, we only have dealt with cases with widths $N = 3,\ 4,\ 5,\ 6,\ 7$. For this calculation, a huge memory is required. To save memory and accelerate the speed, we use a $\mathbb{Z}_3$ invariant basis set.* To solve the mean-field equations and to evaluate the expressions for the coherent anomaly coefficients, three- and four-spin correlations will be involved. By tedious but straightforward algebraic calculation, we can get these expressions of three- and four-spin correlation in this new basis set. We will not present the details here. The resulting numerical values and their coherent anomaly analysis will be given in the next sections.

3.4 NEW EXTRAPOLATION METHOD

If there exist two sequences $\{a(n)\}$ and $\{b(n)\}$, which satisfy
i) $\lim_{n\to\infty} a(n) = c$, $\lim_{n\to\infty} b(n) = c$ and $a(n),\ b(n) \neq c$ for any n,
ii) $\lim_{n\to\infty} \left(a(n+\delta n) - a(n)\right) / \left(b(n+\delta n) - b(n)\right)$ exists and is not 1,
it is possible to construct a third sequence $\{c(n)\}$ with $\lim_{n\to\infty} c(n) = c$ by

$$c(n) = \frac{a(n+\delta n)b(n) - a(n)b(n+\delta n)}{a(n+\delta n) - a(n) - b(n+\delta n) + b(n)}. \tag{3.38}$$

*Indeed, the reflection invariance along the non-chiral direction can be used to reduce the memory requirement even further. But for the computing resources available to us, this reduction is not enough for us to get to larger strips even with width $N = 8$.

Under certain conditions, we can expect that the sequence $\{c(n)\}$ will converge faster than either $\{a(n)\}$ or $\{b(n)\}$. To prove the convergence of the third sequence, let

$$r_1(n) \equiv \frac{a(n+\delta n) - a(n)}{b(n+\delta n) - b(n)}$$

and

$$r_2(n) \equiv \frac{a(n+\delta n) - c}{b(n+\delta n) - c}.$$

It is obvious that $\{r_1(n)\}$ and $\{r_2(n)\}$ will both converge to the same limit. If we define sequence $\{d(n)\}$ by

$$r_1(n) \equiv \frac{a(n+\delta n) - d(n)}{b(n+\delta n) - d(n)},$$

through simple algebraic calculation, we find that $d(n) = c(n)$ for each n and so we can conclude that sequence $\{c(n)\}$ will converge to c.

Now let us check how fast the convergence of sequence $\{c(n)\}$ will be. For our purpose, we consider two cases.

Case 1: Let us assume

$$a(n) = c + (a_1 n + a_2 \ln n)^{-1/\nu} \tag{3.39}$$

and

$$b(n) = c + (b_1 n + b_2 \ln n)^{-1/\nu}. \tag{3.40}$$

Then, using (3.39) and (3.40) for n large enough, we can formally take $\delta n \to 0$ and

$$\delta c(n) = \frac{a(n+\delta n)b(n) - a(n)b(n+\delta n)}{a(n+\delta n) - a(n) - b(n+\delta n) + b(n)} - c \tag{3.41}$$

$$= \frac{\delta a(n)\delta b(n)(a_1 b_2 - a_2 b_1)(n \ln n - n)}{\delta a(n)(a_1 n + a_2)(b_1 n + b_2 \ln n) - \delta b(n)(b_1 n + b_2)(a_1 n + a_2 \ln n)}, \tag{3.42}$$

where $\delta a(n) = a(n) - c$, and similarly for $\delta b(n)$ and $\delta c(n)$. For n large enough, we have

$$\delta c(n) \sim \left(\frac{a_2}{a_1} - \frac{b_2}{b_1}\right) \frac{\delta a(n)\delta b(n)}{\max(|\delta a(n)|, |\delta b(n)|)} \frac{\ln n}{n}. \tag{3.43}$$

Case 2: Let us assume

$$a(n) = c + (a_1 \ln n/n + a_2/n)^{1/\nu} \tag{3.44}$$

and

$$b(n) = c + (b_1 \ln n/n + b_2/n)^{1/\nu}. \tag{3.45}$$

Then, similarly, we have

$$\delta c(n) = \frac{\delta a(n)\delta b(n)(a_2 b_1 - a_1 b_2)(n \ln n - n)}{\delta a(n)(a_1 \ln n - a_1 + a_2)(b_1 \ln n + b_2) - \delta b(n)(b_1 \ln n - b_1 + b_2)(a_1 \ln n + a_2)} \tag{3.46}$$

and

$$\delta c(n) \sim \left(\frac{a_2}{a_1} - \frac{b_2}{b_1}\right) \frac{\delta a(n)\delta b(n)}{\max(|\delta a(n)|, |\delta b(n)|)} \frac{1}{\ln^2 n}. \tag{3.47}$$

From the above two cases, we find that the new sequence may converge much faster than the original ones for n large enough. More interestingly, the new sequence may approach the limit from below monotonically even both of the original sequences approach the limit from above because of the factor $(a_2/a_1 - b_2/b_1)$. In physical problems, it is difficult to get $a(n)$ and $b(n)$ for large n, but in practice the condition can be much looser, as it is often found that the scaling behavior is quite good even for small n. For the new extrapolation method to be reasonable, it is necessary that $a(n)$ and $b(n)$ are dominated by the first three terms in the large-n asymptotic expansion and that $|a(n + \delta n) - a(n)|$ is larger than $|b(n + \delta n) - b(n)|$ if $|\delta a(n)|$ is larger than $|\delta b(n)|$ or vice versa.

We use the square lattice Ising model and rectangular Potts models to see how well the results will be in this new construction.

Hu et al.[57] obtained approximate critical temperatures for the square lattice Ising model using the MFTM method. We present their results in Table 3.1. From Table 3.1 and comparing with the exact value 2.269, we clearly see that the new sequence $T_{\rm n}(N)$ is much closer to the exact value and converges in the right direction.

In the rectangular Potts model ($\Delta = 0$) with $K_n = rK_t$ and r a constant, the critical temperature is exactly known. We now compare the exact critical temperatures with $T_{\rm b}(N)$ the one obtained by Bethe approximation, $T_{\rm w}(N)$ by Weiss approximation and $T_{\rm n}(N)$ by the new construction (3.38) with $\delta N = 2$ from $T_{\rm b}(N)$ and $T_{\rm w}(N)$. From Table 3.2 for $K_n = K_t$, Table 3.3 for $K_n = 10K_t$, and Table 3.4 for $K_n = 100K_t$, we see that even with such short sequences, Eq. (3.38) can give a much better convergence than the original sequences.

N	3	5	7
$T_{\rm b}$	2.5719	2.4852	2.4396
$T_{\rm w}$	2.9221	2.7285	2.6294
$T_{\rm n}$	2.287	2.278	

TABLE 3.1. Table of $T_{\rm b}$, $T_{\rm w}$ and $T_{\rm n}$ for the square lattice Ising model. Critical temperature $T_{\rm b}(N)$ is obtained by the Bethe-type approximation and $T_{\rm w}(N)$ by the Weiss-type approximation where N is the width of the finite strip. $T_{\rm n}(N)$ is obtained by Eq. (3.38) with $\delta N = 2$. The exact value $T_{\rm c}^* = 2.269$.

N	3	4	5	6	7
$T_{\rm b}$	1.56208	1.55004	1.54073	1.53471	1.52965
$T_{\rm w}$	1.65702	1.62624	1.60251	1.58794	1.57563
$T_{\rm n}$	1.5010	1.4992	1.4974		

TABLE 3.2. Table of $T_{\rm b}$, $T_{\rm w}$ and $T_{\rm n}$ for the model with $\Delta = 0$ and $K_n = K_t$. Critical temperature $T_{\rm b}(N)$ is obtained by Bethe-type approximation, $T_{\rm w}(N)$ by Weiss-type approximation, where N is the width of the finite strip, and $T_{\rm n}(N)$ is obtained by (3.38) with $\delta N = 2$. The exact value $T_{\rm c}^* = 1.4925$.

N	3	4	5	6	7
$T_{\rm b}$	6.25082	6.22099	6.19836	6.18422	6.17242
$T_{\rm w}$	6.38835	6.33589	6.29469	6.26873	6.24660
$T_{\rm n}$	6.0757	6.0820	6.0855		

TABLE 3.3. Table of $T_{\rm b}$, $T_{\rm w}$ and $T_{\rm n}$ for the model with $\Delta = 0$ and $K_n = 10K_t$. Critical temperature $T_{\rm b}(N)$ is obtained by Bethe-type approximation, $T_{\rm w}(N)$ by Weiss-type approximation, where N is the width of the finite strip, and $T_{\rm n}(N)$ is obtained by (3.38) with $\delta N = 2$. The exact value $T_{\rm c}^* = 6.0899$.

N	3	4	5	6	7
$T_{\rm b}$	35.8934	35.7828	35.6987	35.6462	35.6023
$T_{\rm w}$	36.3812	36.1933	36.0449	35.9508	35.8706
$T_{\rm n}$	35.223	35.253	35.270		

TABLE 3.4. Table of $T_{\rm b}$, $T_{\rm w}$ and $T_{\rm n}$ for the model with $\Delta = 0$ and $K_n = 100K_t$. Critical temperature $T_{\rm b}(N)$ is obtained by Bethe-type approximation, $T_{\rm w}(N)$ by Weiss-type approximation, where N is the width of the finite strip, and $T_{\rm n}(N)$ is obtained by (3.38) with $\delta N = 2$. The exact value $T_{\rm c}^* = 35.2947$.

We have used $\delta N = 2$ above and also will use it later because the quantity defined in (3.11) in this chapter behaves differently for strips with even width and strips with odd width.

Now let us look at the critical point for $\Delta = 0.50$. The results are shown in Table 3.5 for $K_n = K_t$, Table 3.6 for $K_n = 10K_t$, and Table 3.7 for $K_n = 100K_t$. For $\Delta = 1/2$, Kinzel et al.[42] suggest that the critical point occurs at

$$(\mathrm{e}^{3K_t/2} - 1)(\mathrm{e}^{-3K_n/2} + 1) = 3. \tag{3.48}$$

From Tables 3.5, 3.6 and 3.7, we see that the mean-field transfer matrix results agree qualitatively with (3.48), i.e. in the dependence of $T_{\rm c}$ on K_n/K_t. Both results show that $T_{\rm c}$ increases with K_n/K_t and, when $K_n/K_t \gg 1$, $T_{\rm c}$ shows a very tiny dependence on it. But the mean-field transfer matrix results would suggest a much lower $T_{\rm c}$ than the prediction from (3.48).

3.5 CAM ANALYSIS

The susceptibility of the classical two-dimensional XY model satisfies the form (3.4). This only can be applied as such to the case where there is no oscillating factor in the spin-spin correlation functions. In the 3-state chiral Potts model, there is an oscillating factor in the spin-spin correlation function along chiral direction. Therefore, instead of the usual susceptibility, we should introduce the wavevector-dependent susceptibility as we already did in section 3.3. The divergent quantity

N	3	4	5	6	7
T_{b}	1.13291	1.08831	1.05195	1.02848	1.00791
T_{w}	1.35789	1.29641	1.24498	1.21142	1.18112
T_{n}	0.5628	0.5935	0.6230		

TABLE 3.5. Table of T_{b}, T_{w} and T_{n} for the model with $\Delta = 1/2$ and $K_n = K_t$. Critical temperature $T_{\mathrm{b}}(N)$ is obtained by Bethe-type approximation, $T_{\mathrm{n}}(N)$ by Weiss-type approximation, where N is the width of the finite strip, and $T_{\mathrm{n}}(N)$ is obtained by (3.38) with $\delta N = 2$.

N	3	4	5	6	7
T_{b}	1.50367	1.44230	1.39189	1.35556	1.32355
T_{w}	2.17384	2.02249	1.89716	1.81757	1.74622
T_{n}	1.0494	1.0164	0.9738		

TABLE 3.6. Table of T_{b}, T_{w} and T_{n} for the model with $\Delta = 1/2$ and $K_n = 10K_t$. Critical temperature $T_{\mathrm{b}}(N)$ is obtained by Bethe-type approximation, $T_{\mathrm{w}}(N)$ by Weiss-type approximation, where N is the width of the finite strip, and $T_{\mathrm{n}}(N)$ is obtained by (3.38) with $\delta N = 2$.

N	3	4	5	6	7
T_{b}	1.50374	1.44235	1.39192	1.35558	1.32358
T_{w}	2.17792	2.02472	1.89842	1.81841	1.74679
T_{n}	1.0542	1.0196	0.9763		

TABLE 3.7. Table of T_{b}, T_{w} and T_{n} for the model with $\Delta = 1/2$ and $K_n = 100K_t$. Critical temperature $T_{\mathrm{b}}(N)$ is obtained by Bethe-type approximation, $T_{\mathrm{w}}(N)$ by Weiss-type approximation, where N is the width of the finite strip, and $T_{\mathrm{n}}(N)$ is obtained by (3.38) with $\delta N = 2$.

should be the wavevector-dependent susceptibility in the incommensurate phases. Let us define the quantity more precisely before studying its coherent anomaly behavior. We assume that the spin-spin correlation function can be written as

$$\Big\langle \exp\Big(\mathrm{i}\frac{2\pi}{3}n_{0,0}\Big)\exp\Big(-\mathrm{i}\frac{2\pi}{3}n_{j,k}\Big)\Big\rangle = C(j,k,T)\exp\Big(-\mathrm{i}kq(T)\Big), \tag{3.49}$$

where $C(j,k,T)$ is a function without oscillation. Hence, we can define the wavevector-dependent susceptibility by

$$k_{\mathrm{B}}T\chi(q_t,q_n,T) = \sum_{i,j}\Big\langle \exp\Big(\mathrm{i}\frac{2\pi}{3}n_{0,0}\Big)\exp\Big(-\mathrm{i}\frac{2\pi}{3}n_{j,k}\Big)\Big\rangle \exp\Big(\mathrm{i}(jq_t+kq_n)\Big). \tag{3.50}$$

In the non-chiral case, with $q(T)=0$, we know that $\chi(0,0,T)$ diverges at $T=T_{\mathrm{c}}$ and $\chi(q_t,q_n,T)$ is finite for $q_t,q_n\neq 0$. It is then easily seen that in the chiral case, with chiral field in one direction $\chi(q_t,q_n,T)$ diverges at $q_n=q(T)$, $q_t=0$ and $T=T_{\mathrm{c}}(\Delta)$ where $q(T)$ is defined in (3.49). Therefore, we denote

$$\chi_q(T) = \chi(0,q(T),T). \tag{3.51}$$

If the correlation functions decay algebraically in the incommensurate phase, then $\chi_q(T)$ is divergent there. We expect it to diverge exponentially at the paramagnetic-incommensurate transitions if these phase transitions are of Kosterlitz–Thouless type. We can verify that the mean-field transfer matrix formalism (χ_{Bethe} and χ_{Weiss}) of section 3.3 is still applicable to $\chi_q(T)$, i.e.

$$\chi_q(T) = \frac{\overline{\chi}_q(T_{\mathrm{c}})}{\dfrac{K_{\mathrm{c}}}{K}-1} \tag{3.52}$$

with $\overline{\chi}_q(T_{\mathrm{c}}) = \overline{\chi}_{\mathrm{Bethe}}$ in Bethe approximation and $\overline{\chi}_q(T_{\mathrm{c}}) = \overline{\chi}_{\mathrm{Weiss}}$ in Weiss approximation.

According to the CAM theory, we expect that

$$\overline{\chi}_q(T_{\mathrm{c}}) \simeq f'\exp\left(\frac{c}{(T_{\mathrm{c}}-T_{\mathrm{c}}^*)^{\sigma}}\right) \qquad \text{as } T_{\mathrm{c}}\to T_{\mathrm{c}}^*, \tag{3.53}$$

where we ignore the prefactor $(T-T_{\mathrm{c}}^*)^{\sigma-\psi+1}$ which appears in (3.6). We will comment on the effects of neglecting this prefactor when we try exponential fittings later on.

3.5.1 CAM TEST FOR $\Delta = 0$

Before applying the above theories to the case with general Δ, we shall first test how they work at the point $\Delta = 0$.

The model at $\Delta = 0$ is equivalent to the (scalar) Potts model and both its critical temperature and its susceptibility exponent for general K_n/K_t are known.[68] It provides a good testing ground to see how well the CAM applies to the chiral Potts model and how K_n/K_t affects the convergence of the approximation. We have checked the critical temperatures approximated by our new construction (3.38) in the last section and found it to work very well.

Critical temperatures obtained by Weiss-type approximation are shown in Fig. 3.1 and by Bethe-type approximation in Fig. 3.2, for three different values of K_n/K_t at $\Delta = 0$. Both figures show good convergence of $t_c \to 0$ when $N \to \infty$, where $t_c = (T_c - T_c^*)/T_c^*$.

We use the exact critical temperatures and leave the exponents γ as fitting parameters, see (3.54) in the next section. We plot $\ln(T_c/T_c^* - 1)$ along the x-axis versus $\ln \overline{\chi}(T_c)$ along the y-axis. The slopes are expected to give the values of $1 - \gamma$. These CAM fits are presented in Fig. 3.3 for $K_n = K_t$, in Fig. 3.4 for $K_n = 10K_t$, and in Fig. 3.5 for $K_n = 100K_t$. From Figs. 3.3, 3.4 and 3.5, we get reasonable values for $1 - \gamma$ compared with the exact value of $-4/9$. It looks that both Weiss-type and Bethe-type approximations give reasonable exponents.

Meanwhile, since the exact critical temperatures for general Δ are not known, we also try fitting by leaving the critical temperature as one of the fitting parameters but requiring that both Bethe-type and Weiss-type approximations give the same extrapolated critical temperature and close exponents. These fits give critical temperature $T_c^* = 1.5015$ and $1-\gamma = -0.3655$ for $K_n = K_t$, $T_c^* = 6.1003$ and $1-\gamma = -0.4105$ for $K_n = 10K_t$, and $T_c^* = 35.316$ and $1 - \gamma = -0.4362$ for $K_n = 100K_t$. Compared with the exact information, these fits give both reasonable approximations for critical temperatures and critical exponents.

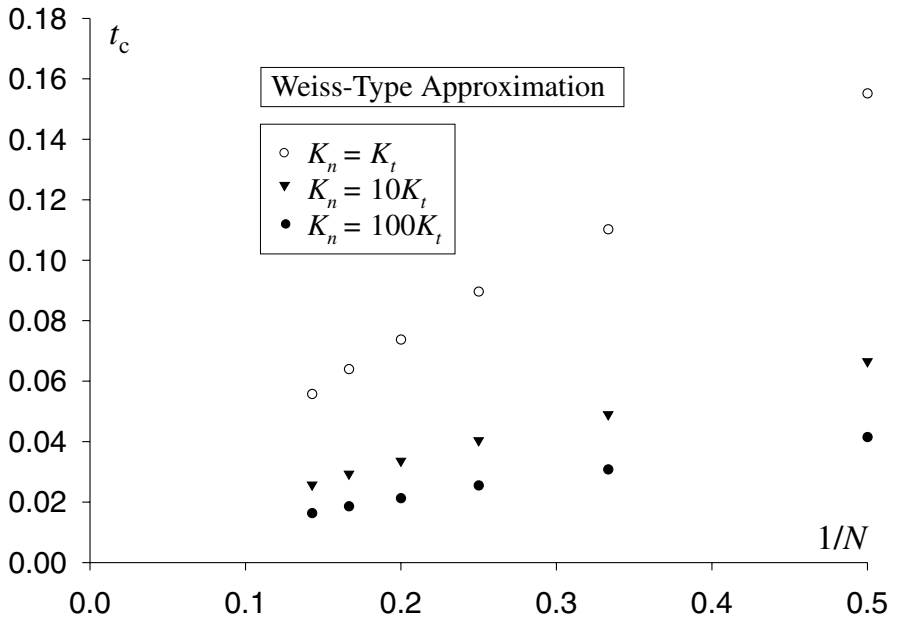

Figure 3.1. Critical temperature shift t_c versus $1/N$ for Potts model, where $t_c = (T_c - T_c^*)/T_c^*$ and N is the width of strip in Weiss-type MFTM method.

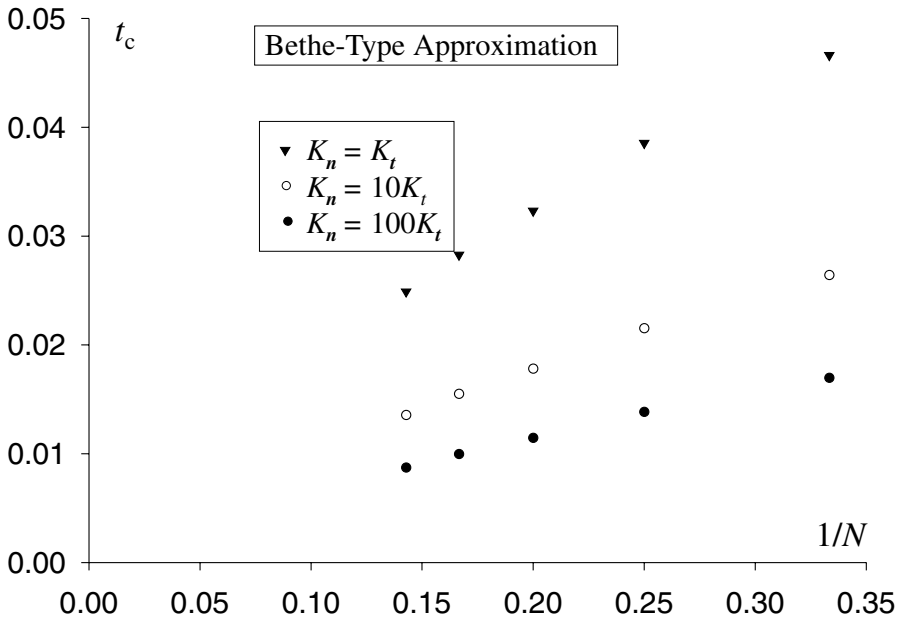

Figure 3.2. Critical temperature shift t_c versus $1/N$ for Potts model, where $t_c = (T_c - T_c^*)/T_c^*$ and N is the width of strip in Bethe-type MFTM method.

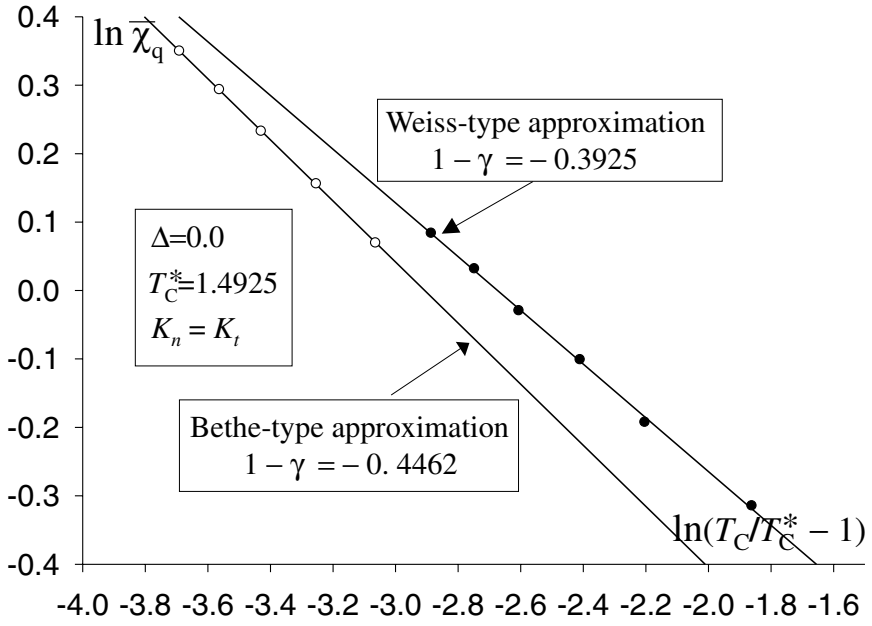

Figure 3.3. Power-law fits of the CAM for the case $K_n = K_t$ and $\Delta = 0$.

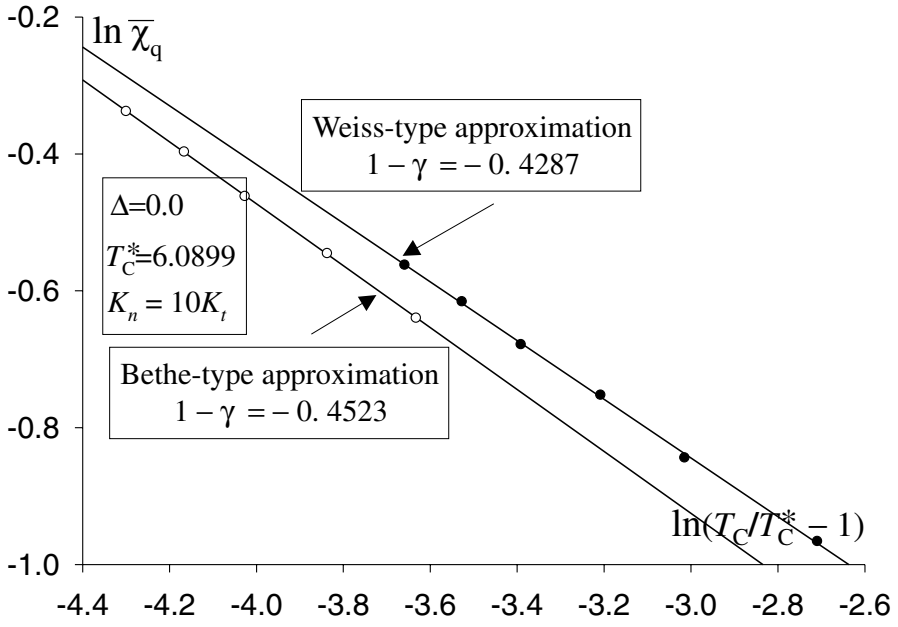

Figure 3.4. Power-law fits of the CAM for the case $K_n = 10K_t$ and $\Delta = 0$.

It seems that the larger values of K_n/K_t give better approximations of both the critical temperature and the critical exponent. One possible explanation of better behavior for larger K_n/K_t is that increasing the value K_n/K_t will increase the correlation length along the chiral direction but reduce the correlation length along the non-chiral direction and the bulk behavior possibly depends on the ratio of the width of the finite strip and the correlation length along the finite direction in the mean-field transfer matrix method.

We might convince ourselves that a power law gives a better fit than exponential fitting for the coherent anomaly coefficients of the susceptibility because it is known to be power-law divergent at this point. However, the plots show almost the same good fit for an exponential form with a small exponent σ and lower extrapolated T_c^* in (3.55). One has to conclude that additional information is necessary to decide which CAM extrapolation scheme to use.

3.5.2 CAM ANALYSIS FOR GENERAL Δ

In this section, we try to fit the data to the power-law form

$$\ln \overline{\chi}_q(T_c) = A + (1-\gamma)\ln(T_c/T_c^* - 1) \tag{3.54}$$

and also the exponential form

$$\ln \overline{\chi}_q(T_c) = A(T_c/T_c^* - 1)^{-\sigma} + B \tag{3.55}$$

for general Δ, where T_c^* is the extrapolated critical temperature, T_c is the finite strip result, and both A and B are fitting parameters.

The power-law fit (3.54) comes from the assumption $\chi_q(T) \propto (T/T_c^* - 1)^{-\gamma}$. Using this, we fit six points (Weiss-type) or five points (Bethe-type) with three parameters, i.e. A, T_c^* and γ. We plot $\ln(T_c/T_c^* - 1)$ along the x-axis versus $\ln \overline{\chi}_q(T_c)$ along the y-axis. The slopes are expected to give the values of $1-\gamma$. We use least-squares fit to a straight line by trying different T_c^* and require the deviation to be less than 3%. We also require both Weiss-type and Bethe-type approximations giving maximal consistency, i.e. that their fits give the same extrapolated critical temperature T_c^* and close critical exponents γ. These fits are presented in Figs. 3.6 and 3.7

for the case of $K_n = 100K_t$. We find that γ increases from 1.4 ± 0.1 at $\Delta = 0$ to about 2.3 ± 0.2 at $\Delta = 0.5$ using this power-law fitting method. We also find that γ for different K_n/K_t are almost the same when $\Delta = 0$, $\Delta = 1/2$ or very small Δ, with only differences within fitting errors. When Δ is large but smaller than $1/2$, we can clearly see the difference of γ for different K_n/K_t. For example, when $\Delta = 0.45$, $\gamma = 2.1 \pm 0.2$ for $K_n/K_t = 1$, $\gamma = 1.65 \pm 0.1$ for $K_n/K_t = 10$ and $\gamma = 1.6 \pm 0.1$ for $K_n/K_t = 100$.

The exponential fit (3.55) comes from the assumption (3.53). Using this formula, we fit six points (Weiss-type) or five points (Bethe-type) with four parameters i.e. A, B, $T_{\rm c}^*$ and σ. We plot $(T_{\rm c}/T_{\rm c}^* - 1)^{-\sigma}$ versus $\ln \overline{\chi}_q(T_{\rm c})$. To find the best fits for this form, we have to try various $T_{\rm c}^*$ and σ with the same accuracy as in the power-law fitting case. We also require both Weiss-type and Bethe-type approximations giving the same extrapolated critical temperature $T_{\rm c}^*$, close exponents σ and close B's. These fits are presented in Figs 3.8 and 3.9 for the case of $K_n = 100K_t$. We find that σ is close to zero for small Δ and about 0.45 ± 0.1 for $\Delta > 0.40$ giving the best fit. For larger Δ, the exponent σ is comparable with the exponent $\sigma = 1/2$ given in the XY model. We also find that the exponents for different K_n/K_t are almost the same in these exponential fits, with only differences within fitting errors.

We also have tried to include the prefactor $(T - T_{\rm c}^*)^{\sigma-\psi+1}$ in our exponential fitting form with ψ from 0 to 1. The inclusion of this prefactor will give a small increase of the exponent σ for small Δ and the resulting extrapolated critical temperature will lie between the one given by power-law fitting and the other given by exponential fitting. This is understandable because the original data of the coherent anomaly coefficients fit both the power-law form and the exponential form very well.

Although both power-law fitting and exponential fitting fit the data very well, the significant difference between the two types of fitting is that power-law fitting gives higher critical temperatures than exponential fitting. Hence, we may expect that higher accuracy for critical temperature and a few more data will provide further understanding of the nature of the phase transition.

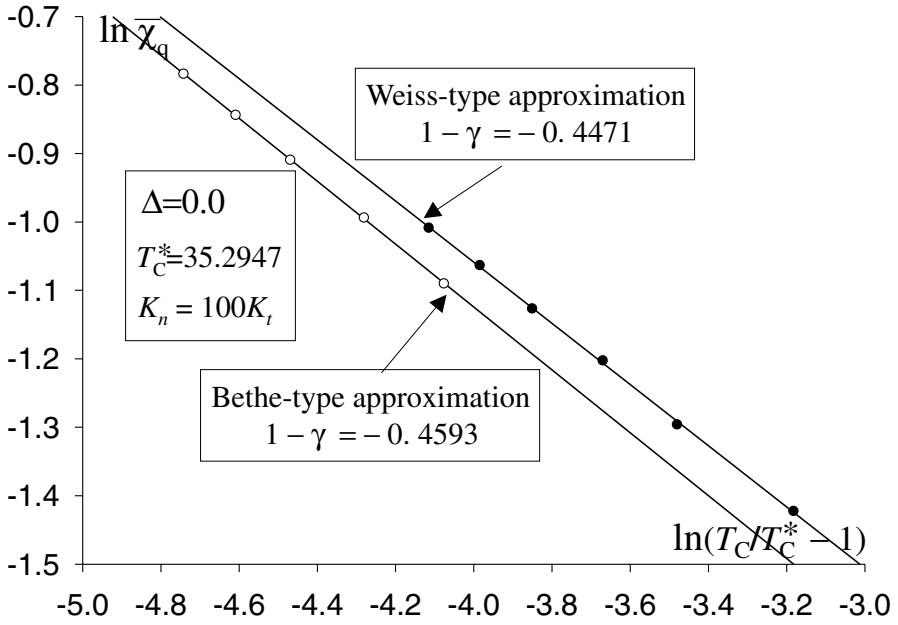

Figure 3.5. Power-law fits of the CAM for the case $K_n = 100K_t$ and $\Delta = 0$.

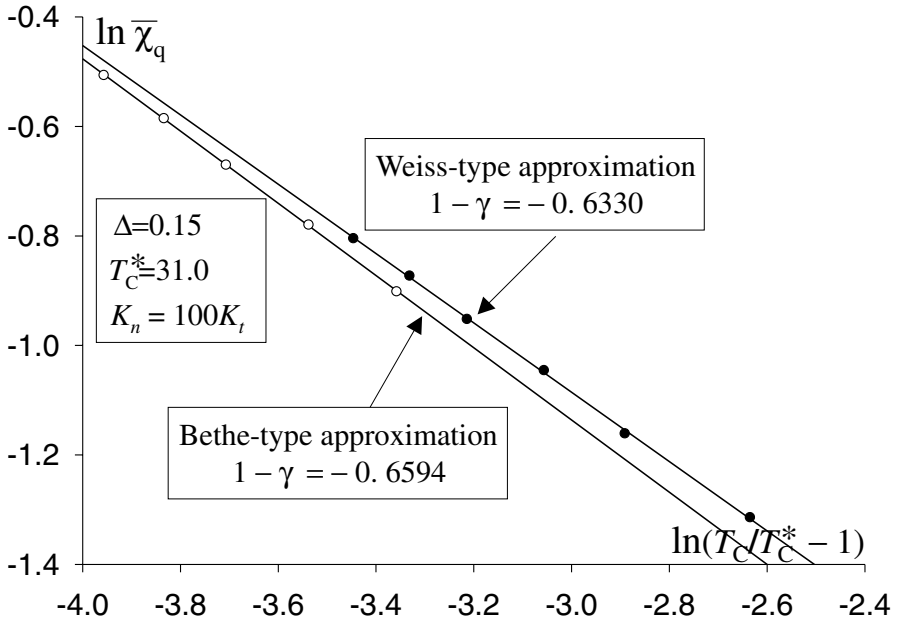

Figure 3.6. Power-law fits of the CAM for the case of $K_n = 100K_t$, $\Delta = 0.15$ and $T_c^* = 31$.

In our fitting procedure, the mean square deviation is always kept less than 3%. But if we require less accuracy, many more fits can be allowed. For example, a different exponential fit is given in Fig. 3.10 with $\sigma = 0.5$ leading to an about three times larger deviation.

Meanwhile, according to mean-field theory and finite-size scaling,[69] we would expect that $(T_c/T_c^* - 1) \propto (1/L + a\ln L/L)^{-1/\nu}$ for both types of approximation,[70] where L denote the system size in which the interactions have been dealt with exactly. As discussed in section 3.4, a new sequence $\{T_n(N)\}$ can be constructed from two sequences $\{T_w(N)\}$ and $\{T_b(N)\}$, where $\{T_w(N)\}$ and $\{T_b(N)\}$ are the critical points obtained by Weiss-type and Bethe-type approximation respectively. We expect this new sequence to give a much better approximation to the critical temperature. Therefore, we can use this sequence as the additional information for judging the accuracy of the two fittings methods. As an example, we study the case $\Delta = 0.45$ and $K_n/K_t = 100$, in order to compare the different critical temperatures given in two previous methods (3.54) and (3.55). We construct the new sequence $\{T_n(3), T_n(4), T_n(5)\}$ as $\{7.7110, 7.7334, 7.7475\}$ using (3.38). Power-law fitting gives T_c^* to be around 7.95 and exponential fitting gives T_c^* to be around 7.78 at $\Delta = 0.45$ and $K_n/K_t = 100$. It looks that exponential fitting is more reasonable at this point. However, the result is far from conclusive. To make a clear conclusion, additional information is necessary.

3.6 WAVEVECTOR ANALYSIS

As is well-known,[44] we should be able to get phase transition information through the analysis of the wavevector at the phase transition point. If a Lifshitz point Δ_L exists at finite chirality, the wavevector along the critical line should vanish if $\Delta \leq \Delta_L$. Although we are not sure how this Lifshitz point Δ_L will depend on K_n/K_t, old works[44,47,48] indicate that there is no big dependence of Δ_L on K_n/K_t. Let us introduce a reduced wavevector $\hat{q} = 3q/(2\pi\Delta)$.

Two cases have been studied at $\Delta = 0.05$. These calculations for the wavevector need an accuracy of 10^{-8} for q. Higher accuracy will be needed for smaller Δ and the numerical values will not be so reliable. The results are presented in Tables 3.8 and

N	3	4	5	6	7
$\hat{q}_{\rm w}$	0.1707023	0.1485028	0.1304893	0.1182574	0.1076384
$\hat{q}_{\rm b}$	0.1347898	0.1168134	0.1026421	0.0929284	0.0846686
$\hat{q}_{\rm n}$	−0.00836	−0.00219	0.00002		

TABLE 3.8. Table of $\hat{q}_{\rm b}$, $\hat{q}_{\rm w}$ and $\hat{q}_{\rm n}$ for $\Delta = 0.05$ and $K_n = 10K_t$. The reduced critical wavevector $\hat{q}_{\rm b}(N)$ is obtained by Bethe-type approximation and $\hat{q}_{\rm w}(N)$ by Weiss-type approximation, where N is the width of the finite strip. Here, $\hat{q}_{\rm c}(N)$ is obtained by (3.38) with $\delta N = 2$.

3.9. Although we only have three members in these new sequences and we cannot make a very conclusive result, it looks very tempting to say that these sequences will converge to the true $\hat{q}_{\rm c}$ from below. Compared with previous results for Δ_L to be around 0.25 to 0.40,[44,47,48] we have $\Delta_L < 0.05$. Hence, we may conclude that even for a very small Δ the wavevector at the transition point is non-zero. This means that the transition should be from the paramagnetic to the incommensurate phase and possibly no Lifshitz point exists at finite chirality at all.

In Fig. 3.11, we plot $\hat{q}_{\rm c}$ versus Δ for different K_n/K_t and the same N based on Weiss approximation. We can see that the reduced wavevectors $\hat{q}_{\rm w}$ decrease as Δ decreases. However, $\hat{q}_{\rm w}$ does not approach 0 as $\Delta \to 0$ as it should. Similar results hold in the Bethe approximation. But the new sequence, which is constructed from $\hat{q}_{\rm w}(N)$ and $\hat{q}_{\rm b}(N)$, approaches 0 as $\Delta \to 0$. This is also suggested by Tables 3.8 and 3.9. We also find that $\hat{q}_{\rm c}$ decreases as K_n/K_t increases for fixed Δ and N. This in turn is consistent with the results of the quantum chain case $K_n/K_t \to \infty$,[50,53] where the incommensurate phase will disappear, i.e. $\hat{q}_{\rm c} = 0$ for $0 < \Delta < 1/2$,[53] when $K_n/K_t \to \infty$. To see the convergence of $\hat{q}_{\rm c}$ with increasing N, plots of $\hat{q}_{\rm c}$ versus Δ for different widths N are shown in Fig. 3.12. We find that for fixed Δ, $\hat{q}_{\rm c}$ decreases as N increases in Weiss approximation, but possibly $\hat{q}_{\rm c}$ will not converge to 0 for $\Delta \neq 0$ as we concluded earlier.

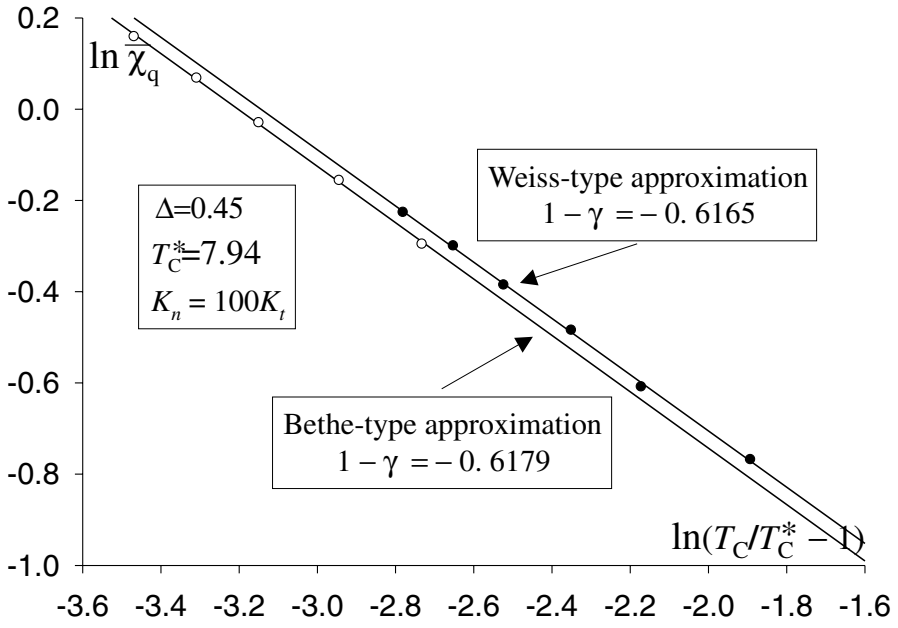

Figure 3.7. Power-law fits of the CAM for the case of $K_n = 100K_t$, $\Delta = 0.45$ and $T_c^* = 7.94$.

N	3	4	5	6	7
$\hat{q}_w$	0.0463680	0.0402710	0.0353594	0.0320544	0.0291924
$\hat{q}_b$	0.0362354	0.0314054	0.0276127	0.0250293	0.0228355
$\hat{q}_n$	−0.00038	0.00069	0.00099		

TABLE 3.9. Table of $\hat{q}_b$, $\hat{q}_w$ and $\hat{q}_n$ for $\Delta = 0.05$ and $K_n = 100K_t$. The reduced critical wavevector $\hat{q}_b(N)$ is obtained by Bethe-type approximation and $\hat{q}_w(N)$ by Weiss-type approximation, where N is the width of the finite strip. Here, $\hat{q}_c(N)$ is obtained by (3.38) with $\delta N = 2$.

3.7 SUMMARY

In conclusion, although we can not exclude the possibility that there exists a Lifshitz point for the asymmetric chiral Potts model, it looks most likely that there is no Lifshitz point at finite chirality at all. Meanwhile, CAM analysis does give consistency with the well-known results at the Potts point and for large Δ cases. The susceptibility does not fit the exponential law very well using our data when Δ is small. From this, one tends to conclude that a Lifshitz point exists at finite chirality contradicting our wavevector analysis. One possibility is that for small Δ, we may need a much better estimate of the critical temperature to make the CAM analysis successful. It is also discomforting to find γ, σ to be possible functions of Δ and K_n/K_t.

To extend the study to larger strips will be very interesting. We may see if the sequence defined in (3.38) is already monotonic for such kind of small width N. (For phenomenological renormalization, it is often found that it is in the scaling region even for small N.) We may also check if the transition is of Kosterlitz–Thouless type when Δ is small and see how the critical exponents change following a change of Δ and possibly K_n/K_t.

Our conclusion that no Lifshitz point exists at finite chirality, is based on the following assumptions:

a) Both Weiss-type and Bethe-type mean-field transfer matrix theories will give the correct critical temperature and wavevector when the width of the strip becomes infinite.

b) The new sequence constructed for the wavevector on the critical line is already in the monotonic region even for a small width N.

c) For all finite K_n/K_t, the phase diagrams have the same global structure.

d) The Δ, for which we calculated $\hat{q}_c$ and find most likely $\hat{q}_c \neq 0$, is small enough. (To calculate $\hat{q}_c$ at smaller Δ will need much higher numerical accuracy.)

3.8 DISCUSSION OF RELATED WORKS

In this section, we will try to reexamine some old results and hopefully get some new insights. Many previous studies of the chiral Potts model are not on the same case. There are several studies concentrating on the quantum Hamiltonian formalism. They are equivalent to either $K_n/K_t \to \infty$ or $K_n/K_t \to 0$ in our formalism.

Howes[48] used the quantum Hamiltonian formalism to study the one-particle excitation mass gap. His case is equivalent to the $K_n/K_t \to 0$ case. He got the series expansion for the mass gap of light and heavy domain wall respectively, then a D log Padé method was employed to analyze the zeroes of the mass gap. He found that the zeroes located at m_1 and m_2 are very close when $\Delta \leq 1/4$ but scattered when $\Delta > 1/4$. Hence he concluded that a possible Lifshitz point is located at $\Delta = 1/4$. He also obtained $\nu_t = \nu_n = 5/6$ when $0 \leq \Delta < 1/4$, $\nu_t = 1$ and $\nu_n = 2/3$ when $\Delta = 1/4$ and that $\nu_t = 1$ and $\nu_n = 1/2$ along the critical line which separates the commensurate phase and the incommensurate phase when $1/4 < \Delta < 1/2$.

Duxbury et al.[44] used the phenomenological renormalization group method[71] to study this model with $K_n = K_t$. They used scaling of the correlation length to determine the critical line which separates the incommensurate phase from the disordered phase and used scaling of the wavevector to determine the critical line which separates the incommensurate phase from the ordered phase. They assumed the anisotropic scaling $X_N(T_c) = N^\theta$ where $X_N = 1/\xi_N$ in the case of correlation length scaling or δq_N for wavevector scaling. They concluded that $\nu_t = \nu_n = 0.85 \pm 0.05$ when $\Delta \leq \Delta_L$ and ν_n becomes small when $\Delta \geq \Delta_L$ for both the critical line which separates the ordered phases from the incommensurate phase and the critical line which separates the incommensurate phase from the disordered phase. Carefully checking Figures 3 (a) and (b) in their letter, it is very tempting to conclude that the wavevector exponent $\beta = \nu_n$.

In the above two works, they locate the two critical lines separately. Since different methods will have different errors and the incommensurate region is so narrow

for small Δ, it may not be surprising if the difference of these two critical lines is covered by these errors.

Houlrik et al.[47] used Monte Carlo renormalization group methods to study the incommensurate phase. Their scheme is built upon a fixed point of the Hamiltonian in the renormalization group theory and the same block scale was used in both directions although the original model was obviously anisotropic. In Fig. 4 of their paper, we see that there are two values ($E^{(m)}(T)$ in their paper) for different size lattices crossing over between a point with temperature 1.09 and wavevector 0 and a point with temperature 1.10 and wavevector $\pi/15$, this indicates that there is at least one point at which the two values equal and this point is in the incommensurate phase according to their algorithm.

The quantum Hamiltonian in Everts' study[50] is equivalent to the case with $K_n/K_t \to \infty$. They concluded that $\nu_t \simeq 0.97$ and $\nu_n \simeq 0.7$ and that there is a possibility that the floating phase extends to Δ in a very narrow strip between the disordered and the ferromagnetic phase, i.e. the non-existence of the Lifshitz point at finite chirality cannot be ruled out.

The quantum Hamiltonian in the study of Vescan et al.[53] is equivalent to the case with $K_n/K_t \to \infty$. In this case, the quantum Hamiltonian will not depend on Δ. The limits $K_n/K_t \to \infty$ and $\Delta \to 0$ do not commute. Vescan et al. concluded that only one kind of phase transition exists for $0 < \Delta \leq 1/2$. It means that the Lifshitz point moves to 1/2 when $K_n/K_t \to \infty$. They also estimated that $\nu_t = 0.95 \pm 0.04$ and $\nu_n = 0.67 \pm 0.07$.

The case von Gehlen et al. studied[52] is equivalent to the case with $K_n/K_t \to 0$. They concluded that short quantum chains or low- and high-temperature expansions will produce fake Lifshitz points and there is no Lifshitz point in this case.

The quantum formalism in Centen et al.[51] is equivalent to the $K_n/K_t \to 0$ case (there is a misprint in formula 2.8 on page 587). Centen et al. estimated the ν_t along the critical line which separates the commensurate phase from the incommensurate phase or from the fluid phase. They found that ν_t varies continuously from 5/6 (corresponding to the Potts case) to 1.

After reviewing these works for the chiral Potts model on the square lattice, we see that it is consistent with our results that for any finite K_n/K_t, the disordered phase and the ordered phase are always separated by the incommensurate phase for $0 < \Delta < 1/2$ and that the incommensurate region shrinks as K_n/K_t is increased.

When $\Delta = 0$, $\nu_t = \nu_n = 5/6$ and when $\Delta \to 1/2$, $\nu_t \to 1$,[50,51,53] $\nu_n \to 1/2$ (from the fermion theory) along the commensurate-incommensurate line for $K_n/K_t \to 0$ and $\nu_n = 0.67 \pm 0.07$ [50,53] for $K_n/K_t \to \infty$. Generally, both ν_t and ν_n continuously vary with Δ.[51] When Δ increases, ν_t increases but ν_n decreases on both critical lines. When $K_n/K_t \to \infty$, the two critical lines merge. Much less information is available for the incommensurate-disorder line. For fixed Δ, the anisotropic exponent which is defined by ν_n/ν_t, decreases with K_n/K_t increasing from 0 to ∞. With these exponents, what has been assumed is that the correlation lengths in both directions diverge simultaneously on the critical lines and this assumption has been taken indirectly in previous works. This assumption can not be taken for certain because at least the exact result of the correlation function at $T = 0$ and $\Delta = 1/2$ shows that the correlation length along the non-chiral direction is infinite but finite along the chiral direction.

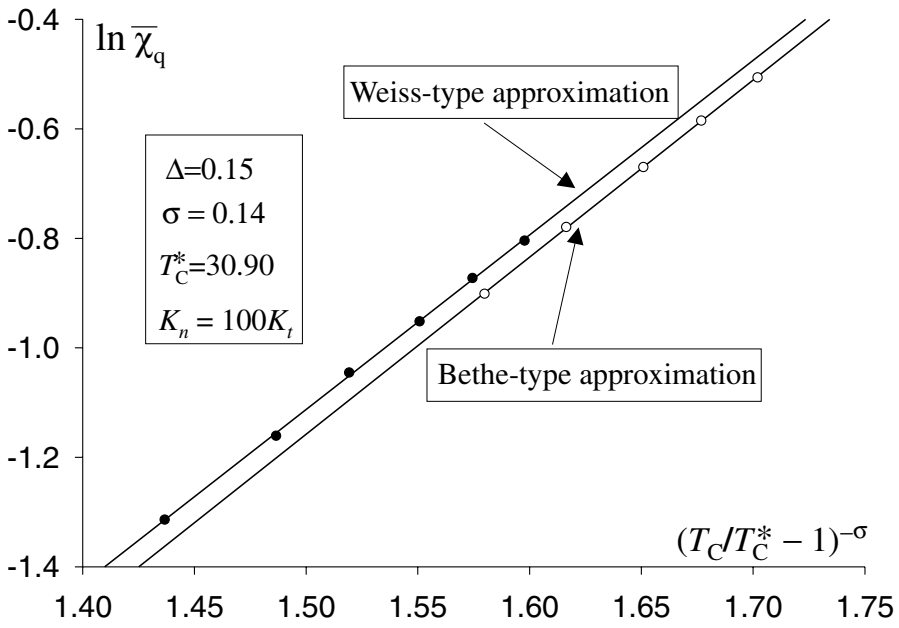

Figure 3.8. Exponential fits of the CAM for the case of $K_n = 100K_t$, $\Delta = 0.15$ and $T_c^* = 30.90$ with $\sigma = 0.14$.

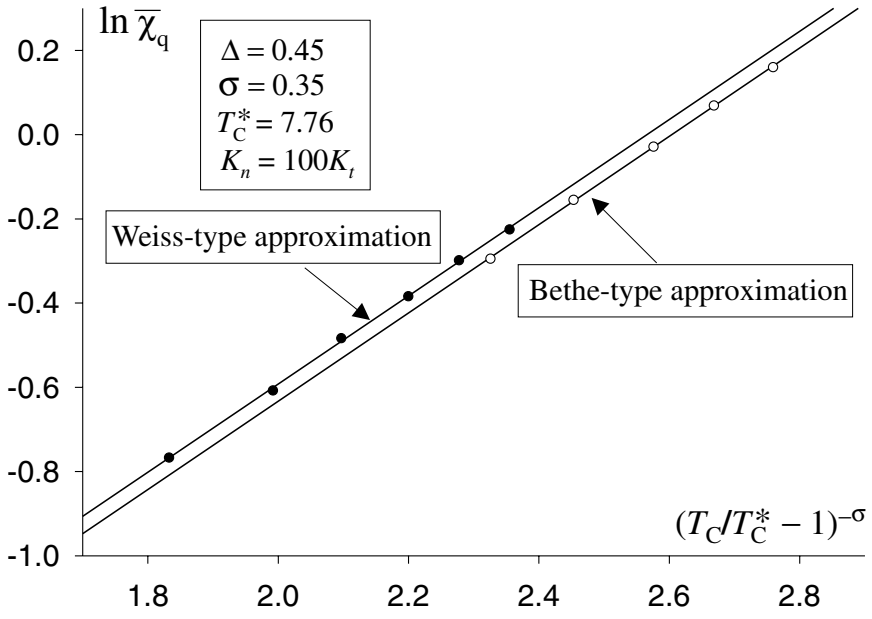

Figure 3.9. Exponential fits of the CAM for the case of $K_n = 100K_t$, $\Delta = 0.45$ and $T_c^* = 7.76$ with $\sigma = 0.35$.

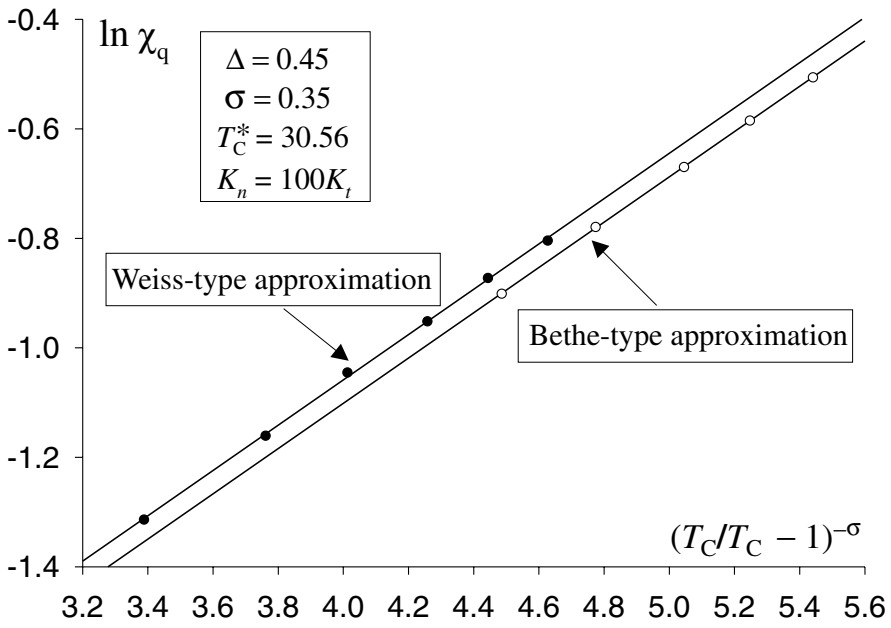

Figure 3.10. Exponential fits of the CAM for the case of $K_n = 100K_t$, $\Delta = 0.15$ and $T_c^* = 30.56$ with $\sigma = 0.5$.

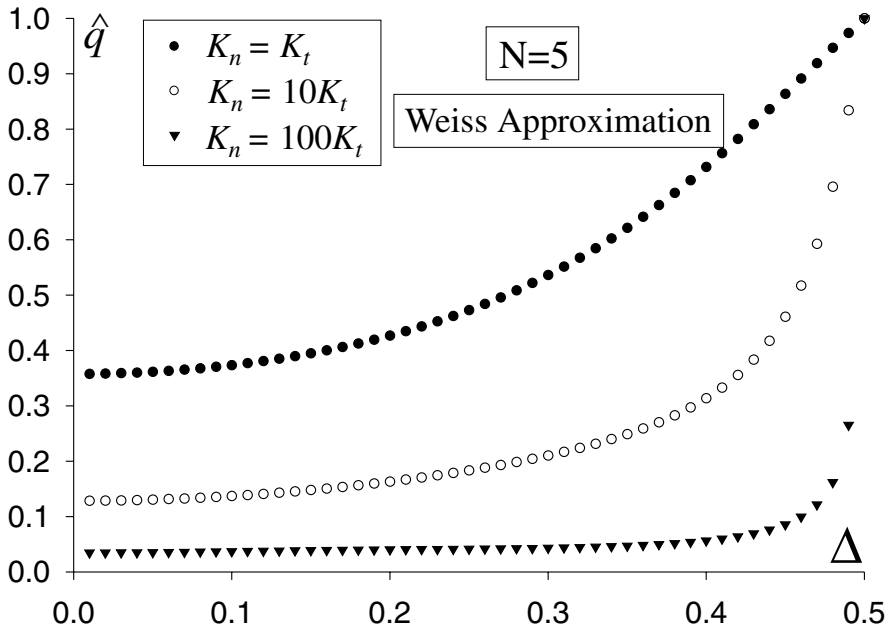

Figure 3.11. Reduced wavevector $\hat{q}_c$ versus Δ with $N = 5$ based on Weiss approximation. As K_n/K_t increases, $\hat{q}_c$ decreases for fixed Δ.

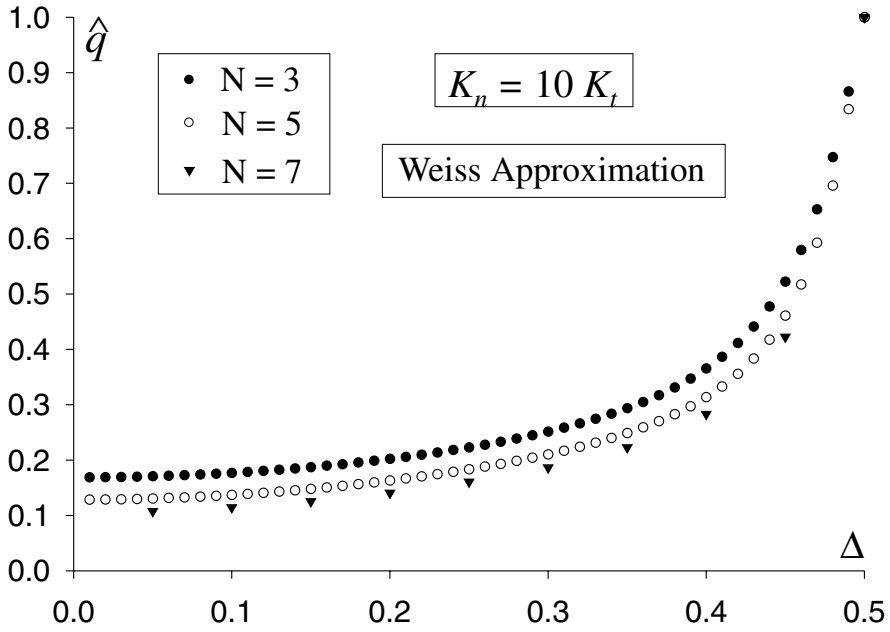

Figure 3.12. Reduced wavevector $\hat{q}_{\mathrm{w}}$ versus Δ with $K_n = 10K_t$ based on Weiss approximation. As N increases, $\hat{q}_{\mathrm{c}}$ decreases for fixed Δ.

CHAPTER 4

SCALING LIMIT FOR THE TWO-POINT CORRELATION FUNCTION IN THE Z-INVARIANT ISING MODEL

In this chapter we shall derive a new result for the two-spin correlation function of the Z-invariant Ising model in the scaling limit. It is well known that knowing the correlation function is very important to understand statistical mechanics systems. For example, the susceptibility is a sum of spin correlation functions. Unfortunately, it cannot be explicitly calculated in most of the solvable models at this time. One exception is the two-dimensional Ising model whose correlation functions have been intensively studied by many authors.[72–93] Baxter[78] gave a formula for the spin correlation function of Z-invariant Ising model. It is beautiful but intractable. Here we use some of Baxter's arguments[78] and a quadratic identity[81] obtained by Perk for the most general planar Ising model to derive a new result for the two-spin correlation function of the Z-invariant Ising model in the scaling limit.

4.1 Z-INVARIANT ISING MODEL

The Z-invariant inhomogeneous Ising model[78,79] has been introduced by Baxter as a natural extension of Onsager's uniform Ising model within the framework of star-triangle equations and commuting transfer matrices. It is defined in terms of a set of oriented straight lines carrying "rapidity" variables u_i. Only two lines can meet at each intersection and the areas separated by the rapidity lines can be colored alternatingly black and white. An Ising spin is associated with each black area and a dual Ising spin with each white area, see also Fig. 4.1.

This defines two Ising models. In the first one each pair of spins meeting at an intersection of two rapidity lines has the usual pair interaction $-K\sigma_x\sigma_y$ with reduced

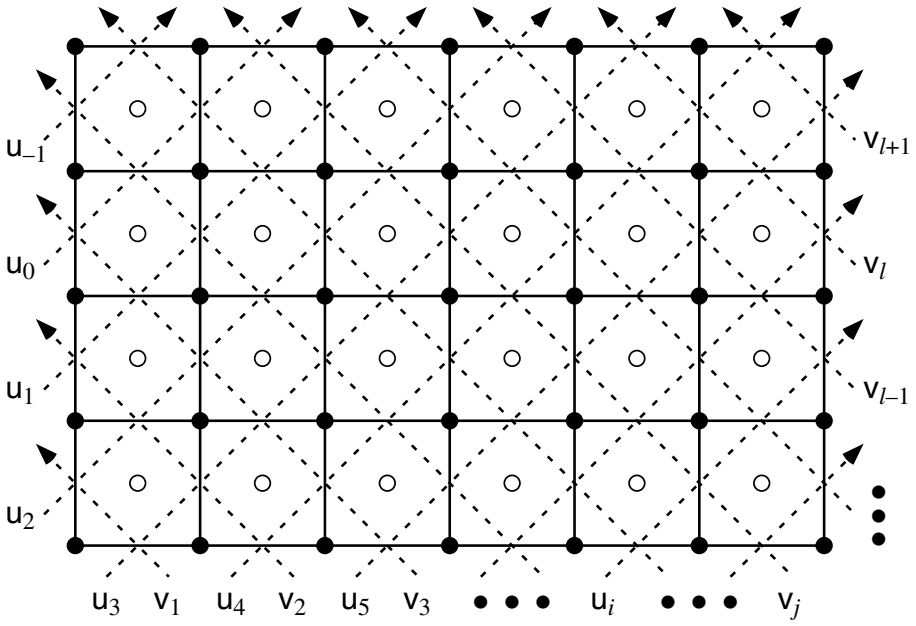

Figure 4.1. The lattice of a two-dimensional Z-invariant Ising model is represented by solid lines, the rapidity lines on the medial graph are represented by oriented dashed lines. These lines carry rapidity variables u_i and v_j. The position of the spins are indicated by small black circles, the positions of the dual spins by white circles.

interaction strength K. In the second model the two dual spins that meet at the same intersection interact as $-K^*\sigma_{x^*}\sigma_{y^*}$, where $\sinh(2K)\sinh(2K^*)=1$. Here K and therefore also K^* only depend on a fixed elliptic modulus k and the two rapidity variables u_1 and u_2 of the two rapidity lines that meet.

We have two possible choices for the reduced interaction strength $K_{x,y}$ of the spins at positions x and y, see Fig. 4.2. If the two rapidity lines with rapidity variables u_1 and u_2 pass through the line connecting the two spins toward the same side of that line, we must choose $K_{x,y} = K(u_1, u_2)$; otherwise, if they pass toward opposite sides, we must take $K_{x,y} = \bar{K}(u_1, u_2)$. These choices $K(u_1, u_2)$ and $\bar{K}(u_1, u_2)$ are given by

$$\begin{aligned}\sinh\left(2K(u_1,u_2)\right) &= k\,\mathrm{sc}(u_1-u_2,k') = \mathrm{cs}(\mathrm{K}(k')+u_2-u_1,k'),\\ \sinh\left(2\bar{K}(u_1,u_2)\right) &= \mathrm{cs}(u_1-u_2,k') = k\,\mathrm{sc}(\mathrm{K}(k')+u_2-u_1,k'),\end{aligned} \tag{4.1}$$

where $k' = \sqrt{1-k^2}$ is the complementary elliptic modulus, $\mathrm{K}(k)$ denotes the complete elliptic integral of the first kind, and $\mathrm{sc}(v,k) = \mathrm{sn}(v,k)/\mathrm{cn}(v,k)$ and $\mathrm{cs}(v,k) = \mathrm{cn}(v,k)/\mathrm{sn}(v,k)$ are Jacobi elliptic functions. There is still a sign ambiguity in definition (4.1) depending on which of the two rapidity lines carries u_1 and which u_2. This ambiguity is removed if we take u_1 to be the rapidity variable of the line that points in a direction (less than 180°) clockwise with respect to the other rapidity line. [In Fig. 4.2 we have to identify u_i as the u_1 and v_j as the u_2 of (4.1).]

Eq. (4.1) also exhibits a remarkable "rotation symmetry" in this Z-invariant Ising model. We can flip the direction of a rapidity line j providing we change its rapidity variable u_j to $u_j \pm \mathrm{K}(k')$. This interchanges the K and $\bar{K}$ choices in (4.1). It is a simple exercise to see that this is consistent using $\mathrm{sc}(v+2\mathrm{K}(k'),k') = \mathrm{sc}(v,k')$ and the corresponding periodicity formula for $\mathrm{cs}(v,k') = 1/\mathrm{sc}(v,k')$. This symmetry plays an important role in the calculation of the correlation functions and was noted before. We shall now exploit it.

In the Z-invariant Ising model, following Baxter's argument,[78,79] the two-point correlation function can only depend on the elliptic modulus k and the values of the $2m$ rapidity variables $u_1, \ldots, u_{2m}$ that pass between the two spins under consideration.

Hence, there should exist universal functions $g_2, \ldots, g_{2m}$ such that for the appropriate m-value

$$\langle \sigma\sigma' \rangle = g_{2m}(k; \bar{u}_1, \ldots, \bar{u}_{2m}) = g_{2m}(k; \bar{u}_{\mathrm{P}(1)} + v, \ldots, \bar{u}_{\mathrm{P}(2m)} + v), \tag{4.2}$$

where $\bar{u}_j = u_j$ if the jth rapidity line passes between the two spins σ and σ' in a fixed chosen direction and[82] $\bar{u}_j = u_j + \mathrm{K}(k')$ if it passes in the opposite direction. The Z-invariance implies that there should be complete permutation symmetry under all permutations P of the rapidities and the "difference property" implies a translation invariance when shifting all the u_j by the same amount v. These properties have been expressed in the above equation.

If two rapidity variables differ by $\mathrm{K}(k')$, they can be viewed as belonging to a single rapidity line passing between the two spins and back. The correlation function cannot depend on them, i.e.

$$\langle \sigma\sigma' \rangle = g_{2m+2}(k; \bar{u}_1, \ldots, \bar{u}_{2m}, \bar{u}_{2m+1}, \bar{u}_{2m+1} + \mathrm{K}(k')) = g_{2m}(k; \bar{u}_1, \ldots, \bar{u}_{2m}). \tag{4.3}$$

4.2 SCALING LIMIT

We can use these properties (4.2) and (4.3) to propose a formula for the two-point function in the scaling limit, where $k \to 1$ and the distance of the spins tends to infinity. In this limit we have $\mathrm{K}(k') = \pi/2$,

$$\sinh\left(2K(u_1, u_2)\right) = \tan(u_1 - u_2) = \cot(\pm\tfrac{1}{2}\pi + u_2 - u_1), \tag{4.4}$$

$$\sinh\left(2\bar{K}(u_1, u_2)\right) = \cot(u_1 - u_2) = \tan(\pm\tfrac{1}{2}\pi + u_2 - u_1). \tag{4.5}$$

The scaling limit is defined by the assumption that the scaled correlation function depends on a single distance variable R. We can view the rapidity variables as angle variables, and the translation symmetry in (4.3) becomes a rotation symmetry in a two-dimensional plane. Writing the u_j in terms of unit vectors $\mathbf{e}_j = (\cos(\lambda u_j), \sin(\lambda u_j))$, the simplest expression for R that exhibits the required rotation and permutation symmetries is

$$R = C\Big|\sum_{j=1}^{2m} \mathbf{e}_j\Big| \quad \text{or} \quad R = \frac{1}{2}\Big[\Big\{\sum_{j=1}^{2m} \cos(2u_j)\Big\}^2 + \Big\{\sum_{j=1}^{2m} \sin(2u_j)\Big\}^2\Big]^{1/2}. \tag{4.6}$$

We set $\lambda = 2$ in view of (4.3) which says that any pair u and $u + \frac{1}{2}\pi$ must cancel out. Furthermore, we choose the scale factor $C = \frac{1}{2}$.

For the special case of diagonal correlations $\langle \sigma_{00}\sigma_{mm}\rangle$ in the uniform rectangular Ising model, for which all $2m$ u_j's are equal, we find from (4.6) $R = m$, justifying the above choice of C. The consistency of our choice is justified by the well known results of the rectangular Ising model. In this special case the correlation length $\xi_{\rm d}$ is known[76] and we can use it to introduce the scaled distance*

$$r = R/\xi_{\rm d}, \quad \text{where} \quad \xi_{\rm d}^{-1} = |\log k|. \tag{4.8}$$

We can now propose the general form of the scaled correlation functions for the lattice and the dual lattices (*) to be

$$\langle \sigma\sigma'\rangle \approx |1-k^{-2}|^{1/4}F(r), \quad \langle \sigma\sigma'\rangle^* \approx |1-k^{-2}|^{1/4}G(r), \tag{4.9}$$

where the functions $F(r)$ and $G(r)$ are expected to be Painlevé functions and the front factor is the square of the spontaneous magnetization for $T < T_{\rm c}$ or $k > 1$.

It is easy to verify that these scaling forms agree with all existing results for the uniform rectangular and triangular Ising models.[77,90] We shall proceed with providing strong evidence that they are also correct for the general Z-invariant Ising model.

For the most general planar Ising model we can use a quadratic identity relating the two-point correlation function $\langle \sigma_{\rm x}\sigma_{\rm y}\rangle$ with its counterpart on the dual lattice $\langle \sigma_{\rm x^*}\sigma_{\rm y^*}\rangle^*$, i.e.[81]

$$\begin{aligned}\sinh(2K_1)\sinh(2K_2)\{&\langle \sigma_{\rm x_1}\sigma_{\rm x_2}\rangle\langle \sigma_{\rm y_1}\sigma_{\rm y_2}\rangle - \langle \sigma_{\rm x_1}\sigma_{\rm y_2}\rangle\langle \sigma_{\rm y_1}\sigma_{\rm x_2}\rangle\}\\ &+\{\langle \sigma_{\rm x_1^*}\sigma_{\rm x_2^*}\rangle^*\langle \sigma_{\rm y_1^*}\sigma_{\rm y_2^*}\rangle^* - \langle \sigma_{\rm x_1^*}\sigma_{\rm y_2^*}\rangle^*\langle \sigma_{\rm y_1^*}\sigma_{\rm x_2^*}\rangle^*\} = 0,\end{aligned} \tag{4.10}$$

see also Fig. 4.3. Here we have two arbitrarily chosen unequal nearest-neighbor pairs of spins at the sites $\{{\rm x}_1, {\rm y}_1\} \neq \{{\rm x}_2, {\rm y}_2\}$ with couplings $K_1 = \beta J_1$, and $K_2 = \beta J_2$. Also

*Strictly spoken, the diagonal distance is not m, but $m\sqrt{2}$, so that the inverse diagonal correlation length really should be $|\log k|/\sqrt{2}$ agreeing with following equation

$$\xi^{-1} = \xi_{>}^{-1}(k) = |2K - 2K^*| = |{\rm arsinh}(k^{\frac{1}{2}}) - {\rm arsinh}(k^{-\frac{1}{2}})|, \tag{4.7}$$

in the limit $k \to 1$.

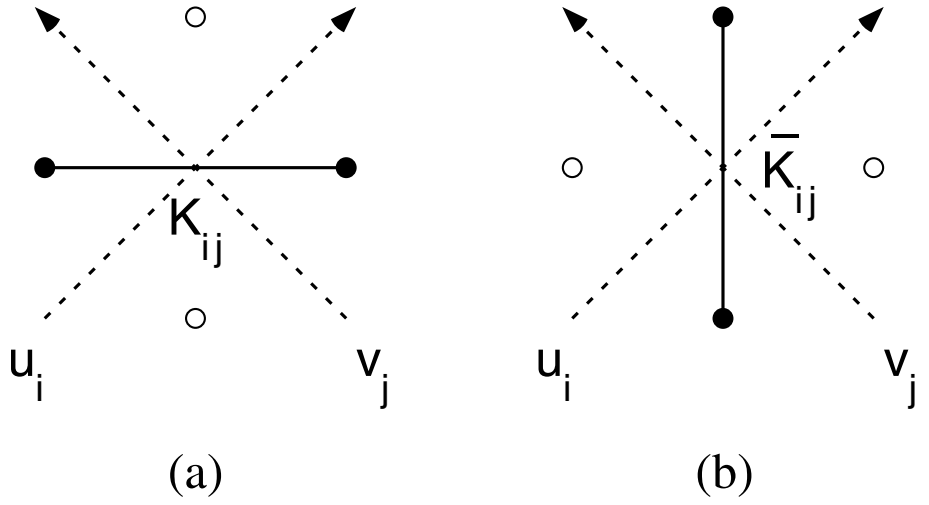

Figure 4.2. (a) The horizontal coupling K_{ij} and (b) the vertical coupling $\bar{K}_{ij}$.

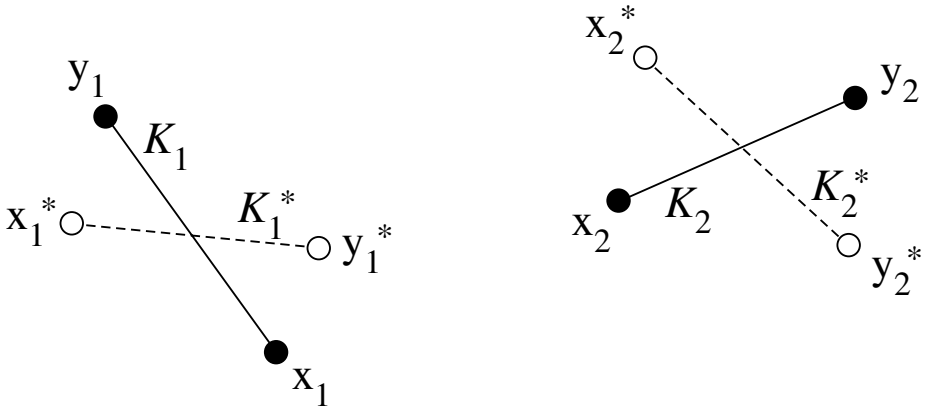

Figure 4.3. Part of an Ising model and its dual on a general planar graph: Indicated are two neighbor pairs of spins indicated by small black circles with their reduced interaction constants K_i (drawn lines). Also indicated are their corresponding two pairs of dual spins indicated by white circles with their reduced interaction constants K_i^* (dashed lines). Note that are both $(\mathrm{x}_1, \mathrm{x}_1^*, \mathrm{y}_1, \mathrm{y}_1^*)$ and $(\mathrm{x}_2, \mathrm{x}_2^*, \mathrm{y}_2, \mathrm{y}_2^*)$ are arranged clockwise.

we have their corresponding two nearest-neighbor pairs of dual spins at sites $\{\mathrm{x}_1^*, \mathrm{y}_1^*\}$ and $\{\mathrm{x}_2^*, \mathrm{y}_2^*\}$ with couplings K_1^* and K_2^* satisfying $\sinh(2K_i)\sinh(2K_i^*)=1$, $(i=1,2)$. The orientations of the two quadruples of points $(\mathrm{x}_1, \mathrm{x}_1^*, \mathrm{y}_1, \mathrm{y}_1^*)$ and $(\mathrm{x}_2, \mathrm{x}_2^*, \mathrm{y}_2, \mathrm{y}_2^*)$ must both be chosen the same for (4.10) to hold with a plus sign on the second line. Many results can be derived from this one equation alone, which is an ultimate statement of the fermionic character of the Ising model.[81]

Restricting ourselves to the Z-invariant Ising model the quadratic identity reduces to

$$\begin{aligned} k^2\mathrm{sc}(u_2-u_1,k')\mathrm{sc}(u_4-u_3,k') \\ \times\{g(u_1,u_2,u_3,u_4,\cdots)g(\cdots)-g(u_1,u_2,\cdots)g(u_3,u_4,\cdots)\} \\ +\{g^*(u_1,u_3,\cdots)g^*(u_2,u_4,\cdots)-g^*(u_1,u_4,\cdots)g^*(u_2,u_3,\cdots)\}=0, \end{aligned} \tag{4.11}$$

suppressing all arguments but the four rapidity variables that differ among the two-point functions g and g^*. This result is easily derived assuming that all rapidity lines pass between the spins in the same direction. Eq. (4.11) is also applicable if some of the rapidity lines go in the opposite direction, providing the corresponding u_j are replaced by $u_j + \mathrm{K}(k')$, as discussed above.

In the scaling limit $k \to 1$, $k' \to 0$, (4.11) reduces to the leading term of

$$\begin{aligned} \tan(u_2-u_1)\tan(u_4-u_3)\{F(r_{1234})F(r)-F(r_{12})F(r_{34})\} \\ +\{G(r_{13})G(r_{24})-G(r_{14})G(r_{23})\}=0, \end{aligned} \tag{4.12}$$

where we introduced the notations r for the scaled distance given in (4.6) with only the u_j variables common to all eight two-point functions occurring and $r_{ij\cdots}$ for the scaled distance with the variables $u_i, u_j, \cdots$ added. Also, F and G are the scaling limit functions corresponding to g and g^*, see (4.9). More specifically, we can write

$$r\cos\psi = \tfrac{1}{2}\xi^{-1}\sum_{j\neq 1,2,3,4}\cos(2u_j), \quad r\sin\psi = \tfrac{1}{2}\xi^{-1}\sum_{j\neq 1,2,3,4}\sin(2u_j). \tag{4.13}$$

Since $\xi \to \infty$ the few omitted terms are infinitesimally small.

Expanding to second order and doing straightforward manipulations we arrive at

$$\begin{aligned}\cos(u_1+u_2-\psi)\cos(u_3+u_4-\psi)(FF''-F'^2+r^{-1}GG')\\ +\sin(u_1+u_2-\psi)\sin(u_3+u_4-\psi)(GG''-G'^2+r^{-1}FF')\\ =0,\end{aligned} \tag{4.14}$$

where the primes denote differentiation with respect to r. Since this must hold for all values of ψ, we conclude

$$FF''-F'^2=-r^{-1}GG', \tag{4.15}$$

$$GG''-G'^2=-r^{-1}FF'. \tag{4.16}$$

These are the same equations as those that would follow from the quadratic identities for the rotational-invariant scaling functions of the uniform case.

4.3 PAINLEVÉ EQUATIONS

We can take the first derivative of (4.15), i.e.

$$FF'''-F'F''=-r^{-1}GG''-r^{-1}G'^2+r^{-2}GG'. \tag{4.17}$$

Eliminating G' and G'' from (4.17) using (4.15) and (4.16), we find

$$G^2=\frac{-2r^3(FF''-F'^2)^2}{r^2(FF'''-F'F'')+r(FF''-F'^2)-FF'}. \tag{4.18}$$

Taking the first derivative of this and substituting it in (4.15), we find a closed equation for $F(r)$, namely

$$\begin{aligned}(FF''-F'^2)(r^4F''''-2r^2F''+rF')+FF'^2\\ +r^4(2F'F''F'''-FF'''^2-F''^3)=0.\end{aligned} \tag{4.19}$$

Clearly, $G(r)$ satisfies the same equation. Following Jimbo and Miwa[91] we can change to a new dependent variable

$$\zeta=rF'/F, \tag{4.20}$$

which satisfies

$$r^3(\zeta'\zeta''' - \zeta''^2) - r^2(\zeta\zeta''' - \zeta'\zeta'') - r\zeta\zeta'' + \zeta\zeta' + 2r^2\zeta'^3 - 6r\zeta\zeta'^2 + 4\zeta^2\zeta' = 0. \quad (4.21)$$

This can be integrated once as

$$\frac{r^2\zeta''^2 + 4\zeta'^2(r\zeta' - \zeta) - \zeta'^2}{4(r\zeta' - \zeta)^2} = \mu^2 \quad (4.22)$$

where μ is a constant setting the scale. Hence, we arrive at the Painlevé V equation[91,93]

$$(r\zeta'')^2 = 4\mu^2(r\zeta' - \zeta)^2 - 4\zeta'^2(r\zeta' - \zeta) + \zeta'^2 \quad (4.23)$$

and its derivative

$$r^2\zeta''' + r\zeta'' = 4\mu^2 r(r\zeta' - \zeta) - 4\zeta'(r\zeta' - \zeta) - 2r\zeta'^2 + \zeta'. \quad (4.24)$$

Eqs. (4.19) and (4.21) are recovered again by eliminating μ^2 between the last two equations. Comparing with the result for the uniform rectangular case,[77,93] we see that we must set $\mu = 1$. Originally these scaling functions $F(r)$ and $G(r)$ were given in terms of a Painlevé III formulation,[77] but this has been shown to agree with the Painlevé V version.[93]

CHAPTER 5

FIBONACCI ISING MODEL

5.1 INTRODUCTION

The wavevector-dependent susceptibility $\chi(\mathbf{q})$ is in many ways similar to the static structure factor $S(\mathbf{q}) = \langle\hat{\rho}(\mathbf{q})\hat{\rho}(-\mathbf{q})\rangle$, with $\hat{\rho}(\mathbf{q})$ the Fourier transform of the local density $\rho(\mathbf{r})$. Just like $S(\mathbf{q})$, $\chi(\mathbf{q})$ gives information on the average relative locations of the atoms. It can also be determined experimentally and for the Ising model $\chi(\mathbf{q})$ even translates into the static structure factor of the equivalent lattice gas model.

Since $\chi(\mathbf{q})$ is a sum of spin correlation functions, at this time it cannot be explicitly calculated in most of the solvable models of statistical mechanics. Models to be considered in this chapter are the one-dimensional Ising model and the two-dimensional Z-invariant Ising model near the critical region whose correlation functions have been studied in the last chapter.

More specifically, we shall study exactly the q-dependent susceptibility of certain Fibonacci Ising models in order to obtain some insight in the theory of aperiodic crystals. More specifically, the aperiodic lattice is a limiting case of a sequence of periodic lattices whose period F_n is the nth element in the Fibonacci sequence, satisfying the defining relation

$$F_{n+1} = F_n + F_{n-1}, \quad F_0 = F_1 = 1. \tag{5.1}$$

We shall compare the results for the periodic case with period F_n with the aperiodic case with $F_n \to \infty$ for different correlation lengths. Meanwhile, this may shed some light on the difference of assuming that the system is quasiperiodic or just a system with a large unit cell. Since these are very crude models, one does not expect them

to represent any existing physical systems, even though with modern experimental techniques one should be able to grow crystals that are well approximated by them.

Our crude models can nevertheless be used to gain theoretical understanding as to what is the most important factor that would reproduce the infinitely many and everywhere dense peaks in the q-dependent susceptibility, or in the diffraction patterns[94–96] in quasicrystals.

The chapter is organized as follows. First, in Section 5.2 we present the work for the one-dimensional Ising model. In Section 5.3 we introduce a purely ferromagnetic Z-invariant Ising model with rapidity variables $\{u_j\}$ and $\{v_j\}$ forming the Fibonacci sequences $\{u_{\rm A}, u_{\rm B}, u_{\rm A}, u_{\rm A}, u_{\rm B}, \cdots\}$ and $\{v_{\rm A}, v_{\rm B}, v_{\rm A}, v_{\rm A}, v_{\rm B}, \cdots\}$. In Section 5.4 we use the results obtained in the last chapter to get the effective connected spin-spin correlation which is the average of the spin-spin correlation over the unit cell in the scaling limit. In Section 5.5, we calculate the wave-dependent susceptibility of this Fibonacci Z-invariant Ising model in the scaling limit. Finally, we present our conclusions in Section 5.6.

5.2 ONE-DIMENSIONAL FIBONACCI ISING MODEL

The infinite set of Fibonacci sequences $\{S_n\}$ is defined recursively by $S_{n+1} = S_n S_{n-1}$ with $S_0 = {\rm B}$ and $S_1 = {\rm A}$; then $S_2 = {\rm AB}$, $S_3 = {\rm ABA}$, $S_4 = {\rm ABAAB}$ and so on. This uses symbols A and B that can represent many different things. The sequence S_n has F_n symbols with F_n the nth Fibonacci number given in (5.1). The n-th Fibonacci chain can be formed by periodically repeating a unit cell which is taken to be the Fibonacci sequence S_n.

The one-dimensional Ising model in zero field is defined by the interaction energy

$$\mathcal{E}/k_{\rm B}T \,=\, -\sum_i K_i \sigma_i \sigma_{i+1}. \tag{5.2}$$

If we choose $\{K_i\}$ to form an n-th Fibonacci sequence of $K_{\rm A}$ and $K_{\rm B}$, then the model will be called the n-th Fibonacci Ising chain. The pair correlation function for an open Ising chain in zero field is simply given by

$$\langle \sigma_m \sigma_n \rangle = \prod_{l=\min(m,n)}^{\max(m,n)-1} \tanh K_l, \quad |\tanh K_l| \equiv \exp(-1/\xi_l), \tag{5.3}$$

with ξ_l the correlation length for the uniform case with all couplings equal K_l. Therefore, it takes only little effort to calculate $\chi(q)$ for the case that the $\{K_j\}$ forms an n-th Fibonacci sequence, i.e. for the n-th Fibonacci Ising chain.

In the limit $n \to \infty$, the model becomes an aperiodic Fibonacci Ising chain. Hence, the q-dependent susceptibility can be calculated by

$$k_{\mathrm{B}}T\chi(q) = \lim_{\mathcal{L}\to\infty} \frac{1}{\mathcal{L}} \sum_{l_1} \sum_{l_2} \mathrm{e}^{\mathrm{i}q(l_2-l_1)} \langle \sigma_{l_1}\sigma_{l_2} \rangle^{(\mathrm{c})}, \tag{5.4}$$

where $\mathcal{L} = LF_n$ is the length of the chain, with L denoting some positive integer and the superscript (c) is used to indicate that we are having connected two-point correlation functions given by

$$\langle \sigma_{i_1}\sigma_{i_2} \rangle^{(\mathrm{c})} = \langle \sigma_{i_1}\sigma_{i_2} \rangle - \langle \sigma_{i_1} \rangle \langle \sigma_{i_2} \rangle. \tag{5.5}$$

We may rewrite

$$k_{\mathrm{B}}T\chi(q) = \sum_{l=-\infty}^{\infty} \mathrm{e}^{\mathrm{i}ql} C^{(\mathrm{c})}(l), \tag{5.6}$$

where

$$C^{(\mathrm{c})}(l) = \lim_{\mathcal{L}\to\infty} \frac{1}{F_n} \sum_{l'=0}^{F_n-1} \langle \sigma_{l'}\sigma_{l+l'} \rangle^{(\mathrm{c})}, \tag{5.7}$$

averaging over the unit cell.

We can simplify this using a result obtained by Tracy.[97] We let $N(m, m')$ be the number of K_{A} in the Fibonacci sequence among the m bonds sandwiched between the m'th and $(m'+m)$th sites. Using Lemma 2.5 in ref. 97, we find that $N(m, m')$ is either $\lfloor N_m \rfloor$ or $\lfloor N_m \rfloor + 1$, where $N_m = mF_{n-1}/F_n$ and $\lfloor x \rfloor$ denotes the integer part of x. Furthermore, in the interval $0 \le m' \le F_n - 1$, the number of times that $N(m, m')$ equals $\lfloor N_m \rfloor$ is $F_n(1 - \{N_m\})$, where $\{x\}$ is the fractional part of x, while the number of times that $N(m, m')$ equals $\lfloor N_m \rfloor + 1$ is $F_n\{N_m\}$. Consequently, if K_{A} and K_{B} are both ferromagnetic, we find

$$k_{\mathrm{B}}T\chi(q) = 1 + 2\sum_{n=1}^{\infty} C^{(\mathrm{c})}(n)\cos(qn), \tag{5.8}$$

with

$$C^{(\mathrm{c})}(n) = C^{(\mathrm{c})}(-n) = (1 - \{\alpha n\})\mathrm{e}^{-\lfloor \alpha n \rfloor/\xi_{\mathrm{A}}} \mathrm{e}^{-(n-\lfloor \alpha n \rfloor)/\xi_{\mathrm{B}}}$$

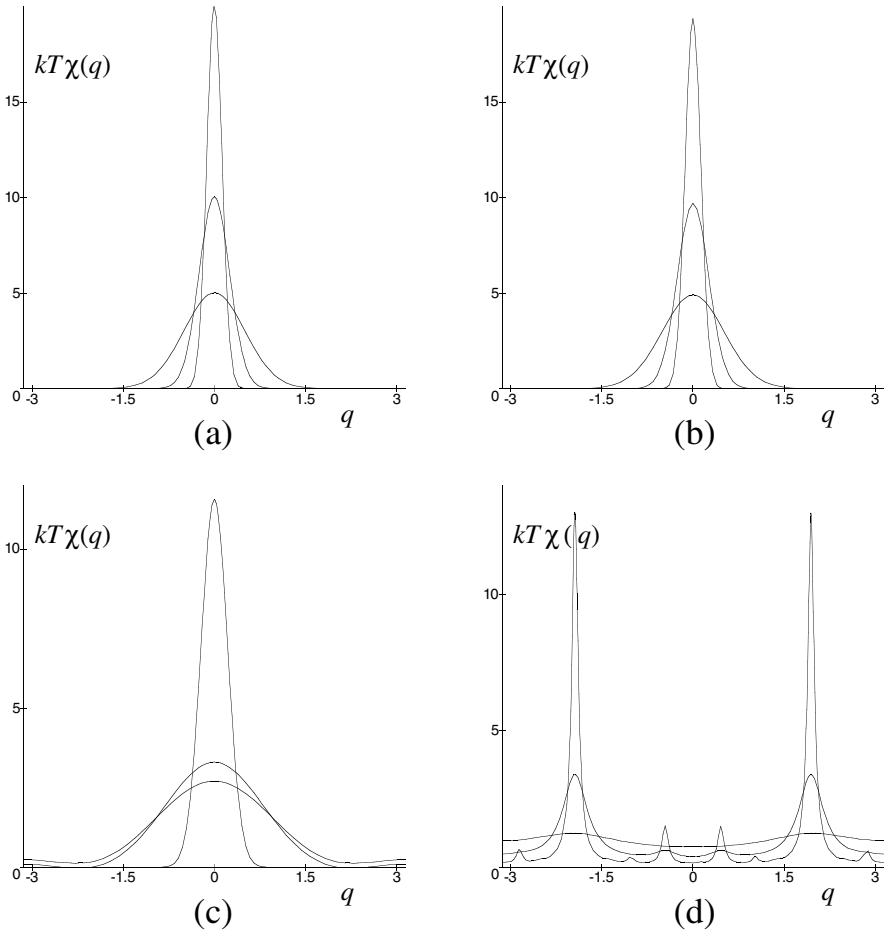

Figure 5.1. Reduced wavevector dependent susceptibility $k_{\mathrm{B}}T\chi(q)$ for the one-dimensional Ising chain. The four cases are: (a) the uniform ferromagnetic case; (b) the $4:1$ Fibonacci case; (c) the $2^{26}:1$ Fibonacci case; and (d) the mixed-sign $1:1$ Fibonacci case. See text.

$$+\{\alpha n\}\mathrm{e}^{-(\lfloor\alpha n\rfloor+1)/\xi_{\mathrm{A}}}\mathrm{e}^{-(n-\lfloor\alpha n\rfloor-1)/\xi_{\mathrm{B}}}, \quad (n\geq 0). \tag{5.9}$$

Using the theory of Fourier series, we can then rewrite (5.9) as

$$\begin{aligned} C^{(\mathrm{c})}(n) &= \Big(1+(\mathrm{e}^{\delta}-1)\{\alpha n\}\Big)\mathrm{e}^{-\delta\{\alpha n\}}\mathrm{e}^{-\kappa n} \\ &= \sum_{m=-\infty}^{\infty}\frac{\sinh^2\frac{1}{2}\delta}{(\frac{1}{2}\delta+\pi\mathrm{i}m)^2}\,\mathrm{e}^{2\pi\mathrm{i}m\alpha n-\kappa n}, \qquad (n\geq 0), \end{aligned} \tag{5.10}$$

where

$$\delta=\frac{1}{\xi_{\mathrm{B}}}-\frac{1}{\xi_{\mathrm{A}}}, \qquad \kappa=\frac{\alpha}{\xi_{\mathrm{A}}}+\frac{1-\alpha}{\xi_{\mathrm{B}}}. \tag{5.11}$$

If $K_{\mathrm{A}}<0$ and $K_{\mathrm{B}}>0$, we still have (5.8), but we have to replace (5.9) by

$$\begin{aligned} C^{(\mathrm{c})}(n) &= C^{(\mathrm{c})}(-n) \\ &= (1-\{\alpha n\})(-1)^{-\lfloor\alpha n\rfloor}\mathrm{e}^{-\lfloor\alpha n\rfloor/\xi_{\mathrm{A}}}\mathrm{e}^{-(n-\lfloor\alpha n\rfloor)/\xi_{\mathrm{B}}} \\ &+ \{\alpha n\}(-1)^{-(\lfloor\alpha n\rfloor+1)}\mathrm{e}^{-(\lfloor\alpha n\rfloor+1)/\xi_{\mathrm{A}}}\mathrm{e}^{-(n-\lfloor\alpha n\rfloor-1)/\xi_{\mathrm{B}}} \\ &= \sum_{m=-\infty}^{\infty}\frac{\cosh^2\frac{1}{2}\delta}{(-\frac{1}{2}\delta\mathrm{i}+\pi(m+\frac{1}{2}))^2}\,\mathrm{e}^{2\pi\mathrm{i}(m+\frac{1}{2})\alpha n-\kappa n}, \quad (n\geq 0). \end{aligned} \tag{5.12}$$

Eq. (5.12) is equivalent to replacing $1/\xi_{\mathrm{A}}$ by $1/\xi_{\mathrm{A}}-\pi\mathrm{i}$ in (5.9) and (5.11), or δ has to be replaced by $\delta+\pi\mathrm{i}$ and κ by $\kappa-\pi\mathrm{i}\alpha$.

Since the effective correlation function (5.9) decays exponentially, it is trivial to calculate the sum (5.8) numerically using software packages like Maple. Therefore, without too many further details we shall present plots for four cases in Fig. 5.1.

The first plot is for the uniform ferromagnetic case at three different temperatures, with the highest and sharpest peak at $q=0$ for the lowest temperature. The reduced wavevector-dependent susceptibility in this case is given by

$$k_{\mathrm{B}}T\chi_0(q)=\frac{\sinh\xi^{-1}}{\cosh\xi^{-1}-\cos q}, \quad \xi^{-1}=-\log\tanh K. \tag{5.13}$$

The peaks get higher and narrower as the temperature goes down, while the area under the curve remains constant, namely 2π.

The second plot is for the case that ξ_{A} and ξ_{B} have a ratio of $4:1$. It is hard to see any difference with the first plot; this is also true for the case with ratio $1:4$,

which is not shown. The third case has ratio $2^{26} : 1$, very close to the decoupling limit; even though there is a clear quantitative difference, qualitatively it still looks like the uniform case. Indeed, in the ferromagnetic Fibonacci case we have from (5.8) and (5.10) that

$$k_{\rm B}T\chi(q) = \sum_{m=-\infty}^{\infty} \frac{\sinh^2 \frac{1}{2}\delta}{(\frac{1}{2}\delta + \pi {\rm i} m)^2} \, \frac{\sinh(\kappa - 2\pi {\rm i} m\alpha)}{\cosh(\kappa - 2\pi {\rm i} m\alpha) - \cos q}. \tag{5.14}$$

In the limit $T \to T_{\rm c} = 0$, both δ and κ tend to zero exponentially fast, and it is not difficult to see that the $m = 0$ term totally dominates (5.14), or $\chi(q) \approx \chi_0(q)$ with $\xi^{-1} = \kappa$. This clear universal behavior, with only a single delta-function divergence at $q = 0$, holds as long as both $K_{\rm A}$ and $K_{\rm B}$ are positive. Similarly, when $K_{\rm A}$ and $K_{\rm B}$ are both negative there is only one divergence at $q = \pi$, as $\chi(q)$ then equals $\chi(q \pm \pi)$ of the ferromagnetic case.

The final plot is for the mixed case with ferro- and antiferromagnetic couplings of equal strength. This last case is very different with clear incommensurate peaks at the lowest temperature. In this mixed case, (5.12) can be rewritten as

$$C^{({\rm c})}(n) \;\; = \;\; \sum_{m=-\infty}^{\infty} \frac{1}{(\pi(m + \frac{1}{2}))^2} \, {\rm e}^{2\pi {\rm i}(m+\frac{1}{2})\alpha n} C_0^{({\rm c})}(n). \tag{5.15}$$

Hence, we have

$$\chi_{\rm m}(q) = \sum_{m=-\infty}^{\infty} \frac{1}{(m + \frac{1}{2})^2 \pi^2} \, \chi_0(q + 2\pi(m + \tfrac{1}{2})\alpha), \quad \alpha = \tfrac{1}{2}(\sqrt{5} - 1), \tag{5.16}$$

indicating the locations and heights of the visible peaks. In fact, $\chi_0(q)$ is periodic mod 2π, so that the peaks are located at $q = 2\pi(m + \frac{1}{2})\alpha + 2\pi n$, with m and n arbitrary integers. The number of visible peaks increases as the temperature decreases and the correlation length ξ increases. It does not matter that we have chosen the antiferromagnetic coupling to be the more abundant one, as the other case follows from this one simply replacing $\chi(q) \to \chi(q \pm \pi)$, corresponding to a flip of sign of every other spin.

It may be worthwhile to note that also in this mixed case we have strong universality, with $\chi(q) \approx \chi_{\rm m}(q)$ as $T \to 0$. Now $\delta \to \pi {\rm i}$ instead of 0, causing all terms in (5.14) to contribute, rather than just the $m = 0$ term.

5.3 Z-INVARIANT FIBONACCI ISING MODEL

We study the simplest two-dimensional ferromagnetic case, which is the Z-invariant Ising model with quasiperiodicity in one or two diagonal directions.

This model is described in terms of two perpendicular sets of diagonal rapidity lines, shown in Fig. 4.1. The rapidity variables $\{u_j\}$ and $\{v_j\}$ form the Fibonacci sequences $\{u_{\rm A}, u_{\rm B}, u_{\rm A}, u_{\rm A}, u_{\rm B}, \cdots\}$ and $\{v_{\rm A}, v_{\rm B}, v_{\rm A}, v_{\rm A}, v_{\rm B}, \cdots\}$. If $v_{\rm A} = v_{\rm B}$, the aperiodicity in the corresponding diagonal direction disappears. As shown in Fig. 4.1, the rapidity lines define a checkerboard lattice with alternatingly black and white faces, where the order variables (spins $\sigma = \pm 1$) and disorder variables (dual spins $\mu \equiv \sigma^*$) live. Two adjacent spins share one vertex which is the intersection of two rapidity lines u_i and v_j.

The pair interaction energies between such pairs of spins are either K_{ij} shown in Fig. 4.2a, or $\bar{K}_{ij}$ shown in Fig. 4.2b. We have given a real elliptic parametrization in (4.1). Two other parametrizations have been used by Baxter[78,79] and Martínez.[84,85] They are

$$\sinh 2K_{ij} = -\mathrm{i}k\,\mathrm{sn}(\mathrm{i}u_i - \mathrm{i}v_j, k), \quad \sinh 2\bar{K}_{ij} = \mathrm{i}/\mathrm{sn}(\mathrm{i}u_i - \mathrm{i}v_j, k), \tag{5.17}$$

suitable for $T > T_{\rm c}$ (or $k < 1$) and

$$\sinh 2K_{ij} = -\mathrm{i}\,\mathrm{sn}(\mathrm{i}u'_i - \mathrm{i}v'_j, 1/k), \quad \sinh 2\bar{K}_{ij} = \mathrm{i}k/\mathrm{sn}(\mathrm{i}u'_i - \mathrm{i}v'_j, 1/k), \tag{5.18}$$

more suited for $T < T_{\rm c}$ (or $k > 1$). This last representation involves an implicit rescaling of the rapidity variables by a factor k, $u'_i = ku_i$, $v'_j = kv_j$, in view of Jacobi's real transformation $k\,\mathrm{sn}(x,k) = \mathrm{sn}(kx, 1/k)$.

The pair correlation functions of the order and disorder variables have been discussed in Chapter IV. Therefore, we can write

$$\langle \sigma_{m,n}\sigma_{m',n'}\rangle = g_{2m'-2m}(k; u_{m-n+1}, \cdots, u_{m'-n'}, v_{m+n}, \cdots, v_{m'+n'-1}),$$

$$\langle \sigma^*_{m,n}\sigma^*_{m',n'}\rangle = g^*_{2m'-2m}(k; u_{m-n+1}, \cdots, u_{m'-n'}, v_{m+n+1}, \cdots, v_{m'+n'}), \tag{5.19}$$

assuming $m + n \le m' + n'$ and $m - n \le m' - n'$, in which case all rapidity lines pass between the spins (or dual spins) in the same direction. Clearly, the same result

holds if $m+n \geq m'+n'$ and $m-n \geq m'-n'$, interchanging (m,n) with (m',n'). On the other hand, if $m+n \leq m'+n'$ and $m-n \geq m'-n'$, we have

$$\langle \sigma_{m,n}\sigma_{m',n'}\rangle = g_{2n'-2n}(k; u_{m'-n'+1},\cdots,u_{m-n},\bar{v}_{m+n},\cdots,\bar{v}_{m'+m'-1}),$$

$$\langle \sigma^*_{m,n}\sigma^*_{m',n'}\rangle = g^*_{2n'-2n}(k; u_{m'-n'+1},\cdots,u_{m-n},\bar{v}_{m+n+1},\cdots,\bar{v}_{m'+n'}), \tag{5.20}$$

where $\bar{v}_j = v_j + \mathrm{K}(k')$. Finally, for $m+n \geq m'+n'$ and $m-n \leq m'-n'$, we have to interchange (m,n) with (m',n') in (5.20). There exist several multiple integral, determinant, and Pfaffian representations[78,82–85] for these functions g_{2m}. In our study of the Fibonacci Ising model in the scaling limit, it is not necessary to use any of these results. We can use the results derived in Chapter 4.

5.4 EFFECTIVE CONNECTED PAIR CORRELATION FUNCTION IN THE SCALING LIMIT

If we assume that the rapidity variables take at most four different values $u_1,\ldots,u_4$ and if we let M_j be the number of times that the value u_j occurs as argument of a given g_{2m} function, then we can define the short-hand notation

$$\begin{aligned} &G(M_1,M_2,M_3,M_4) \\ &\quad = g^{(\mathrm{c})}_{2m}(k; \overbrace{u_1,\cdots,u_1}^{M_1},\overbrace{u_2,\cdots,u_2}^{M_2},\overbrace{u_3,\cdots,u_3}^{M_3},\overbrace{u_4,\cdots,u_4}^{M_4}), \end{aligned} \tag{5.21}$$

with $M_1+M_2+M_3+M_4 = 2m$. Next, if we write $u_1 = u_{\mathrm{A}}$, $u_2 = u_{\mathrm{B}}$, $u_3 = v_{\mathrm{A}}$, $u_4 = v_{\mathrm{B}}$ for the Fibonacci Ising model of this section, then we can apply lemma 2.5 in ref. [97]. This yields the effective connected pair correlation function

$$\begin{aligned} C^{(\mathrm{c})}(m,n) &= \lim_{\mathcal{L}\to\infty} \mathcal{L}^{-2} \sum_{m',n'} \langle \sigma_{m',n'}\sigma_{m'+m,n'+n}\rangle^{(\mathrm{c})} \\ &= (1-\{(m+n)\alpha\})(1-\{(m-n)\alpha\})G(N_1,N_2,N_3,N_4) \\ &\quad +(1-\{(m+n)\alpha\})\{(m-n)\alpha\}G(N_1+1,N_2-1,N_3,N_4)) \end{aligned}$$

$$+\{(m+n)\alpha\}(1-\{(m-n)\alpha\})G(N_1,N_2,N_3+1,N_4-1)$$

$$+\{(m+n)\alpha\}\{(m-n)\alpha\}G(N_1+1,N_2-1,N_3+1,N_4-1), \tag{5.22}$$

where

$$N_1 = m-n-N_2 = \lfloor (m-n)\alpha \rfloor,$$

$$N_3 = m+n-N_4 = \lfloor (m+n)\alpha \rfloor. \tag{5.23}$$

The Fourier transform of (5.22) gives the exact q-dependent susceptibility.

It is to be expected that at temperatures for which the correlation length is short, the q-dependent susceptibility of the aperiodic lattice does not show much difference from that of the periodic lattice. We really need only to examine the case that T is close to T_c. For the remainder of this section we shall restrict ourselves to the scaling limit and use the results of Chapter IV. From (4.8) and (4.9) we find

$$g^{(c)}_{2m}(k;u_1,\cdots,u_{2m}) \approx |1-k^{-2}|^{1/4} f_{\pm}(|t|R), \tag{5.24}$$

with $t = 1-k$ and with f_+ and f_- the connected versions of F and G. In other words, f_- for $T < T_c$ includes a subtraction of the contribution due to the square of the spontaneous magnetization. For correlation functions of the form (5.21), (4.6) reduces to

$$4R^2 = (M_1\cos 2u_1 + M_2\cos 2u_2 + M_3\cos 2u_3 + M_4\cos 2u_4)^2$$

$$+ (M_1\sin 2u_1 + M_2\sin 2u_2 + M_3\sin 2u_3 + M_4\sin 2u_4)^2. \tag{5.25}$$

If the rapidity lines with rapidity variable u_j pass between the two spins in the opposite direction compared to a preferred direction, we have to replace u_j by $u_j \pm \mathrm{K}(0) = u_j \pm \frac{1}{2}\pi$, as explained in Chapter IV. Equivalently, we can replace $M_j > 0$ by $-M_j < 0$. Because of this, R continues smoothly across a boundary where $M_j = 0$.

The spin correlation function of the regular two-dimensional Ising model has this scaling form with $u_1 = u$ and $u_2 = v$, whereas u_3 and u_4 are absent. More precisely, (5.24) reduces to

$$\langle \sigma_{0,0}\sigma_{m,n}\rangle^{(c)} = G(m-n, m+n, 0, 0) \approx |1-k^{-2}|^{1/4} f_{\pm}(|t|R), \tag{5.26}$$

with

$$R = \sqrt{m^2\cos^2(u-v) + n^2\sin^2(u-v)}. \tag{5.27}$$

Here one may have assumed that $m+n$, $m-n \geq 0$. However, (5.27) is valid generally for R large taking in account the remark below (5.25). Therefore, the scaled correlation function is indeed rotationally invariant and, as shown also in Chapter 4, it is given in terms of Painlevé equations[77,91,93].

In order to compare with Vaidya's[90] work on the triangular Ising model, we must study a quadratic Ising model with "SW–NE" diagonal interactions. At criticality, the horizontal interactions K_1, the vertical interactions K_2, and the diagonal interactions K_3 are given by

$$\sinh 2K_1 = \tan(u_1 - u_3), \quad \sinh 2K_2 = \tan(u_3 - u_2), \quad \sinh 2K_3 = \cot(u_1 - u_2). \tag{5.28}$$

Here we have vertical rapidities u_1 pointing north, horizontal rapidities u_2 pointing east, and diagonal rapidities u_3 pointing northeast. Each rapidity line intersects each bond it meets in the middle. Using (5.25), we find that the scaled correlation function is given by

$$\langle \sigma_{0,0}\sigma_{m,n}\rangle^{(c)} = G(m, -n, m-n, 0), \quad \text{for } m \geq 0 \text{ and } n \leq 0. \tag{5.29}$$

Substituting M_i and u_i into (5.25), we find that vector (m, n) corresponds to the scaled distance

$$R^2 = m^2\cos(u-w)^2 + n^2\cos(v-w)^2$$

$$-2mn\cos(u-w)\cos(v-w)\cos(u-v). \tag{5.30}$$

Again, taking in account the remark below (5.25), (5.30) gives R also for the regions with $m < 0$ or $n > 0$. This result for R is proportional to the one of Vaidya[90] after

some simplifications and after identifying $N \equiv m$, $M \equiv n$. Eq. (5.30) gives the most general positive definite quadratic form in m and n. Therefore, the scaled correlation function of the most general periodic Z-invariant Ising model cannot be distinguished from that of the triangular lattice.

5.5 WAVEVECTOR DEPENDENT SUSCEPTIBILITY OF THE FIBONACCI ISING MODEL IN THE SCALING LIMIT

The effective pair correlation of the Z-invariant Fibonacci Ising model has been evaluated exactly in (5.22). We now use (5.24) with R given by (5.25) to rewrite it in the scaling limit as

$$\begin{aligned} C^{(\mathrm{c})}(m,n)|1-k^{-2}|^{-1/4} &\approx f_{\pm}(|t|R_1) \\ &+\{(m-n)\alpha\}[f_{\pm}(|t|R_2)-f_{\pm}(|t|R_1)] \\ &+\{(m+n)\alpha\})[f_{\pm}(|t|R_3)-f_{\pm}(|t|R_1)] \\ &+\{(m-n)\alpha\}\{(m+n)\alpha\}[f_{\pm}(|t|R_1)-f_{\pm}(|t|R_2)-f_{\pm}(|t|R_3)+f_{\pm}(|t|R_4)], \end{aligned} \tag{5.31}$$

where $u_1 = u_{\mathrm{A}}$, $u_2 = u_{\mathrm{B}}$, $u_3 = v_{\mathrm{A}}$, and $u_4 = v_{\mathrm{B}}$. The R_j, for $j = 1,2,3,4$, follow from (5.25) with the substitutions

$$\begin{aligned} R_1: &\quad (M_1,M_2,M_3,M_4) = (N_1,N_2,N_3,N_4), \\ R_2: &\quad (M_1,M_2,M_3,M_4) = (N_1+1,N_2-1,N_3,N_4), \\ R_3: &\quad (M_1,M_2,M_3,M_4) = (N_1,N_2,N_3+1,N_4-1), \\ R_4: &\quad (M_1,M_2,M_3,M_4) = (N_1+1,N_2-1,N_3+1,N_4-1), \end{aligned} \tag{5.32}$$

in accordance with (5.22). Since $\lfloor \alpha(m \pm n) \rfloor \approx \alpha(m \pm n)$ for m,n large, we expand the R_j around R_0, which is given by

$$4R_0^2 = [(m-n)(\alpha \cos 2u_{\mathrm{A}} + (1-\alpha)\cos 2u_{\mathrm{B}})$$

$$+(m+n)(\alpha\cos 2v_{\rm A}+(1-\alpha)\cos 2v_{\rm B})]^2$$

$$+[(m-n)(\alpha\sin 2u_{\rm A}+(1-\alpha)\sin 2u_{\rm B})$$

$$+(m+n)(\alpha\sin 2v_{\rm A}+(1-\alpha)\sin 2v_{\rm B})]^2, \tag{5.33}$$

which has the general quadratic form $A(m-an)^2+B(n+am)^2$ with A, B, and a some constants, no more general than Vaidya's form[90] for the triangular lattice (5.30).

It is straightforward to verify that

$$R_1-R_0+\{(m-n)\alpha\}(R_2-R_1)+\{(m+n)\alpha\}(R_3-R_1)=\mathrm{O}(R_0^{-1}),$$

$$R_i-R_0=\mathrm{O}(1),\qquad R_1-R_2-R_3+R_4=\mathrm{O}(R_0^{-1}), \tag{5.34}$$

when $R_0\to\infty$. Also, we can Taylor expand

$$f_\pm(|t|R_i)=f_\pm(|t|R_0)+|t|(R_i-R_0)f'_\pm(|t|R_0)+\cdots. \tag{5.35}$$

Therefore, in the scaling limit, we find that (5.31) becomes

$$C^{(\mathrm{c})}(m,n)\approx|1-k^{-2}|^{1/4}f_\pm(|t|R_0), \tag{5.36}$$

where the error is of the same order of magnitude as corrections to scaling. In the scaling limit, we have to ignore those higher-order corrections and substitute (5.36) into (5.6), converting the sum to an integral. It is easily seen by comparing (5.36) with (5.27) that the only difference is the change in R, which corresponds to a combination of a rotation and a scale transformation. Hence, the scaled q-dependent susceptibility of the Z-invariant ferromagnetic Fibonacci Ising model is the same as the one of a ferromagnetic Ising model on a triangular lattice. There is only one peak at $q_x=q_y=0 \bmod 2\pi$, whose height is given by the form of the susceptibility of the ferromagnetic uniform two-dimensional Ising model, i.e.

$$\chi(0,0)\approx c_\pm|t|^{-7/4},\qquad t=\frac{T}{T_{\rm c}}-1\propto 1-k. \tag{5.37}$$

except for a change in the constant $c_\pm$. This is another manifestation of universality.

5.6 CONCLUSIONS

Even though several authors have shown that the quasi-periodic Ising model is in the same universality class as the regular Ising model, with the same critical exponents, its wavevector-dependent susceptibility can have multiple incommensurate peaks. However, this only happens when the pair interactions are both attractive and repulsive and the sign of the interactions varies in an incommensurate way.

Indeed, for the mixed Fibonacci Ising model (with an incommensurate sequence of ferro- and antiferromagnetic bonds), $\chi(\mathbf{q})$ has infinitely many divergencies at T_c, which are everywhere dense in the unit cell $0 \leq q_x, q_y \leq 2\pi$. Away from T_c there is a finite number of incommensurate peaks, and more and more of these peaks become invisible as T moves farther away from T_c.

When all pair interactions are ferromagnetic, however, the q-dependent susceptibility behaves just like the one in the regular ferromagnetic Ising model, with only one diverging peak per unit cell located at $(q_x, q_y) = (0, 0)$, in spite of aperiodicity present in the lattice. This is explained by the fact that the spin correlation function in a ferromagnetic Ising Fibonacci lattice decays as a function of distance without changing sign. We have shown this in two examples, the one-dimensional case ($T_c = 0$) in Section 5.2 and the scaling limit of the Z-invariant Ising model in Section 5.5.

In other words, when there are no oscillations in the pair correlation, then there is no trace of the multi-peaks in the q-dependent susceptibility. This is a confirmation of work by Nelson and Widom, that the interference pattern in the icosahedral alloy is a result of the many oscillations in the radial pair correlation functions[98–100].

Not only does the wavevector-dependent susceptibility $\chi(\mathbf{q})$ have but one pronounced peak at $\mathbf{q} = (0, 0)$, leading to a single $T = 0$ divergence, if all the interactions are ferromagnetic; also if the interactions on the quadratic lattice are purely antiferromagnetic we expect only one such peak at $\mathbf{q} = (\pi, \pi)$, even if the magnitudes of the interactions vary quasiperiodically.

For the case with aperiodic mixed signs of the bonds, the pair correlations as seen from (5.12) pick up oscillating phase factors. Thus it follows that the everywhere dense set of overlapping peaks is a result of aperiodic oscillations of the pair correlations. The difference in the number of peaks at different temperatures shows that the number of oscillations per correlation length in the pair correlation function determines the number of visible peaks.

If—instead of aperiodic oscillations—the pair correlation picks up a periodic phase factor, then the diffraction patterns as well as the q-dependent susceptibilities in the two cases differ in two ways. As the correlation length increases, the peaks move and approach their different sets of positions for the two cases, one commensurate and the other incommensurate. Moreover, as $\xi \to \infty$ there is an ever-increasing number of peaks for the aperiodic case, while the number of peaks for the periodic case has an upper bound.

Finally, in our present work we have chosen the underlying lattice to be regular. With our increased knowledge of the correlation functions we should be able to repeat the calculations for certain aperiodic lattices[101–110] like Penrose tilings.

CHAPTER 6

FREE ENERGY OF THE INTEGRABLE CHIRAL POTTS MODEL

6.1 INTRODUCTION

The integrable chiral Potts model is a two-dimensional lattice model—to each site of the lattice we associate a spin which takes N different values and two "rapidity lines" cross each edge.[111] Here we shall consider a square lattice rotated 45° so that the rapidity lines are oriented horizontally and vertically marking the commuting diagonal transfer matrices, which also commute with Hamiltonians of certain quantum spin chains.[112] A recent review of the model is given by Au-Yang et al.[113].

The Boltzmann weights for the pair interaction between the two spins on an edge are given by

$$W_{\rm pq}(n) = \Big(\frac{\mu_{\rm p}}{\mu_{\rm q}}\Big)^n \prod_{j=1}^{n} \frac{y_{\rm q} - x_{\rm p}\omega^j}{y_{\rm p} - x_{\rm q}\omega^j}, \quad \overline{W}_{\rm pq}(n) = (\mu_{\rm p}\mu_{\rm q})^n \prod_{j=1}^{n} \frac{\omega x_{\rm p} - x_{\rm q}\omega^j}{y_{\rm q} - y_{\rm p}\omega^j}, \tag{6.1}$$

in which $\omega = {\rm e}^{2\pi i/N}$. The weights are shown in Fig. 6.1, where the subscripts p and q are the two rapidity variables. We associate with every rapidity line p (or q), a variable $t_{\rm p}$ (or $t_{\rm q}$). Let $\lambda_{\rm p} = \mu_{\rm p}^N$, then λ is related to t by

$$\lambda_{\rm p} + \lambda_{\rm p}^{-1} = (1 + {\rm k'}^2 - {\rm k}^2 {t_{\rm p}}^N)/{\rm k'}, \tag{6.2}$$

where ${\rm k}^2 + {\rm k'}^2 = 1$. The variables k and k′ are fixed and the same for all the rapidity lines, and they are related to the temperature of the the system (with ${\rm k'} \to 0$ for $T \to 0$ and ${\rm k'} \to 1$ for $T \to T_c$). We can uniquely determine λ from this quadratic equation by choosing the branch with either $\lambda > 1$ or $\lambda < 1$. Now, let

$$y_{\rm p}^N = (1 - {\rm k'}\lambda_{\rm p})/{\rm k}, \quad x_{\rm p}^N = (1 - {\rm k'}/\lambda_{\rm p})/{\rm k}. \tag{6.3}$$

Consequently, $x_{\rm p}$, $y_{\rm p}$ and $\mu_{\rm p}$ are given in terms of $t_{\rm p}$ up to an integral power of ω. Since $x_{\rm p}^N y_{\rm p}^N = t_{\rm p}^N$, we make the further restriction $x_{\rm p} y_{\rm p} = t_{\rm p}$. Thus the variables x, y and μ (with subscript p or q) on the right-hand side of (6.1) are now completely determined except for some irrelevant ω factors. It is easily seen from (6.3), that $\lambda \to 1/\lambda$ corresponds to interchanging x and y; thus moving from one Riemann sheet to the other corresponds to interchanging x and y in the weights.

The transfer matrices are defined by

$$T(x_{\rm q}, y_{\rm q})_{\sigma\sigma'} = \prod_{J=1}^{L} W_{\rm pq}(\sigma_J - \sigma'_J)\overline{W}_{\rm p'q}(\sigma_{J+1} - \sigma'_J), \tag{6.4}$$

$$\widehat{T}(x_{\rm q'}, y_{\rm q'})_{\sigma'\sigma''} = \prod_{J=1}^{L} \overline{W}_{\rm pq'}(\sigma'_J - \sigma''_J)W_{\rm p'q'}(\sigma'_J - \sigma''_{J+1}), \tag{6.5}$$

where $L \times M$ denotes the size of the lattice. They have been shown[114] to satisfy some functional relations:

$$\Lambda_{\rm q}^{(j)} T(x_{\rm q}, y_{\rm q})\widehat{T}(\omega^j y_{\rm q}, x_{\rm q}) = \mathbf{X}^{-j}\bar{H}_{\rm p'q}^{(j)}\tau_j(t_{\rm q}) + H_{\rm pq}^{(j)}\tau_{N-j}(\omega^j t_{\rm q}), \tag{6.6}$$

$$\tau_j(t_{\rm q})\tau_2(\omega^{j-1}t_{\rm q}) = {\rm z}(\omega^{j-1}t_{\rm q})\mathbf{X}\tau_{j-1}(t_{\rm q}) + \tau_{j+1}(t_{\rm q}), \tag{6.7}$$

$$\tau_{N+1}(t_{\rm q}) = {\rm z}(t_{\rm q})\mathbf{X}\tau_{N-1}(\omega t_{\rm q}) + (\alpha_{\rm q} + \bar{\alpha}_{\rm q})\mathbf{1}, \tag{6.8}$$

where $\mathbf{X}$ is the spin shift operator,

$$\mathbf{X}_{\sigma,\sigma'} = \prod_{J=1}^{L} \delta(\sigma_J, \sigma'_J + 1), \quad \delta(n,j) = \begin{cases} 1 & \text{if } n = j \bmod N, \\ 0 & \text{otherwise.} \end{cases} \tag{6.9}$$

Unlike the eigenvalues of transfer matrices, whose dependences on $t_{\rm q}$ are very complicated, the elements and the eigenvalues of the matrices $\tau_j(t_{\rm q})$ are polynomials in $t_{\rm q}$ of degree $(j-1)L$ with $\tau_0(t) = 0$ and $\tau_1(t) = 1$. The scalar variables in these equations are

$$\begin{aligned} H_{\rm pq}^{(j)} &= \Big[{\rm k}(\omega\mu_{\rm p})^j \lambda_{\rm q} \prod_{l=0}^{j-1}(t_{\rm p} - \omega^l t_{\rm q})\Big]^L \Big/ [{\rm k}'(1 - \lambda_{\rm q}\lambda_{\rm p})]^L, \\ \bar{H}_{\rm p'q}^{(j)} &= [(1 - \lambda_{\rm q}\lambda_{\rm p'})]^L \Big/ \Big[{\rm k}\mu_{\rm p'}^j \prod_{l=0}^{j-1}(t_{\rm p'} - \omega^l t_{\rm q})\Big]^L, \end{aligned} \tag{6.10}$$

while $\Lambda_{\rm q}^{(j)} = \Lambda_{\rm q}^{(j,0)}$ with

$$\Lambda_{\rm q}^{(j)} = \Big[\mu_{\rm p}^j \prod_{l=0}^{j-1}(y_{\rm q} - \omega^{-l}x_{\rm p}) \prod_{l=0}^{N-j-1}(y_{\rm q} - \omega^l y_{\rm p'})\Big]^L \Big/ [N(y_{\rm p} - x_{\rm q})(y_{\rm q} - y_{\rm p'})]^L, \tag{6.11}$$

$$\mathrm{z}(t_\mathrm{q}) = [\omega\mu_\mathrm{p}\mu_{\mathrm{p}'}(t_\mathrm{p} - t_\mathrm{q})(t_{\mathrm{p}'} - t_\mathrm{q})]^L, \tag{6.12}$$

$$\alpha_\mathrm{q} = [\mathrm{k}'(1 - \lambda_\mathrm{p}\lambda_\mathrm{q})(1 - \lambda_{\mathrm{p}'}\lambda_\mathrm{q})/\mathrm{k}^2\lambda_\mathrm{q}]^L, \tag{6.13}$$

$$\bar{\alpha}_\mathrm{q} = [\mathrm{k}'(\lambda_\mathrm{q} - \lambda_\mathrm{p})(\lambda_\mathrm{q} - \lambda_{\mathrm{p}'})/\mathrm{k}^2\lambda_\mathrm{q}]^L. \tag{6.14}$$

Since all the matrices commute, these relations are the functional relations between their eigenvalues. It is straightforward to verify that

$$\prod_{j=0}^{N-1} \mathrm{z}(\omega^j t_\mathrm{q}) = \alpha_\mathrm{q}\bar{\alpha}_\mathrm{q}. \tag{6.15}$$

It is easily seen from (6.10) that

$$H^{(j)}_{\mathrm{pq}} \Big/ \bar{H}^{(j)}_{\mathrm{p}'\mathrm{q}} = \prod_{l=0}^{j-1} \mathrm{z}(\omega^l t_\mathrm{q}) \Big/ \alpha_\mathrm{q}. \tag{6.16}$$

Consequently, if we let

$$\Gamma^{(j)}_\mathrm{q} = \alpha_\mathrm{q}\Lambda^{(j)}_\mathrm{q} \Big/ \bar{H}^{(j)}_{\mathrm{p}'\mathrm{q}}, \tag{6.17}$$

then (6.6) is equivalent to

$$\Gamma^{(j)}_\mathrm{q} T(x_\mathrm{q}, y_\mathrm{q})\widehat{T}(\omega^j y_\mathrm{q}, x_\mathrm{q}) = \mathbf{X}^{-j}\alpha_\mathrm{q}\tau_j(t_\mathrm{q}) + \prod_{l=0}^{j-1} z(\omega^l t_\mathrm{q})\tau_{N-j}(\omega^j t_\mathrm{q}), \tag{6.18}$$

Iterating (6.7) $N-1$ times, and then combining with (6.8), we find

$$\tau_2(t_\mathrm{q})\tau_2(\omega t_\mathrm{q}) \cdots \tau_2(\omega^{N-1} t_\mathrm{q}) = (\alpha_\mathrm{q} + \bar{\alpha}_\mathrm{q}) + \xi(t), \tag{6.19}$$

where $\xi(t)$ is a sum of products of the polynomials $\tau_2(t)$ and $\mathrm{z}(t)$. From this equation all the coefficients of the polynomial $\tau_2(t)$ can be evaluated in principle by solving a system of $L-1$ coupled Nth order polynomial equations. However, as the lattice size L increases, it becomes a numerical nightmare. When $\tau_2(t)$ is obtained, we can use (6.7) to obtain $\tau_j(t)$ for $j = 3, \cdots, N$ successively.

It is easily verifiable[115] that

$$T(x_\mathrm{q}, y_\mathrm{q})T(\omega x_\mathrm{q}, y_\mathrm{q}) \cdots T(\omega^{N-1} x_\mathrm{q}, y_\mathrm{q}) = d_\mathrm{q} S(\lambda_\mathrm{q}),$$

$$\widehat{T}(y_\mathrm{q}, x_\mathrm{q})\widehat{T}(\omega y_\mathrm{q}, x_\mathrm{q}) \cdots \widehat{T}(\omega^{N-1} y_\mathrm{q}, x_\mathrm{q}) = \hat{d}_\mathrm{q} S(1/\lambda_\mathrm{q}), \tag{6.20}$$

where $S(\lambda)$ is a polynomial in λ of degree $(N-1)L$, and

$$1/d_{\rm q} = c\prod_{j=1}^{N-1}(y_{\rm p'} - \omega^j y_{\rm q})^{jL}\prod_{j=0}^{N-1}(x_{\rm p} - \omega^j y_{\rm q})^{(N-1-j)L},$$
$$1/\hat{d}_{\rm q} = c\prod_{j=1}^{N-1}(y_{\rm p} - \omega^j x_{\rm q})^{jL}\prod_{j=0}^{N-1}(x_{\rm p'} - \omega^j x_{\rm q})^{(N-1-j)L}, \tag{6.21}$$

with $c = [(\lambda_{\rm p}\lambda_{\rm p'})^{(N-1)/2}/N^N]^{L/2}$. Letting $j = 0$ in (6.6), we find

$$\Lambda_{\rm q}^{(0)} T(x_{\rm q}, y_{\rm q})\widehat{T}(y_{\rm q}, x_{\rm q}) = H_{\rm pq}^{(0)}\tau_N(t_{\rm q}), \tag{6.22}$$

whereas letting $j = N$ in (6.6), we obtain

$$\Lambda_{\rm q}^{(N)} T(x_{\rm q}, y_{\rm q})\widehat{T}(y_{\rm q}, x_{\rm q}) = \bar{H}_{\rm pq}^{(N)}\tau_N(t_{\rm q}). \tag{6.23}$$

Thus the identity

$$\bar{H}_{\rm pq}^{(N)}/\Lambda_{\rm q}^{(N)} = H_{\rm pq}^{(0)}/\Lambda_{\rm q}^{(0)} \tag{6.24}$$

must hold, as can be easily verified.

Replacing $x_{\rm q}$ in (6.22) by $\omega x_{\rm q}, \cdots, \omega^{N-1}x_{\rm q}$, and multiplying together all the N resulting equations, we get

$$S(\lambda_{\rm q})S(1/\lambda_{\rm q}) = \mathbf{X}^{-\frac{1}{2}N(N-1)}\tau_N(t_{\rm q})\tau_N(\omega t_{\rm q})\cdots\tau_N(\omega^{N-1}t_{\rm q}). \tag{6.25}$$

Whenever $\tau_N(t)$ is given, this equation can be used together with (6.2) to obtain all the zeroes of $S(\lambda)$. Letting $j = 0, \cdots, N-1$ in (6.6) and multiplying these N equations together, we get

$$T(x_{\rm q}, y_{\rm q})^N \hat{d}_{\rm q} S(\lambda_{\rm q}^{-1}) = \prod_{j=0}^{N-1}\left\{[\bar{H}_{\rm p'q}^{(j)}\tau_j(t_{\rm q}) + H_{\rm pq}^{(j)}\tau_{N-j}(\omega^j t_{\rm q})]\Big/\Lambda_{\rm q}^{(j)}\right\}. \tag{6.26}$$

From this equation, all the eigenvalues of the transfer matrix can be evaluated in principle when the polynomials $S(\lambda_{\rm q})$ and $\tau_j(t_{\rm q})$ are given.

The outline of this chapter is as follows: We review, in Section 2, the steps used by Baxter to obtain the free energy for the N-state chiral Potts model for two different regimes. The results then are extended, in Section 3, to other regimes by rotations and symmetries.

6.2 THE LARGEST EIGENVALUE

To calculate the free energy, we need to calculate the largest eigenvalue of the transfer matrix. To determine which one is the largest eigenvalue, we need to examine the zero-temperature limit, where for the ferromagnetic case, the largest eigenvalue is known. In the chiral Potts model, the limit $T \to 0$ corresponds to $\mathrm{k}' \to 0$. It can be seen from (6.2) that, for given t, λ is either k' or $1/\mathrm{k}'$, depending on the choice of the Riemann sheet with $\lambda < 1$ or $\lambda > 1$. If both t_{q} and t_{p} are arbitrary, then the weights in (6.1) cannot be made to correspond to the zero-temperature ferromagnetic weights with

$$W_{\mathrm{pq}}(n) = \delta(n,0), \quad \overline{W}_{\mathrm{pq}}(-n) = \delta(n,0). \tag{6.27}$$

If, however, we have $t^N \to 1$ for one of the rapidity variables, then the corresponding λ is finite. In this section, the case $|\mu_{\mathrm{q}}| > 1$ but $|\mu_{\mathrm{p}}\mu_{\mathrm{p}'}| < 1$ and $|\mu_{\mathrm{p}}\mu_{\mathrm{p}'}| > 1$ will be considered. We choose

$$\lambda_{\mathrm{q}} \propto 1/\mathrm{k}', \quad x_{\mathrm{p}}, y_{\mathrm{p}}, x_{\mathrm{p}'}, y_{\mathrm{p}'}, x_{\mathrm{q}} \to 1, \quad y_{\mathrm{q}} \to t_{\mathrm{q}}. \tag{6.28}$$

Consequently, (6.1) becomes

$$W_{\mathrm{pq}}(n) \propto \mathrm{k}'^{n/N}, \quad \overline{W}_{\mathrm{pq}}(-n) \propto \mathrm{k}'^{n/N}. \tag{6.29}$$

There are seemingly many other choices—these are the subtleties which we have not yet understood. From (6.29) we find that, as $\mathrm{k}' \to 0$, the Boltzmann weights are zero except when the adjacent spins are equal. Since the shift operator $\mathbf{X}$, the transfer matrices, and the $\tau_j(t_q)$ all commute, they can be simultaneously diagonalized. The common eigenvector, which gives the largest eigenvalue of the transfer matrix in the Q sector, is

$$|Q\rangle = \sum_{\sigma=0}^{N-1} \omega^{Q\sigma} |\sigma\rangle, \quad |\sigma\rangle = |\sigma_1 = \sigma_2 \cdots = \sigma_L = \sigma\rangle, \tag{6.30}$$

such that

$$\mathbf{X}|Q\rangle = \omega^Q |Q\rangle. \tag{6.31}$$

From (BBP3.44) and (BBP3.48),* for a given choice of Q, we can explicitly calculate the corresponding eigenvalue of $\tau_2(t)$ as

$$\tau_2(t_{\rm q}) = (1-\omega t_{\rm q})^L + \omega^{Q+L}(\mu_{\rm p}\mu_{\rm p'})^L(1-t_{\rm q})^L. \tag{6.32}$$

From here on, we shall assume that all the matrices in the functional relations are in their diagonalized form, and we are considering now the functional relation between the leading eigenvalues whose common eigenvector gives the largest eigenvalue of the transfer matrix.

As $L \to \infty$, we find that the case $|\mu_{\rm p}\mu_{\rm p'}| > 1$ is very different from the case $|\mu_{\rm p}\mu_{\rm p'}| < 1$, namely

$$\tau_2(t_{\rm q}) = \begin{cases} (1-\omega t_{\rm q})^L & \text{for } |\mu_{\rm p}\mu_{\rm p'}| < 1, \\ \\ \omega^{Q+L}(\mu_{\rm p}\mu_{\rm p'})^L(1-t_{\rm q})^L & \text{for } |\mu_{\rm p}\mu_{\rm p'}| > 1. \end{cases} \tag{6.33}$$

Consequently, for $|\mu_{\rm p}\mu_{\rm p'}| < 1$, $\tau_2(t) \sim {\rm O}(1)$ and its L zeroes are at ω^{-1}. As the temperature increases, we expect the L zeroes of $\tau_2(t)$ to move away but still to stay around ω^{-1}; while for $|\mu_{\rm p}\mu_{\rm p'}| > 1$, we expect $\tau_2(t) \propto (\mu_{\rm p}\mu_{\rm p'})^L$ and its L zeroes to be around 1. Now from (6.12) we find that ${\rm z}(t) \propto (\mu_{\rm p}\mu_{\rm p'})^L$, thus by comparing the order of magnitude we find from (6.7) that

$$\tau_j(t) = \tau_2(t)\tau_2(\omega t)\cdots\tau_2(\omega^{j-2}t) \begin{cases} \propto 1 & \text{for } |\mu_{\rm p}\mu_{\rm p'}| < 1, \\ \\ \propto (\mu_{\rm p}\mu_{\rm p'})^{(j-1)L} & \text{for } |\mu_{\rm p}\mu_{\rm p'}| > 1. \end{cases} \tag{6.34}$$

In the limit ${\rm k}' \to 0$, we have $\lambda_{\rm q} \gg 1$ and

$$\alpha_{\rm q} \to [\lambda_{\rm q}\lambda_{\rm p}\lambda_{\rm p'}]^L = \lambda_{\rm q}^L[\mu_{\rm p}\mu_{\rm p'}]^{NL}, \qquad \bar{\alpha}_{\rm q} \to \lambda_{\rm q}^L. \tag{6.35}$$

Using (6.34) to estimate the order of magnitude, we find in the limit $L \to \infty$, that (6.19) becomes

$$\tau_2(t_{\rm q})\tau_2(\omega t_{\rm q})\cdots\tau_2(\omega^{N-1}t_{\rm q}) \to \begin{cases} \bar{\alpha}_{\rm q} & \text{if } |\mu_{\rm p}\mu_{\rm p'}| < 1, \\ \\ \alpha_{\rm q} & \text{if } |\mu_{\rm p}\mu_{\rm p'}| > 1. \end{cases} \tag{6.36}$$

*We shall quote equations in ref. 114 as (BBPx.xx) in the following.

Thus when the right-hand side of the equation is given as a function of λ, the problem of finding $\tau_2(t)$ whose zeroes are on one of the Riemann sheets, may be viewed as a generalization of the factorization problem in Wiener-Hopf sum or integral equations. From (6.2), we write

$$t = \omega^m \widehat{\Delta}(\lambda), \qquad \widehat{\Delta}(\lambda) = [(1 + \mathrm{k}'^2 - \mathrm{k}'\lambda - \mathrm{k}'/\lambda)/\mathrm{k}^2]^{1/N}, \tag{6.37}$$

such that the complex λ-plane consists of N Riemann sheets. If all the zeroes of $\tau_2(t)$ are on the lth sheet, then the $N-1$ functions $\tau_2(\omega^m t)$ for $m \neq 0$ have no zeroes on this sheet. Using Cauchy's integral formula, O'Rourke and Baxter derived that for $\lambda_q > 1$, $|\mu_{\mathrm{p}}\mu_{\mathrm{p}'}| < 1$ and $l = -1$ (or $N-1$)

$$\ln \tau_2(t_{\mathrm{q}}) = \frac{1}{2\pi i} \oint_{|\lambda|=1} d\lambda \ln[\widehat{\Delta}(\lambda) - \omega t_{\mathrm{q}}] \frac{d}{d\lambda} \ln \bar{\alpha}_{\mathrm{q}}. \tag{6.38}$$

Letting

$$\lambda = \mathrm{e}^{i\theta}, \qquad \Delta(\theta) = [(1 + \mathrm{k}'^2 - 2\mathrm{k}'\cos\theta)/\mathrm{k}^2]^{1/N} = \widehat{\Delta}(\lambda), \tag{6.39}$$

the above integral can be rewritten as

$$\ln \tau_2(t_{\mathrm{q}}) = \frac{L}{4\pi} \int_0^{2\pi} d\theta \left[\frac{1 + \lambda_{\mathrm{p}} \mathrm{e}^{i\theta}}{1 - \lambda_{\mathrm{p}} \mathrm{e}^{i\theta}} + \frac{1 + \lambda_{\mathrm{p}'} \mathrm{e}^{i\theta}}{1 - \lambda_{\mathrm{p}'} \mathrm{e}^{i\theta}} \right] \ln[\Delta(\theta) - \omega t_{\mathrm{q}}]. \tag{6.40}$$

It is clearly seen from (6.37) and (6.39) that in these integrals, the functions $\Delta(\theta)$ and $\widehat{\Delta}(\lambda)$ are single-valued and their arguments are in $[-\pi/N, \pi/N]$. This expression is exact subject to Baxter's assumption about the location of the zeros, for L large and the argument of t_{q} out of $[-3\pi/N, -\pi/N]$.

Similarly for $|\mu_{\mathrm{p}}\mu_{\mathrm{p}'}| > 1$, when the zeroes of $\tau_2(t)$ are around 1, we find

$$\ln \tau_2(t_{\mathrm{q}}) = L \ln(\omega \mu_{\mathrm{p}} \mu_{\mathrm{p}'}) + \frac{1}{2\pi i} \oint_{|\lambda|=1} d\lambda \, \ln[\widehat{\Delta}(\lambda) - t_{\mathrm{q}}] \frac{d}{d\lambda} \ln \alpha_{\mathrm{q}}, \tag{6.41}$$

yielding

$$\ln \frac{\tau_2(t_{\mathrm{q}})}{(\omega \mu_{\mathrm{p}} \mu_{\mathrm{p}'})^L} = \frac{L}{4\pi} \int_0^{2\pi} d\theta \left[\frac{1 + \lambda_{\mathrm{p}}^{-1} \mathrm{e}^{i\theta}}{1 - \lambda_{\mathrm{p}}^{-1} \mathrm{e}^{i\theta}} + \frac{1 + \lambda_{\mathrm{p}'}^{-1} \mathrm{e}^{i\theta}}{1 - \lambda_{\mathrm{p}'}^{-1} \mathrm{e}^{i\theta}} \right] \ln[\Delta(\theta) - t_{\mathrm{q}}]. \tag{6.42}$$

where the argument of t_{q} is out of range $[-\pi/N, \pi/N]$. For the argument of t_{q} to be in $[-\pi/N, \pi/N]$ and $m \neq 0$, from (6.42) we have

$$\ln \frac{\tau_2(\omega^m t_{\mathrm{q}})}{(\omega \mu_{\mathrm{p}} \mu_{\mathrm{p}'})^L} = \frac{L}{4\pi} \int_0^{2\pi} d\theta \left[\frac{1 + \lambda_{\mathrm{p}}^{-1} \mathrm{e}^{i\theta}}{1 - \lambda_{\mathrm{p}}^{-1} \mathrm{e}^{i\theta}} + \frac{1 + \lambda_{\mathrm{p}'}^{-1} \mathrm{e}^{i\theta}}{1 - \lambda_{\mathrm{p}'}^{-1} \mathrm{e}^{i\theta}} \right] \ln[\Delta(\theta) - \omega^m t_{\mathrm{q}}]. \tag{6.43}$$

Adding (6.43) by taking $m = 1, 2, \cdots, N-1$, we have

$$\sum_{m=1}^{N-1} \ln \frac{\tau_2(\omega^m t_{\rm q})}{(\omega \mu_{\rm p} \mu_{\rm p'})^L} = \frac{L}{4\pi} \int_0^{2\pi} d\theta \left[\frac{1+\lambda_{\rm p}^{-1} {\rm e}^{i\theta}}{1-\lambda_{\rm p}^{-1} {\rm e}^{i\theta}} + \frac{1+\lambda_{\rm p'}^{-1} {\rm e}^{i\theta}}{1-\lambda_{\rm p'}^{-1} {\rm e}^{i\theta}} \right] \sum_{m=1}^{N-1} \ln[\Delta(\theta) - \omega^m t_{\rm q}]. \quad (6.44)$$

We may write

$$\frac{1}{2\pi} \int_0^{2\pi} d\theta \, \frac{1+\lambda {\rm e}^{i\theta}}{1-\lambda {\rm e}^{i\theta}} \sum_{m=0}^{N-1} \ln[\Delta(\theta) - \omega^m t] = \frac{1}{\pi} \int_0^{\pi} d\theta \, \frac{(1-\lambda^2) \ln[\Delta(\theta)^N - t^N]}{1 + \lambda^2 - 2\lambda \cos\theta}, \quad (6.45)$$

and use (6.2) and (6.39) and the integral formulae, valid for $|\lambda|, |\mu| < 1$,

$$\int_0^{\pi} \frac{d\theta \, (1-\lambda^2)}{1 + \lambda^2 - 2\lambda \cos\theta} = \pi, \quad \int_0^{\pi} d\theta \, \frac{\ln(1 + \mu^2 - 2\mu \cos\theta)}{1 + \lambda^2 - 2\lambda \cos\theta} = \frac{2\pi \ln(1-\lambda\mu)}{(1-\lambda^2)}, \quad (6.46)$$

to verify that the $\tau_2(t)$ given by (6.42) is correct for case the argument of $t_{\rm q}$ in $[-\pi/N, \pi/N]$ hence for any $t_{\rm q}$ if $\lambda_q > 1$, $|\mu_{\rm p} \mu_{\rm p'}| > 1$. Similarly, $\tau_2(t)$ given by (6.40) is correct for any $t_{\rm q}$ if $\lambda_q > 1$, $|\mu_{\rm p} \mu_{\rm p'}| < 1$. To summarize, when the right-hand side of (6.36) is given, being a polynomial in λ related to t by (6.2), then $\tau_2(t_{\rm q})$ for $|\lambda_{\rm q}| > 1$, whose zeroes are on the lth sheet of the complex λ plane, is given by

$$\ln \tau_2(t_{\rm q}) = d_0 + \frac{1}{2\pi i} \oint_{|\lambda|=1} d\lambda \, \ln[\omega^l \widehat{\Delta}(\lambda) - t_{\rm q}] \begin{cases} \dfrac{d \ln \bar{\alpha}_{\rm q}}{d\lambda}, & \text{if } |\mu_{\rm p} \mu_{\rm p'}| < 1, \\ \dfrac{d \ln \alpha_{\rm q}}{d\lambda}, & \text{if } |\mu_{\rm p} \mu_{\rm p'}| > 1, \end{cases} \quad (6.47)$$

where d_0 is some constant. From (6.34), we find

$$\tau_N(t) = \tau_2(t) \tau_2(\omega t) \cdots \tau_2(\omega^{N-2} t). \quad (6.48)$$

Consequently, for $|\mu_{\rm p} \mu_{\rm p'}| < 1$, we find that the zeroes of $\tau_N(t)$ are around $\omega^{-1}, \omega^{-2}, \cdots, \omega^{1-N}$; but not on the Riemann sheets with $t = \widehat{\Delta}(\lambda)$. Therefore, we can see from (6.22), that $T(x_{\rm q}, y_{\rm q})$ cannot have zeroes on this sheet also; similarly for $|\mu_{\rm p} \mu_{\rm p'}| > 1$, we find that $T(x_{\rm q}, y_{\rm q})$ has no zeroes on the Riemann sheet $t = \omega \widehat{\Delta}(\lambda)$. Rewriting (6.26) as

$$T(x_{\rm q}, y_{\rm q})^N \hat{d}_{\rm q} \hat{S}(\lambda_{\rm q}) = \lambda_{\rm q}^{(N-1)L} [H_{\rm pq}^{(0)} \tau_N(t_{\rm q}) / \Lambda_{\rm q}^{(0)}] r(\lambda_{\rm q}, t_{\rm q}), \quad (6.49)$$

where $\hat{S}(\lambda_{\rm q}) = \lambda_{\rm q}^{(N-1)L} S(1/\lambda_{\rm q})$ and

$$r(\lambda_{\rm q}, t_{\rm q}) = \prod_{j=1}^{N-1} [\bar{H}_{\rm p'q}^{(j)} \tau_j(t_{\rm q}) / \Lambda_{\rm q}^{(j)}] + \prod_{j=1}^{N-1} [H_{\rm pq}^{(j)} \tau_{N-j}(\omega^j t_{\rm q}) / \Lambda_{\rm q}^{(j)}] \quad (6.50)$$

Baxter and O'Rourke[115,116] then examine (6.49) for $|\mu_{\rm p}\mu_{\rm p'}|<1$, around $t_{\rm q}\sim 1$, where $T(x_{\rm q},y_{\rm q})$ and $\tau_N(t_{\rm q})$ have no zeroes; therefore the zeroes of $r(\lambda_{\rm q},t_{\rm q})$ are the zeroes of $\hat{S}(\lambda_{\rm q})$. Considering the limit ${\rm k}'\to 0$, they[115] then show that the $(N-1)L$ zeroes of $r(\lambda_{\rm q},t_{\rm q})$ lie on $N-1$ circles of different radius, inside the annulus $1<|\lambda_{\rm q}|<1/{\rm k}'$. These zeroes can be surrounded by two contours $\mathcal{C}_-$ and $\mathcal{C}_+$. On the $N-1$ circles where the zeroes of $r(\lambda_{\rm q},t_{\rm q})$ are, the two terms in (6.50) must be of the same order of magnitude, but of opposite sign. As one moves away from these circles, the difference in magnitude of these two terms becomes big. Using Cauchy's integral formula, they write

$$\frac{d}{d\lambda}\ln\hat{S}(\lambda)=\frac{1}{2\pi i}\left[\oint_{\mathcal{C}_+}\frac{d\lambda'}{\lambda-\lambda'}\frac{d}{d\lambda'}\ln r(\lambda',t')-\oint_{\mathcal{C}_-}\frac{d\lambda'}{\lambda-\lambda'}\frac{d}{d\lambda'}\ln r(\lambda',t')\right], \tag{6.51}$$

in which $t'=\widehat{\Delta}(\lambda')$. Guided by the results obtained in the limit ${\rm k}'\to 0$, Baxter and O'Rourke found that on the contour $\mathcal{C}_+$ the second term of $r(\lambda,t)$ in (6.50) dominates in the limit $L\to\infty$, and on the contour $\mathcal{C}_-$ the first term dominates. After dropping the exponentially small terms, the two contours can be shifted to the unit circle. Performing integration with respect to λ, they obtain

$$\ln\hat{S}(\lambda)=d_1+\frac{1}{2\pi i}\oint_{|\lambda'|=1}d\lambda'\,\ln(\lambda-\lambda')\frac{d}{d\lambda'}\sum_{j=1}^{N-1}\ln\left[\frac{H^{(j)}_{\rm pq}\tau_{N-j}(\omega^j t')}{\bar{H}^{(j)}_{\rm p'q}\tau_j(t')}\right], \tag{6.52}$$

where d_1 is some constant. We use (6.16) to find

$$\prod_{j=1}^{N-1}[H^{(j)}_{\rm pq}/\bar{H}^{(j)}_{\rm p'q}]=\alpha_{\rm q}^{-(N-1)}\prod_{l=0}^{N-1}{\rm z}(\omega^l t_{\rm q})^{N-1-l}=\bar{\alpha}_{\rm q}^{(N-1)}\prod_{l=1}^{N-1}{\rm z}(\omega^l t_{\rm q})^{-l}, \tag{6.53}$$

where (6.15) is also used, and from (6.34) obtain

$$\sum_{j=1}^{N-1}\ln[\tau_{N-j}(\omega^j t')/\tau_j(t')]=\sum_{j=1}^{N-1}(N-2j)\ln\tau_2(\omega^{j-1}t'). \tag{6.54}$$

Since the zeroes of $\tau_2(t)$ are around ω^{-1}, we find $\tau_2(\omega^{j-1}t)$ for $j=1,\cdots,N-1$ have no zeroes on the sheet $t=\widehat{\Delta}(\lambda)$, thus the above function is single-valued on this Riemann sheet. Similarly, we find ${\rm z}(\omega^j t)$ for $j=1,\cdots,N-1$ have no zeroes on the sheet $t=\widehat{\Delta}(\lambda)$ either, as seen from (6.12) and (6.28).

After substituting the second identity in (6.53) and (6.54) into (6.52), the integration involving $\bar{\alpha}_{\rm q}$ can be carried out explicitly, while the rest of the integrand has

been shown to be a single-valued function on the sheet $t = \widehat{\Delta}(\lambda)$. Using the identity

$$\oint d\lambda\, f(\lambda)\frac{dg(\lambda)}{d\lambda} = -\oint d\lambda\, g(\lambda)\frac{df(\lambda)}{d\lambda}, \tag{6.55}$$

which is valid if $f(\lambda)$ and $g(\lambda)$ are singled-valued, and (6.40), we arrive at the final result

$$\ln \hat{S}(\lambda_{\rm q}) = d_1 + (N-1)\ln \bar{\alpha}_{\rm q} - \tfrac{1}{2}L[A(\lambda_{\rm q}^{-1}, t_{\rm p})$$

$$+A(\lambda_{\rm q}^{-1}, t_{\rm p'}) + B(\lambda_{\rm p}, \lambda_{\rm q}^{-1}) + B(\lambda_{\rm p'}, \lambda_{\rm q}^{-1})], \tag{6.56}$$

where

$$A(\lambda_{\rm q}, t_{\rm p}) = \frac{1}{2\pi}\int_0^{2\pi} d\theta\, \frac{1+\lambda_{\rm q}{\rm e}^{i\theta}}{1-\lambda_{\rm q}{\rm e}^{i\theta}} \sum_{j=1}^{N-1}(N-j)\ln[\omega^{-j/2}\Delta(\theta) - \omega^{j/2}t_{\rm p}], \tag{6.57}$$

and

$$B(\lambda_{\rm p}, \lambda_{\rm q}) = \frac{1}{8\pi^2}\int_0^{2\pi} d\theta\, \frac{1+\lambda_{\rm p}{\rm e}^{i\theta}}{1-\lambda_{\rm p}{\rm e}^{i\theta}} \int_0^{2\pi} d\phi\, \frac{1+\lambda_{\rm q}{\rm e}^{i\phi}}{1-\lambda_{\rm q}{\rm e}^{i\phi}}$$

$$\times \sum_{j=1}^{N-1}(N-2j)\ln[\omega^{-j/2}\Delta(\theta) - \omega^{j/2}\Delta(\phi)]. \tag{6.58}$$

If instead, we use the first identity in (6.53), we would obtain the identical result, even though it is more difficult to justify using (6.55).

These are the most crucial steps. If one uses (6.25) to determine the zeroes of $\hat{S}(\lambda)$, one would find from (6.48) that they are the image of the zeroes of $\tau_2(t)$. This means that instead of the zeroes of $\hat{S}(\lambda)$ lying on the $N-1$ circles of different radius, as implied by the solution in (6.56), they would be lying on just one circle. This just shows the ingenuity of Baxter in being able to choose the right path.

Similarly, for $|\mu_{\rm p}\mu_{\rm p'}| > 1$, we again find from (6.50) that the zeroes of $\hat{S}(\lambda)$ can be surrounded by two contours $\mathcal{C}_-$ and $\mathcal{C}_+$, and that Cauchy's integral formula (6.51) still holds. We then estimate the order of magnitude of the two terms in (6.50) for $t' \sim \omega$ in the limit ${\rm k}' \to 0$. We now find on the contour $\mathcal{C}_+$ the first term in (6.50) dominating instead, while on the contour $\mathcal{C}_-$ the second term dominates. We

again drop the insignificant terms, shift the two contours to the unit circle, and then integrate with respect to λ to obtain a similar equation,

$$\ln \hat{S}(\lambda) = d_2 - \frac{1}{2\pi i}\oint_{|\lambda'|=1} d\lambda' \, \ln(\lambda-\lambda')\frac{d}{d\lambda'}\sum_{j=1}^{N-1} \ln\left[\frac{H^{(j)}_{\mathrm{pq}}\tau_{N-j}(\omega^j t')}{\bar{H}^{(j)}_{\mathrm{p'q}}\tau_j(t')}\right]. \tag{6.59}$$

This equation differs from (6.52) not only in the sign in front of the integral, but also in the variable t'. Here we have $t' = \omega\widehat{\Delta}(\lambda')$ instead of $t' = \widehat{\Delta}(\lambda')$. It may be worthwhile to mention again, that calculating the largest eigenvalue of the transfer matrix, we find for $|\mu_{\mathrm{p}}\mu_{\mathrm{p'}}| < 1$, the zeroes of $r(\lambda_{\mathrm{q}}, t_{\mathrm{q}})$ on the Riemann sheet $t' = \widehat{\Delta}(\lambda')$ are the zeroes of $\hat{S}(\lambda')$, whereas for $|\mu_{\mathrm{p}}\mu_{\mathrm{p'}}| > 1$, the zeroes of $r(\lambda_{\mathrm{q}}, t_{\mathrm{q}})$ on the sheet $t' = \omega\widehat{\Delta}(\lambda')$ are the zeroes of $\hat{S}(\lambda')$. Using (6.53), (6.54) and (6.42), we find (6.59) becomes

$$\ln \hat{S}(\lambda_{\mathrm{q}}) = d_2 + (N-1)\ln\alpha_{\mathrm{q}} - \tfrac{1}{2}L[C(\lambda_{\mathrm{q}}^{-1}, t_{\mathrm{p}})$$

$$+C(\lambda_{\mathrm{q}}^{-1}, t_{\mathrm{p'}}) - B(\lambda_{\mathrm{p}}^{-1}, \lambda_{\mathrm{q}}^{-1}) - B(\lambda_{\mathrm{p'}}^{-1}, \lambda_{\mathrm{q}}^{-1})], \tag{6.60}$$

where

$$C(\lambda_{\mathrm{q}}, t_{\mathrm{p}}) = \frac{1}{2\pi}\int_0^{2\pi} d\theta \frac{1+\lambda_{\mathrm{q}}\mathrm{e}^{i\theta}}{1-\lambda_{\mathrm{q}}\mathrm{e}^{i\theta}} \sum_{j=1}^{N-1} j \ln[\omega^{-j/2}\Delta(\theta) - \omega^{j/2}t_{\mathrm{p}}]. \tag{6.61}$$

Finally as $\hat{S}(\lambda)$ is now given, (6.49) can be used to calculate the largest eigenvalue of the transfer matrix, by dropping the exponentially small term in (6.50). From (6.16) and (6.14), we find that the ratio of the first term to the second term in (6.50) is of the order $(\mu_{\mathrm{p}}\mu_{\mathrm{p'}})^{N(N-1)L/2}$, thus for $|\mu_{\mathrm{p}}\mu_{\mathrm{p'}}| < 1$, the first term is exponentially small, while for $|\mu_{\mathrm{p}}\mu_{\mathrm{p'}}| > 1$, the second term is exponentially small. That is

$$\hat{S}(\lambda_{\mathrm{q}})T(x_{\mathrm{q}}, y_{\mathrm{q}})^N = \begin{cases} \epsilon_{\mathrm{q}}\,\bar{\alpha}_{\mathrm{q}}^{(N-1)} \prod_{j=0}^{N-1}[\tau_{N-j}(\omega^j t_{\mathrm{q}})\mathrm{z}(\omega^j t_{\mathrm{q}})^{-j}], & \text{if } |\mu_{\mathrm{p}}\mu_{\mathrm{p'}}| < 1, \\ \epsilon_{\mathrm{q}} \prod_{j=1}^{N}\tau_j(t_{\mathrm{q}}), & \text{if } |\mu_{\mathrm{p}}\mu_{\mathrm{p'}}| > 1, \end{cases} \tag{6.62}$$

where

$$\epsilon_{\mathrm{q}} = \hat{d}_{\mathrm{q}}^{-1}\lambda_{\mathrm{q}}^{(N-1)L}\prod_{j=1}^{N}[\bar{H}^{(j)}_{\mathrm{p'q}}/\Lambda^{(j)}_{\mathrm{q}}], \tag{6.63}$$

and (6.24) and (6.53) are used for the first case. It is easy to show from (6.10) and (6.11) that

$$\epsilon_{\rm q} = [\rho_{\rm pq}\bar{D}_{\rm p'q}\Phi_0]^{NL}[\lambda_{\rm q}^2\lambda_{\rm p}/\lambda_{\rm p'}]^{(N-1)L/4}, \tag{6.64}$$

in which

$$\rho_{\rm pq}^N = \prod_{n=1}^{N-1} W_{\rm pq}(n), \qquad \bar{\rho}_{\rm pq}^N = \prod_{n=1}^{N-1} \overline{W}_{\rm pq}(n),$$

$$D_{\rm pq}^N = \det_N[W_{\rm pq}(i-j)], \qquad \bar{D}_{\rm pq}^N = \det_N[\overline{W}_{\rm pq}(i-j)]. \tag{6.65}$$

It was shown in these papers[113,117,118] that

$$\bar{D}_{\rm pq}^N = N^{N/2}\Phi_0^{-N}\prod_{j=1}^{N-1}\frac{(t_{\rm p}-\omega^j t_{\rm q})^j}{(y_{\rm q}-\omega^{-j}y_{\rm p})^j(x_{\rm p}-\omega^j x_{\rm q})^j} \tag{6.66}$$

with

$$\Phi_0 \equiv {\rm e}^{i\pi(N-1)(N-2)/12N} \tag{6.67}$$

and

$$[\bar{D}_{\rm pq}/\bar{\rho}_{\rm pq}]^N = N^{N/2}\Phi_0^{-N}[(y_{\rm q}^N-y_{\rm p}^N)(x_{\rm p}^N-x_{\rm q}^N)]^{-\frac{1}{2}(N-1)}\prod_{j=1}^{N-1}(t_{\rm p}-\omega^j t_{\rm q})^j,$$

$$[\bar{D}_{\rm pq}D_{\rm pq}/\rho_{\rm pq}\bar{\rho}_{\rm pq}]^N = N^N/{\rm k}^{N-1}. \tag{6.68}$$

From (6.34), we find

$$\sum_{j=0}^{N-1}\ln\tau_{N-j}(\omega^j t_{\rm q}) = \sum_{j=1}^{N-1} j\ln\tau_2(\omega^{j-1}t_{\rm q}), \tag{6.69}$$

$$\sum_{j=1}^{N}\ln\tau_j(t_{\rm q}) = \sum_{j=1}^{N-1}(N-j)\ln\tau_2(\omega^{j-1}t_{\rm q}). \tag{6.70}$$

Consequently, equations (6.62) and (6.64) can be used to give the largest eigenvalue of the transfer matrix as

$$N\ln T_{\rm q} = \tfrac{1}{2}LN(\ln\tilde{\kappa}_{\rm pq}+\ln\tilde{\kappa}_{\rm p'q}+\ln\rho_{\rm pq}+\ln\bar{D}_{\rm p'q}), \tag{6.71}$$

in which we substitute (6.40) into (6.69) and use (6.56) for $\hat{S}$ to obtain, for $|\mu_{\rm p}\mu_{\rm p'}|<1$,

$$N\ln\tilde{\kappa}_{\rm pq} = \tfrac{1}{2}(N-1)\ln(\lambda_{\rm q}/\lambda_{\rm p}) - 2\sum_{j=1}^{N-1}(N-j)\ln[\omega^{-j/2}t_{\rm q}-\omega^{j/2}t_{\rm p}]$$

$$+C(\lambda_{\rm p},t_{\rm q})+A(\lambda_{\rm q}^{-1},t_{\rm p})+B(\lambda_{\rm p},\lambda_{\rm q}^{-1}). \tag{6.72}$$

As can be seen from (6.28) and the fact that the zeroes of $\hat{S}$ are evaluated on the Riemann sheet $t_{\rm q}=\widehat{\Delta}(\lambda_{\rm q})$, we find that the above expression is valid for

$$|\lambda_{\rm q}|>1 \text{ and } -\frac{\pi}{N}\le \arg t_{\rm p}, \arg t_{\rm q}\le \frac{\pi}{N}.$$

Similarly, we use (6.42) in (6.70) and (6.60) for $\hat{S}$ to express (6.62) for $|\mu_{\rm p}\mu_{\rm p'}|>1$ as

$$N\ln\tilde{\kappa}_{\rm pq}=\tfrac{1}{2}(N-1)\ln(\lambda_{\rm q}/\lambda_{\rm p})-(N-1)\ln[{\rm k}'(1-\lambda_{\rm q}\lambda_{\rm p})^2/\lambda_{\rm q}{\rm k}^2]$$

$$+A(\lambda_{\rm p}^{-1},\omega^{-1}t_{\rm q})+C(\lambda_{\rm q}^{-1},t_{\rm p})-B(\lambda_{\rm p}^{-1},\lambda_{\rm q}^{-1})+d_3, \tag{6.73}$$

where d_3 is again some constant to be determined. It is easily seen from (6.57) and (6.61) that

$$I(\lambda_{\rm p},t_{\rm q})\equiv A(\lambda_{\rm p},t_{\rm q})+C(\lambda_{\rm p},\omega t_{\rm q})$$

$$=\frac{(N-1)}{2\pi}\int_0^{2\pi}d\theta\,\frac{1+\lambda_{\rm p}{\rm e}^{i\theta}}{1-\lambda_{\rm p}{\rm e}^{i\theta}}\ln\{[\Delta(\theta)^N-t_{\rm q}^N]\,\omega^{-N^2/2}\}. \tag{6.74}$$

From (6.45) and (6.46) we find the identity, for $|\lambda_{\rm p}|<1$,

$$I(\lambda_{\rm p},t_{\rm q})=-N(N-1)\frac{\pi}{2}+\begin{cases}(N-1)\ln[{\rm k}'(\lambda_{\rm q}-\lambda_{\rm p})^2/\lambda_{\rm q}{\rm k}^2] & \text{for } |\lambda_{\rm q}|>1,\\ \\ (N-1)\ln[{\rm k}'(1-\lambda_{\rm p}\lambda_{\rm q})^2/\lambda_{\rm q}{\rm k}^2] & \text{for } |\lambda_{\rm q}|<1.\end{cases} \tag{6.75}$$

Now we use (6.75) in (6.73) to obtain

$$N\ln\tilde{\kappa}_{\rm pq}=\tfrac{1}{2}(N-1)\ln(\lambda_{\rm q}/\lambda_{\rm p})$$

$$-C(\lambda_{\rm p}^{-1},t_{\rm q})+C(\lambda_{\rm q}^{-1},t_{\rm p})-B(\lambda_{\rm p}^{-1},\lambda_{\rm q}^{-1}). \tag{6.76}$$

We may also use (6.75) when p and q are interchanged to write (6.73) as

$$\ln\tilde{\kappa}_{\rm pq}^N=\tfrac{1}{2}(N-1)\ln(\lambda_{\rm p}/\lambda_{\rm q})$$

$$+A(\lambda_{\rm p}^{-1},\omega^{-1}t_{\rm q})-A(\lambda_{\rm q}^{-1},\omega^{-1}t_{\rm p})-B(\lambda_{\rm p}^{-1},\lambda_{\rm q}^{-1}). \tag{6.77}$$

Since $\hat{S}$ given by (6.60) is evaluated on the Riemann sheet $t_{\rm q}=\omega\widehat{\Delta}(\lambda_{\rm q})$, we find from (6.28), that equations (6.73), (6.76) and (6.77) are valid for the regime $-\pi/N\le \arg t_{\rm p}, \arg(t_{\rm q}/\omega)\le \pi/N$.

When the rapidity lines satisfy ${\rm p}={\rm p}'$, the partition function is denoted by $Z_{\rm pq}$ and the partition function per site[117] is then

$$\kappa_{\rm pq}=Z_{\rm pq}^{1/ML}=\tilde{\kappa}_{\rm pq}\rho_{\rm pq}\bar{D}_{\rm pq}. \tag{6.78}$$

From the inversion relation, Baxter[117] has shown

$$\tilde{\kappa}_{\rm pq}\tilde{\kappa}_{\rm qp}=1. \tag{6.79}$$

On the other hand, from (6.58), we find

$$B(\lambda_{\rm p}^{-1},\lambda_{\rm q}^{-1})=-B(\lambda_{\rm q}^{-1},\lambda_{\rm p}^{-1}). \tag{6.80}$$

Consequently, we can see easily that (6.76) and (6.77) indeed satisfy this inversion relation (6.79). This shows that the constants are correctly chosen.

Baxter[116] has also shown that, for $|\mu_{\rm p}|<1$ and $|\mu_{\rm q}|<1$,

$$N\ln\tilde{\kappa}_{\rm pq}=\tfrac{1}{2}(N-1)\ln(\lambda_{\rm q}/\lambda_{\rm p})+A(\lambda_{\rm p},t_{\rm q})-A(\lambda_{\rm q},t_{\rm p})-B(\lambda_{\rm p},\lambda_{\rm q}), \tag{6.81}$$

valid in $-\pi/N\le \arg t_{\rm p}, \arg t_{\rm q}\le \pi/N$. It is shown by Baxter[115] that (6.72) is an analytic continuation of (6.81) as $\lambda_{\rm q}$ moves from the inside of the unit circle to the outside.

6.3 ROTATIONS AND SYMMETRIES

The weights satisfy the properties[111,117]

$$W_{\rm pq}(n)=\overline{W}_{\rm q^*p}(n),\quad \overline{W}_{\rm pq}(n)=W_{\rm q^*p}(-n), \tag{6.82}$$

where ${\rm q}^*={\rm R}^{-1}{\rm q}$, namely

$$\mu_{\rm q^*}=1/\mu_{\rm q},\quad x_{\rm q^*}=\omega^{-1}y_{\rm q},\quad y_{\rm q^*}=x_{\rm q}; \tag{6.83}$$

and

$$W_{\rm pq}(n) = \overline{W}_{\rm q,Rp}(-n), \quad \overline{W}_{\rm pq}(n) = W_{\rm q,Rp}(-n), \tag{6.84}$$

in which

$$\mu_{\rm Rp} = 1/\mu_{\rm p}, \quad x_{\rm Rp} = y_{\rm p}, \quad y_{\rm Rp} = \omega x_{\rm p}. \tag{6.85}$$

Combining them, we find

$$W_{\rm pq}(n) = W_{\rm Rp,Rq}(-n), \quad \overline{W}_{\rm pq}(n) = \overline{W}_{\rm Rp,Rq}(-n). \tag{6.86}$$

From the definitions in (6.65), we obtain

$$\rho_{\rm Rp,Rq} = \rho_{\rm pq}\,, \qquad \rho_{\rm q,Rp} = \bar{\rho}_{\rm pq}\,, \qquad \rho_{\rm q^*p} = \bar{\rho}_{\rm pq}\,,$$

$$\bar{D}_{\rm Rp,Rq} = \bar{D}_{\rm pq}\,, \qquad \bar{D}_{\rm q,Rp} = D_{\rm pq}\,, \qquad \bar{D}_{\rm q^*p} = D_{\rm pq}\,. \tag{6.87}$$

From these relations, we find that the partition per site defined in (6.78) satisfies

$$\kappa_{\rm pq} = \kappa(x_{\rm p}, y_{\rm p}, x_{\rm q}, y_{\rm q}) = \kappa_{\rm Rp,Rq} = \kappa(\omega y_{\rm p}, x_{\rm p}, \omega y_{\rm q}, x_{\rm q}) \tag{6.88}$$

$$= \kappa_{\rm q^*p} = \kappa(\omega^{-1} y_{\rm q}, x_{\rm q}, x_{\rm p}, y_{\rm p}) \tag{6.89}$$

$$= \kappa_{\rm q,Rp} = \kappa(x_{\rm q}, y_{\rm q}, \omega y_{\rm p}, x_{\rm p}) \tag{6.90}$$

$$= \kappa_{\rm R^2p,R^2q} = \kappa(\omega x_{\rm p}, \omega y_{\rm p}, \omega x_{\rm q}, \omega y_{\rm q}) = \kappa_{\rm R^mp,R^mq}. \tag{6.91}$$

Hence,

$$\kappa_{\rm R^mp,R^mq} = \begin{cases} \kappa(\omega^{\frac{1}{2}m} x_{\rm p}, \omega^{\frac{1}{2}m} y_{\rm p}, \omega^{\frac{1}{2}m} x_{\rm q}, \omega^{\frac{1}{2}m} y_{\rm q}), & m \text{ even}, \\ \kappa(\omega^{\frac{1}{2}(m+1)} y_{\rm p}, \omega^{\frac{1}{2}(m-1)} x_{\rm p}, , \omega^{\frac{1}{2}(m+1)} y_{\rm q}, \omega^{\frac{1}{2}(m-1)} x_{\rm q}), & m \text{ odd}. \end{cases} \tag{6.92}$$

As mentioned earlier, interchanging x and y is equivalent to changing λ to $1/\lambda$. Thus, these rotations allow one to extend (6.72), (6.77) and (6.81) to other regimes.

We first consider the automorphism T, given in refs. [111,114], that leaves $t = xy$ and λ unchanged. Let

$$\mu_{\rm Tq} = \omega^{-1}\mu_{\rm q}, \quad x_{\rm Tq} = \omega x_{\rm q}, \quad y_{\rm Tq} = \omega^{-1} y_{\rm q}. \tag{6.93}$$

Then we find from (6.1) that

$$W_{\rm p,Tq}(n) = \frac{W_{\rm pq}(n+1)}{W_{\rm pq}(1)}, \quad \overline{W}_{\rm p,Tq}(n) = \frac{\overline{W}_{\rm pq}(n+1)}{\overline{W}_{\rm pq}(1)}. \tag{6.94}$$

As a consequence, the partition function satisfies

$$Z_{\mathrm{p,Tq}} = [W_{\mathrm{pq}}(1)\overline{W}_{\mathrm{pq}}(1)]^{-ML} Z_{\mathrm{pq}}. \tag{6.95}$$

From (6.65), it is seen that

$$\rho_{\mathrm{p,Tq}} = \frac{\rho_{\mathrm{pq}}}{W_{\mathrm{pq}}(1)}, \quad \bar{D}_{\mathrm{p,Tq}} = (-1)^{(N-1)/N} \frac{\bar{D}_{\mathrm{pq}}}{\overline{W}_{\mathrm{pq}}(1)}. \tag{6.96}$$

Therefore, for odd $N = 2n+1$, we find from (6.95), (6.96) and (6.78) that

$$\tilde{\kappa}_{\mathrm{p,Tq}} = \tilde{\kappa}(x_{\mathrm{p}}, y_{\mathrm{p}}, \omega x_{\mathrm{q}}, \omega^{-1} y_{\mathrm{q}}) = \tilde{\kappa}(x_{\mathrm{p}}, y_{\mathrm{p}}, x_{\mathrm{q}}, y_{\mathrm{q}}). \tag{6.97}$$

Similarly, we find

$$\tilde{\kappa}_{\mathrm{Tp,q}} = \tilde{\kappa}(\omega x_{\mathrm{p}}, \omega^{-1} y_{\mathrm{p}}, x_{\mathrm{q}}, y_{\mathrm{q}}) = \tilde{\kappa}(x_{\mathrm{p}}, y_{\mathrm{p}}, x_{\mathrm{q}}, y_{\mathrm{q}}). \tag{6.98}$$

This shows that the automorphism T leaves the normalized partition function per site $\tilde{\kappa}$ invariant for odd $N = 2n+1$.

Letting $m = 2n = N-1$ in (6.92), and using (6.87), (6.97) and (6.98), we find that (6.91) becomes

$$\tilde{\kappa}_{\mathrm{pq}} = \tilde{\kappa}(\omega^n x_{\mathrm{p}}, \omega^n y_{\mathrm{p}}, \omega^n x_{\mathrm{q}}, \omega^n y_{\mathrm{q}}) = \tilde{\kappa}(\omega^{-1} x_{\mathrm{p}}, y_{\mathrm{p}}, \omega^{-1} x_{\mathrm{q}}, y_{\mathrm{q}}), \tag{6.99}$$

in which the λ remains unchanged, but in which $t_{\mathrm{q}}, t_{\mathrm{p}}$ shift to $\omega^{-1} t_{\mathrm{q}}, \omega^{-1} t_{\mathrm{p}}$.

Similarly, we let $m = 2n+1 = N$ in (6.92) to obtain

$$\tilde{\kappa}_{\mathrm{pq}} = \tilde{\kappa}(\omega^{-n} y_{\mathrm{p}}, \omega^n x_{\mathrm{p}}, \omega^{-n} y_{\mathrm{q}}, \omega^n x_{\mathrm{q}}) = \tilde{\kappa}(y_{\mathrm{p}}, x_{\mathrm{p}}, y_{\mathrm{q}}, x_{\mathrm{q}}). \tag{6.100}$$

Thus this transformation relates the normalized partition functions where the $t_{\mathrm{q}}, t_{\mathrm{p}}$ are unchanged but λ is replaced by $1/\lambda$.

For $|\lambda_{\mathrm{p}}|, |\lambda_{\mathrm{q}}| < 1$, we find $|\lambda_{\mathrm{Rp}}|, |\lambda_{\mathrm{Rq}}| > 1$. If also $-\pi/N \le \arg t_{\mathrm{Rp}} \le \pi/N$, and $\pi/N \le \arg t_{\mathrm{Rq}} \le 3\pi/N$, then (6.77) hold for $\tilde{\kappa}_{\mathrm{Rp,Rq}}$. Consequently, we find using (6.87) that

$$\ln \tilde{\kappa}_{\mathrm{pq}}^N = \ln \tilde{\kappa}_{\mathrm{Rp,Rq}}^N = \tfrac{1}{2}(N-1) \ln(\lambda_{\mathrm{Rp}}/\lambda_{\mathrm{Rq}})$$

$$+ A(\lambda_{\mathrm{Rp}}^{-1}, \omega^{-1} t_{\mathrm{Rq}}) - A(\lambda_{\mathrm{Rq}}^{-1}, \omega^{-1} t_{\mathrm{Rp}}) - B(\lambda_{\mathrm{Rp}}^{-1}, \lambda_{\mathrm{Rq}}^{-1}), \tag{6.101}$$

which, as seen from (6.85), is identical to (6.81), except for the regime of validity. Combining the two regimes we find (6.105) listed in the table below and valid for $-3\pi/N \le \arg(t_{\rm p}) \le \pi/N$ and $-\pi/N \le \arg(t_{\rm q}) \le \pi/N$.

For $|\lambda_{\rm p}|, |\lambda_{\rm q}| > 1$, $-3\pi/N \le \arg(t_{\rm p}) \le \pi/N$ and $-\pi/N \le \arg(t_{\rm q}) \le \pi/N$, we use (6.100) to invert (6.105), and the result is (6.106) which is also listed in the table, and it differs from (6.77) in that $\omega^{-1}t$ in (6.77) becomes t in (6.106). Since the regimes of validity for the two equations are different by a multiplicative ω factor, this is consistent with (6.99).

From (6.87), we find

$$\ln \tilde{\kappa}_{\rm q,Rp} = \ln \tilde{\kappa}_{\rm q^*p} = \ln \tilde{\kappa}_{\rm pq} + \ln(\rho_{\rm pq}/\bar{\rho}_{\rm pq}) + \ln(\bar{D}_{\rm pq}/D_{\rm pq}). \tag{6.102}$$

For $|\lambda_{\rm p}| < 1$, $|\lambda_{\rm q}| > 1$, such that $|\lambda_{\rm q*}| < 1$, we consider the regime where $-3\pi/N \le \arg(t_{\rm q*}) \le \pi/N$ and $-\pi/N \le \arg(t_{\rm p}) \le \pi/N$, such that (6.105) holds for $\tilde{\kappa}_{\rm q^*p}$,

$$\ln \tilde{\kappa}^N_{\rm q^*p} = \tfrac{1}{2}(N-1)\ln(\lambda_{\rm p}\lambda_{\rm q}) + A(\lambda_{\rm q}^{-1}, t_{\rm p}) - A(\lambda_{\rm p}, \omega^{-1}t_{\rm q}) - B(\lambda_{\rm q}^{-1}, \lambda_{\rm p}). \tag{6.103}$$

Using (6.68) and (6.75), we may rewrite (6.102) as

$$\ln \tilde{\kappa}^N_{\rm q^*p} = \ln \tilde{\kappa}^N_{\rm pq} + (N-1)\ln\lambda_{\rm p} + 2\sum_{j=1}^{N-1}(N-j)\ln(\omega^{-j/2}t_{\rm q} - \omega^{j/2}t_{\rm p})$$

$$-A(\lambda_{\rm p}, \omega^{-1}t_{\rm q}) - C(\lambda_{\rm p}, t_{\rm q}). \tag{6.104}$$

Consequently, we find (6.107) in the table, which is again identical to (6.72), but with region of validity extended. This shows that all the calculations are consistent.

Finally, for $|\lambda_{\rm p}| > 1$, $|\lambda_{\rm q}| < 1$, we again use (6.100) in (6.107) to obtain (6.108) which is given also in the table. Even though equations (6.97)–(6.100) are proven here for odd N only, the results in (6.105), (6.106), (6.107) and (6.108) are valid for even N also, because we have derived these formulae using a more tedious way, namely by taking a different low-temperature $\mathrm{k}' \to 0$ limit choosing $\mu_{\rm q} \to \mathrm{k}'$ instead of $\mu_{\rm p} \to \mathrm{k}'$ as Baxter did in ref. 116.

The regime of $t_{\rm p}, t_{\rm q}$ for which (6.105) is valid is different from the regime for which (6.107) holds. In the intersection of these two regimes, it is found that (6.107) is

TABLE 6.1. Free energy of integrable chiral Potts model for different regions.

$\lvert\lambda_{\rm p}\rvert < 1,\ \lvert\lambda_{\rm q}\rvert < 1$	$-\pi/N \le \arg(t_{\rm q}) \le \pi/N$ and $-3\pi/N \le \arg(t_{\rm p}) \le \pi/N$

$$N \ln \tilde{\kappa}_{\rm pq} = \tfrac{1}{2}(N-1)\ln(\lambda_{\rm q}/\lambda_{\rm p}) + A(\lambda_{\rm p}, t_{\rm q}) - A(\lambda_{\rm q}, t_{\rm p}) - B(\lambda_{\rm p}, \lambda_{\rm q}), \tag{6.105}$$

$\lvert\lambda_{\rm p}\rvert > 1,\ \lvert\lambda_{\rm q}\rvert > 1$	$-\pi/N \le \arg(t_{\rm q}) \le \pi/N$ and $-3\pi/N \le \arg(t_{\rm p}) \le \pi/N$

$$N \ln \tilde{\kappa}_{\rm pq} = \tfrac{1}{2}(N-1)\ln(\lambda_{\rm p}/\lambda_{\rm q}) + A(\lambda_{\rm p}^{-1}, t_{\rm q}) - A(\lambda_{\rm q}^{-1}, t_{\rm p}) - B(\lambda_{\rm p}^{-1}, \lambda_{\rm q}^{-1}), \tag{6.106}$$

$\lvert\lambda_{\rm p}\rvert < 1,\ \lvert\lambda_{\rm q}\rvert > 1$	$-\pi/N \le \arg(t_{\rm q}) \le 3\pi/N$ and $-\pi/N \le \arg(t_{\rm p}) \le \pi/N$

$$N \ln \tilde{\kappa}_{\rm pq} = \tfrac{1}{2}(N-1)\ln(\lambda_{\rm q}/\lambda_{\rm p}) - 2\sum_{j=1}^{N-1}(N-j)\ln(\omega^{-j/2}t_{\rm q} - \omega^{j/2}t_{\rm p})$$
$$+ C(\lambda_{\rm p}, t_{\rm q}) + A(\lambda_{\rm q}^{-1}, t_{\rm p}) + B(\lambda_{\rm p}, \lambda_{\rm q}^{-1}), \tag{6.107}$$

$\lvert\lambda_{\rm p}\rvert > 1,\ \lvert\lambda_{\rm q}\rvert < 1$	$-\pi/N \le \arg(t_{\rm q}) \le 3\pi/N$ and $-\pi/N \le \arg(t_{\rm p}) \le \pi/N$

$$N \ln \tilde{\kappa}_{\rm pq} = \tfrac{1}{2}(N-1)\ln(\lambda_{\rm p}/\lambda_{\rm q}) - 2\sum_{j=1}^{N-1}(N-j)\ln(\omega^{-j/2}t_{\rm q} - \omega^{j/2}t_{\rm p})$$
$$+ C(\lambda_{\rm p}^{-1}, t_{\rm q}) + A(\lambda_{\rm q}, t_{\rm p}) + B(\lambda_{\rm p}^{-1}, \lambda_{\rm q}). \tag{6.108}$$

an analytic continuation of (6.105) as the variable $\lambda_{\rm q}$ moves from inside the unit circle to outside the unit circle. However, since the two regimes do not coincide, it shows that this is not true in general. Thus even though the regimes of validity for (6.108) and (6.106) do intersect, we found that (6.106) is not the analytic continuation of (6.108) when $\lambda_{\rm p}$ is continued from inside the unit circle to outside. When $|\lambda_{\rm p}|, |\lambda_{\rm q}| < 1$ or $|\lambda_{\rm p}|, |\lambda_{\rm q}| > 1$ we find from (6.105) or from (6.106) that the inversion relation (6.79) holds. However, if $|\lambda_{\rm p}| < 1$ and $|\lambda_{\rm q}| > 1$, then we need to use (6.107) for $\tilde{\kappa}_{\rm pq}$; and

(6.108) for $\tilde{\kappa}_{\rm qp}$; we find that inversion relation (6.79) does not hold. This is rather perplexing.

6.4 CONCLUSION

In this chapter, we follow the technique given by Baxter[115,116,119,120] to obtain the free energy of the N-state chiral Potts model for two different regimes. There are more quantities and regimes in this integrable model which have not been solved yet.

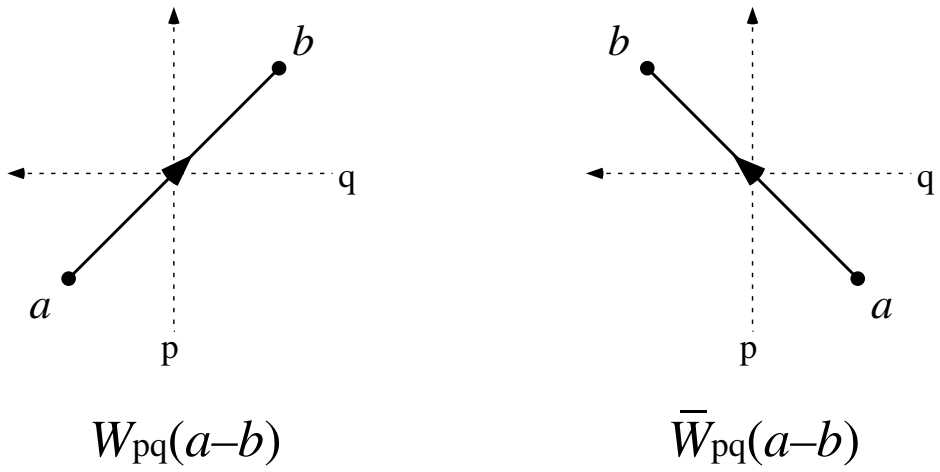

Figure 6.1. Boltzmann weights $W_{\mathrm{pq}}(a-b)$ and $\overline{W}_{\mathrm{pq}}(a-b)$ for the two types of edge interaction between the spins a and b.

BIBLIOGRAPHY

1. Tanisaki, S., J. Phys. Soc. Jpn. **16**, 579, (1961)

2. Blinc, R., Levanyuk, A. P., eds. *Incommensurate Phases in Dielectrics*, (North-Holland, Amsterdam, 1986)

3. Yoshimori, A., J. Phys. Soc. Jpn. **14**, 807, (1959)

4. Nagamiya, T., in *Solid State Physics*, Vol. **20**, F. Seitz, H. Ehrenreich and D. Turnbull, eds., (Academic Press, New York, 1967)

5. Ertl, G. and Kuppers, J., Surface Sci. **21**, 61, (1970)

6. Yeomans, J. M., in *Solid State Physics*, Vol. **41**, H. Ehrenreich and D. Turnbull, eds., (Academic Press, Orlando, 1988)

7. Scott, H. L., McCullough, W. S., Int. J. Mod. Phys. **B5**, 2479, (1991)

8. Villain, J., Gordon, M. B., Surf. Sci. **125**, 1 (1983)

9. Pokrovsky, V. L., Talapov, A. L., in *Theory of Incommensurate Crystals*, Soviet Scientific Reviews **1**, (Harwood Academic, 1984)

10. Huse, D. A. and Fisher, M. E., Phys. Rev. **B29**, 239, (1984)

11. Bak, P., Rep. Prog. Phys. **45**, 587, (1982)

12. Hering, S. V., van Sciver, S. W., and Vilches, O. E., J. Low Temp. Phys. **25**, 793 (1976)

13. Stephens, P. W., Heiney, P. A., Birgeneau, R. J. and Horn, P. M., Phys. Rev. Lett. **43**, 47, (1979)

14. Fain, S. C., Chinn, M. D. and Diehl, R. D., Phys. Rev. **B21** , 4170, (1980)

15. Stephens, P. W., Heiney, P. A., Birgeneau, R. J., Horn, P. M., Stoltenberg, J. and Vilches, O. E., Phys. Rev. Lett. **45**, 1959, (1980)

16. Stephens, P. W., Heiney, P. A., Birgeneau, R. J., Horn, P. M., Moncton, D. E. and Brown G. S., Phys. Rev. **B29**, 3512, (1984)

17. Jaubert, M., Glachant, A., Bienfait, M., and Boato, G., Phys. Rev. Lett. **46**, 1679, (1981)

18. Den Nijs, M. P. M., in *Phase Transitions and Critical Phenomena*, Vol. **12**, C. Domb and J. L. Lebowitz, eds., (Academic Press, London and Orlando, 1988)

19. Pokrovsky, V. L., Talapov, A. L., Phys. Rev. Lett. **42**, 65, (1979)

20. Pokrovsky, V. L., Talapov, A. L., Zh. Exp. Teor. Fys. **78**, 269, (1980)

21. Schulz, H. J., Phys. Rev. **B22**, 5274, (1980)

22. Schulz, H. J., Phys. Rev. Lett. **46**, 1685, (1981)

23. Luther, A., Timonen, J. and Pokrovsky, V., in *Phase Transitions in Surface Films*, J. G. Dash and J. Duvalds, eds, (Plenum Press, New York, 1980), 115

24. Okwamoto, Y., J. Phys. Soc. Jpn. **49**, 8, (1980)

25. Selke, W., Phys. Rep. **170** (1988) and References therein

26. Ostlund, S., Phys. Rev. **B24**, 398, (1981)

27. Huse, D. A., Phys. Rev. **B24**, 5180, (1981)

28. Elliott, R. J., Phys. Rev. **124**, 346, (1961)

29. Selke, W. and Fisher, M., Phys. Rev. **B20**, 257, (1979)

30. Bak, P. and von Boehm, J., Phys. Rev. **B21**, 5297, (1980)

31. Imbihl, R., Behm, R. J., Christmann, K., Ertl, G. and Matsushima, T., Surf. Sci. **117**, 257, (1982)

32. Villain, J., Bak, P., J. Physique **42**, 657 (1981)

33. Kosterlitz, J. M., Thouless, D. J., J. Phys. **C6**, 1181, (1973)

34. Kosterlitz, J. M., J. Phys. **C7**, 1046, (1974)

35. Blinc, R., De Sa Barreto, F. C., Phys. Stat. Sol. **B87**, K105, (1978)

36. Huang, J. and Ho, T. T., Phys. Rev. Lett. **58**, 2239, (1987)

37. Levstik, A., Filipic, C., Prelovsek, P. and Blinc, R., Phys. Rev. Lett. **54**, 1567, (1985)

38. Schobinger-Papamantellos, P. and Buschow, K. H. J., J. Magn. Magn. Mater. **71**, 134, (1988)

39. Shapira, Y., Becerra, C. C., Oliveira, N. F. and Chang, T. S., Phys. Rev. **B24**, 2780, (1981)

40. Haldane, F. D. M., Bak, P. and Bohr, T., Phys. Rev. **B28**, 2743, (1983)

41. Schulz, H. J., Phys. Rev. **B28**, 2746, (1983)

42. Kinzel, W., Selke, W. and Wu, F. Y., J. Phys. **A14**, L399, (1981)

43. Au-Yang, H. and Perk, J. H. H., J. Stat. Phys. **78**, 17-78, (1995)

44. Duxbury, P. M., Yeomans, J. and Beale, P. D., J. Phys. **A17**, L179, (1984)

45. Yeomans, J. M. and Derrida, B., J. Phys. **A18**, 2343, (1985)

46. Selke, W. and Yeomans, J., Z. Phys. **B46**, 311, (1982)

47. Houlrik, J. M., Jensen, S. J. K., Phys. Rev. **B34**, 325, (1986)

48. Howes, S. F., Phys. Rev. **B27**, 1762, (1983)

49. Howes, S. F., Kadanoff, L. P. and den Nijs, M. P. M., Nucl. Phys. **B215**, 169, (1983)

50. Everts, H. U. and Roder, H., J. Phys. **A22**, 2475, (1989)

51. Centen, P., Rittenberg, V. and Marcu, M., Nucl. Phys. **B205[FS5]**, 585, (1982)

52. Von Gehlen, G., Rittenberg, V., Nucl. Phys. **B230[FS10]**, 455, (1984)

53. Vescan, T., Rittenberg, V. and von Gehlen, G., J. Phys. **A19**, 1957, (1986)

54. Den Nijs, M. P. M., J. Phys. **A17**, L95, (1984)

55. Suzuki, M., J. Phys. Soc. Jpn. **55**, 4205, (1986)

56. *Coherent Anomaly Method, Mean field, Fluctuations and Systematics*, edited by Suzuki, M. et al., (World Scientific, Singapore, 1995)

57. Hu, X., Katori, M. and Suzuki, M., J. Phys. Soc. Jpn. **56**, 3865, (1987)

58. McCullough, W. S., Phys. Rev. **B46**, 5084, (1992)

59. Wu, F. Y., Rev. Mod. Phys. **54**, 235-268, (1982)

60. Weiss, P., J. Phys. Radium **6**, 661, (1907)

61. Bethe, H. A., Proc. Roy. Soc. **A150**, 552, (1935)

62. Fujiki, S., J. Phys. Soc. Jpn. **62**, 556, (1993)

63. Hu, X., Prog. Theor. Phys. **89**, 545, (1993)

64. Baxter, R. J., J. Phys. **C6**, L94-L96, (1973)

65. Baxter, R. J., J. Stat. Phys. **9**, 145-182, (1973)

66. Nomura, Y. and Suzuki, M., J. Phys. Soc. Jpn. **62**, 3774, (1993)

67. Suzuki, M., Katori, M., Hu, X., J. Phys. Soc. Jpn. **56**, 3092, (1987)

68. Baxter, R. J., *Exactly Solved Models in Statistical Mechanics*, (Academic Press, London, 1982)

69. Fisher, M. E., J. Math. Phys. **5**, 944, (1964)

70. Ito, N. and Suzuki, M., Phys. Rev. B **43**, 3483, (1991)

71. Nightingale, M. P. M., J. Appl. Phys. **53**, 7927, (1982)

72. Kaufman, B. and Onsager, L., Phys. Rev. **76**, 1244-1252, (1949)

73. Montroll, E. W., Potts, R. B. and Ward, J. C., J. Math. Phys. **4**, 308-322, (1963)

74. Wu, T. T., Phys. Rev. **149**, 380-401, (1966)

75. Kadanoff, L. P., Nuovo Cimento (ser. 10) **B44**, 276-305, (1966)

76. McCoy, B. M. and Wu, T. T., *The Two-Dimensional Ising Model* (Harvard Univ. Press, Cambridge, Mass., 1973)

77. Wu, T. T., McCoy, B. M., Tracy, C. A. and Barouch, E., Phys. Rev. **B13**, 316-374, (1976)

78. Baxter, R. J., Phil. Trans. R. Soc. Lond. **A289**, 315-346, (1978)

79. Baxter, R. J., Proc. R. Soc. Lond. **A404**, 1-33, (1986)

80. Au-Yang, H. and Perk, J. H. H., Physica **D18**, 365-366, (1986)

81. Perk, J. H. H., Phys. Lett. **A79**, 3-5, (1980)

82. Au-Yang, H. and Perk, J. H. H., Physica **A144**, 44-104, (1987)

83. Au-Yang, H. and Perk, J. H. H., in Proc. 1987 Summer Research Institute on Theta Functions, Proc. Symp. Pure Math. **49**, part 1, L. Ehrenpreis and R. C. Gunning, eds., Am. Math. Soc., Providence, R.I., 1989, 287-293

84. Reyes Martínez, J. R., Phys. Lett. **A227**, 203-208, (1997)

85. Reyes Martínez, J. R., Physica **A256**, 463-484, 1998

86. Tracy, C. A. and McCoy, B. M., Phys. Rev. Lett. **31**, 1500-1504, (1973)

87. Stephenson, J., J. Math. Phys. **5**, 1009-1024, (1964)

88. Stephenson, J., J. Math. Phys. **7**, 1123-1132, (1966)

89. Stephenson, J., J. Math. Phys. **11**, 413-419, (1970)

90. Vaidya, H. G., Phys. Lett. **A57**, 1-4, (1976)

91. Jimbo, M. and Miwa, T., Proc. Japan Acad. **A56**, 405-410, (1980), **A57**, 347, (1981)

92. Au-Yang, H. and Perk, J. H. H., Phys. Lett. **A104**, 131-134, (1984)

93. McCoy, B. M. and Perk, J. H. H., Nucl. Phys. **B285[FS19]**, 279-294, (1987)

94. Lubensky, T. C., in *Introduction to Quasicrystals*, M. V. Jarić, ed. (Academic Press, Boston, 1988), 199-280

95. Henley, C. L., Comments Cond. Mat. Phys. **13**, 59-117, (1987)

96. Janot, C. *Quasicrystals: A Primer*, (Clarendon Press, Oxford, 2nd ed., 1994)

97. Tracy, C. A., J. Stat. Phys. **51**, 481-490, (1988)

98. Widom, M., in *Introduction to Quasicrystals*, M. V. Jarić, ed., (Academic Press, Boston, 1988), 59-110

99. Nelson, D. R. and Widom, M., Nucl. Phys. **B240[FS12]**, 113-139, (1984)

100. Sadoc, J. F. and Mosseri, R., *Extended Icosahedral Structures*, M. V. Jarić and D. Gratias, eds., (Academic Press, Boston, 1989), 163-188

101. Antonov, N. V. and Korepin, V. E., Zap. Nauch. Semin. LOMI **161**, 13-23, (1987), J. Sov. Math. **46**, 2058-2065, (1989)

102. Antonov, N. V. and Korepin, V. E., Teor. Mat. Fiz. **77**, 402-411, (1988), Theor. Math. Phys. **77**, 1282-1288, (1988)

103. Korepin, V. E., Phys. Lett. **A118**, 285-287, (1986)

104. Korepin, V. E., Commun. Math. Phys. **110**, 157-171, (1987)

105. Choy, T. C., Intern. J. Mod. Phys. **B2**, 49-63, (1988)

106. Baake, M., Grimm, U. and Baxter, R. J., Intern. J. Mod. Phys. **B8**, 3579-3600, (1994)

107. Grimm, U., Baake, M. and Simon, H., in *Proc. of the 5th International Conference on Quasicrystals*, C. Janot and R. Mosseri, eds. (World Scientific, Singapore, 1995), 80-83

108. Grimm, U., Baake, M., in *The Mathematics of Long-Range Aperiodic Order*, R. V. Moody, ed. (Kluwer, Dordrecht, 1997), 199-237

109. Baake, M., Grimm, U. and Pisani, C., J. Stat. Phys. **78**, 285-297, (1995)

110. Repetowicz, P., Grimm, U. and Schreiber, M., J. Phys. **A32**, 4397-4418, (1999)

111. Baxter, R. J., Perk, J. H. H. and Au-Yang, H., Phys. Lett. **A128**, 138-142, (1988)

112. Au-Yang, H., McCoy, B. M., Perk, J. H. H., Tang, S. and Yan, M.-L., Phys. Lett. **A123**, 219-223, (1987)

113. Au-Yang, H. and Perk, J. H. H., Intern. J. Mod. Phys. **B11**, 11-26, (1997)

114. Baxter, R. J., Bazhanov, V. V. and Perk, J. H. H., Int. J. Mod. Phys. **B4**, 803-870, (1990)

115. O'Rourke, M. J. and Baxter, R. J., J. Stat. Phys. **82**, 1-29, (1996)

116. Baxter, R. J., in *Proc. of Fourth Asia Pacific Physics Conference*, S. H. Ahn, I.-T. Cheon, S. H. Choh, and C. Lee eds. (World Scientific, Singapore, 1991), 42-58

117. Baxter, R. J., J. Stat. Phys. **82**, 1219-1234, (1996)

118. Baxter, R. J., J. Stat. Phys. **52**, 639-667, (1988)

119. Baxter, R. J., J. Stat. Phys. **73**, 461-495, (1993)

120. Baxter, R. J., J. Phys. **A27**, 1837-1849, (1994)

APPENDICES

APPENDIX A

DIFFERENCE SEQUENCE

We have introduced the difference sequence to denote spin configurations along one row in the chiral direction because only the differences between the successive spins are important in view of the $\mathbb{Z}_3$ invariance of the original model. We use the smallest periodic unit to denote a spin configuration. For example, if we have a spin configuration along one row such as $\cdots$ 11122001112200 $\cdots$, the sequence of differences between successive spins is $\cdots$ 20020202002020 $\cdots$ and the smallest unit of this sequence is any one of 2002020, 0020202, $\cdots$, 0200202. So these sequences denote the equivalent spin configuration and we only need take one of them to denote this configuration. We take the smallest one in numerical value i.e. 0020202 if these sequences are treated as numbers. A set of difference sequences is called independent if it doesn't contain any two elements representing the same $\mathbb{Z}_3$ equivalent spin configuration.

Thus, element $m_1 m_2 \cdots m_l$ in an independent difference sequence set satisfies:

1)$m_1\ m_2\ \cdots\ m_l$ is the smallest among $m_2\ m_3\ \cdots\ m_l\ m_1$, $m_3\ m_4\ \cdots\ m_l\ m_1\ m_2$, $\cdots$, $m_l\ m_1\ \cdots\ m_{l-1}$, if these sequences are treated as numbers.

2)$m_1\ m_2\ \cdots\ m_l$ can not be separated into more than one identical subsequences.

Generally, m_i can take any value of 0, 1, and 2 and if the length of a difference sequence is l, the period of this spin configuration is l or $3l$ depending on the value of $P \equiv \sum_{i=1}^{l} m_i \pmod 3$. If $P = 0$, then the period of this spin configuration is l. Otherwise, the period will be $3l$. We introduce the difference sequence also because the complexity and time consumption of our numerical calculation depends on the

length of the sequence instead of the period of the spin configuration. The difference sequence for the ground state is 0 when $0 \leq \Delta < 1/2$ and 2 when $1/2 < \Delta \leq 1$.

APPENDIX B

SIMPLIFIED FORMALISM FOR A SPECIAL CASE

For a set of boundary fields $\{\boldsymbol{\eta}_i\}$, let us look at the following situation,

$$\boldsymbol{\eta}_{i+l} = \mathbf{R}\boldsymbol{\eta}_i \tag{B.1}$$

where

$$\mathbf{R} = \begin{pmatrix} \cos(2\pi P/3) & -\sin(2\pi P/3) \\ \sin(2\pi P/3) & \cos(2\pi P/3) \end{pmatrix} \tag{B.2}$$

and P can take any value of $0, 1$ and 2. If $P = 0$, we have $\boldsymbol{\eta}_{i+l} = \boldsymbol{\eta}_i$ and (2.33) and (2.32) can be applied directly with period $L = l$. If $P \neq 0$, clearly,

$$\boldsymbol{\eta}_{i+3l} \;=\; \mathbf{R}^3\boldsymbol{\eta}_i \;=\; \boldsymbol{\eta}_i. \tag{B.3}$$

Hence, the period for boundary fields $L = 3l$ and (2.33) and (2.32) can be applied. However, not all equations in (2.33) are independent for $P \neq 0$. Following, we find a set of independent mean field equations and give similar formula for calculation of approximated free energy for this case. From (B.2) and (2.23), we can show

$$T(\boldsymbol{\eta}_{j+l})_{\{n_i\},\{n'_i\}} \;=\; T(\boldsymbol{\eta}_j)_{\{n_i-P\},\{n'_i-P\}}. \tag{B.4}$$

We defined τ^k in (2.27), hence if we denote its largest eigenvalue, corresponding left and right eigenvectors as λ^k, $\langle\lambda^k|$ and $|\lambda^k\rangle$ (with $\langle\lambda^k|\lambda^k\rangle = 1$) respectively, it is easy to show that

$$\tau^{k+l}_{\{n_i\},\{n'_i\}} \;=\; \tau^{k}_{\{n_i-P\},\{n'_i-P\}}, \tag{B.5}$$

$$\lambda^k \;=\; \lambda^0 \quad \text{for any } k, \tag{B.6}$$

$$(\langle\lambda^{k+l}|)_{\{n_i\}} \;=\; (\langle\lambda^k|)_{\{n_i-P\}}, \tag{B.7}$$

$$(|\lambda^{k+l}\rangle)_{\{n_i\}} \;=\; (|\lambda^k\rangle)_{\{n_i-P\}}. \tag{B.8}$$

Meanwhile $\mathbf{m}_k$ can be calculated as

$$\mathbf{m}_k = \langle \lambda^k | \mathbf{M} | \lambda^k \rangle \tag{B.9}$$

where $\mathbf{M}$ is defined in (2.24). Through simple algebraic calculation, we can get

$$\mathbf{m}_{i+l} = \mathbf{R}\mathbf{m}_i. \tag{B.10}$$

By iteration procedure (2.34), we can expect this relation to be kept by $\{\boldsymbol{\eta}_i^{(n)}\}$ for arbitrary n and hence by final solutions of $\{\boldsymbol{\eta}_i\}$. With the help of (B.4) and (B.10), the calculation can be reduced as

$$F_{MF} = -\frac{1}{3Nl\beta} \ln \lambda^0(\{\boldsymbol{\eta}_j\}) + \frac{K_t}{Nl\beta} \sum_{j=0}^{l-1} (2\boldsymbol{\eta}_j \cdot \mathbf{m}_j - \mathbf{m}_j \cdot \mathbf{m}_j), \tag{B.11}$$

the independent mean field equations

$$\boldsymbol{\eta}_j = \mathbf{m}_j \quad \text{where } j = 0, 1, \cdots, l-1. \tag{B.12}$$

and

$$\mathbf{m}_i = (\lambda^0)^{-1} \langle \lambda^0 | T(\boldsymbol{\eta}_0) T(\boldsymbol{\eta}_1) \cdots \mathbf{M} T(\boldsymbol{\eta}_i) \cdots T(\boldsymbol{\eta}_{l-1}) VW | \lambda^0 \rangle \quad \text{for } i = 0, 1, \cdots, l-1 \tag{B.13}$$

where we define

$$U = \prod_{i=0}^{l-1} T(\boldsymbol{\eta}_i), \tag{B.14}$$

$$V_{\{n_i\},\{n_i'\}} = U_{\{n_i - P\},\{n_i' - P\}}, \tag{B.15}$$

$$W_{\{n_i\},\{n_i'\}} = V_{\{n_i - P\},\{n_i' - P\}}, \tag{B.16}$$

$$\tau^0 = UVW. \tag{B.17}$$

APPENDIX C

MAIN FORTRAN PROCEDURE FOR CHAPTER 2

```
c       This program is to search for upper limit of Lifshitz point
        parameter(ichain=9,mult=1,iper=55,itl=2184)
c       ichain is the length of period and mult is the width of strip
c       nps is number of Potts states, iper is repeating times in
c       searching for phase boundary. The accuracy is -/2**iper.
c       itl is the number of different boundary conditions.
c       mnps is the dimension of transfer matrix intrix(i,j), i means
c       row index in transfer matrix and j means column index
        parameter(nps=3,mnps=nps**mult)
        integer intrix
       double precision tdum1
       double precision so,pie,temp,dta
       double precision nsb,erf
        common so(mnps,2),pie
c    above first class
        common temp,dta
c    above second class
        common nsb(2,0:ichain-1)
        common tdum1(mnps,mnps)
        common erf,ipmt(2,mnps),intrix(mnps,mult)
c    above third class
        double precision tpt,dmax,dmin
```

```
      double precision tpdis,tpord,kxy
      double precision fret0,fret,fretf,fretf0,sum
      double precision sb0,sb,func,erff,erff0
      dimension sb(2,0:ichain-1), sb0(2,0:ichain-1)
      dimension it(0:ichain,itl)
      integer s(0:ichain-1)
      integer it,ipf
      character*6 ppout
      character*4 ppbin
      character*2 cwidth,clength
      if (mult .le. 9) cwidth='w'//char(mult+48)
      if (mult .gt. 9) cwidth='w'//char(mult+55)
      if (ichain .le. 9) clength='b'//char(ichain+48)
      if (ichain .gt. 9) clength='b'//char(ichain+55)
      ppout=cwidth//clength//'.p'
      ppbin=clength//'.p'
      open (unit=2,file=ppout,status='new')
      open (unit=3,file=ppbin,status='old')
      read(3,*) ((it(i,j),i=0,ichain),j=1,itl)
ccccccccccccccccccccccccccccc
      kxy=10.0d0
      dmax=0.50d0
      dmin=0.00d0
ccccccccccccccccccccccccccccc
      erf=0.10d-13
      pie =2.0d0*3.14159265358979324d0/dble(nps)
      do 10 irow=1,mnps
      do 10 icol=1,mult
```

```
          intrix(irow,icol)=mod(int((irow-1)/(nps**(icol-1))),nps)
 10       continue
           do 25 irow=1,mnps
          ipmt(1,irow)=1
          ipmt(2,irow)=1
          do 20 icol=1,mult
          ipmt(1,irow)=ipmt(1,irow)+nps**(icol-1)
     z      * mod((intrix(irow,icol)+1),nps)
          ipmt(2,irow)=ipmt(2,irow)+nps**(icol-1)
     z      * mod((intrix(irow,icol)+2),nps)
 20       continue
 25       continue
          do 30 i1=1,mnps
          So(i1,1) =cos(pie*intrix(i1,1))
          So(i1,2) =sin(pie*intrix(i1,1))
 30      continue
          do 190 itdta=1,iper
             dta=(dmax+dmin)*0.50d0
             tpord=2.0d0
             tpdis=0.10d0
c         following sentence is the do loop searching for o-d point
           do 180 ittmp=1,60
c         above sentence is the do loop searching for o-d point
          tpt=(tpord+tpdis)*0.50d0
          temp=tpt
c         following gives transfer matrix which is not related to MF
          do 60 i1=1,mnps
          do 60 i2=1,mnps
```

```
          sum=0.d0
          do 40 im =1,mult
          sum=sum+kxy*temp*(cos((intrix(i1,im)-
     z    intrix(i2,im)+dta)*pie))
  40      continue
          do 50 im =1,mult-1
          sum=sum+temp*(cos((intrix(i1,im)-
     z    intrix(i1,im+1))*pie))
  50      continue
          tdum1(i1,i2)=exp(sum)
  60      continue
c         above gives transfer matrix which is not related to MF
c         following calculates either ordered or disordered phase
c         following gives the free energy of disordered phase
          do 70 i=0,ichain-1
          do 70 j1=1,2
          sb(j1,i)=0.0d0
 70       continue
          fret=func(sb,0)
          fretf=fret
c         above gives the free energy of disordered phase
c         following gives the free energy of ordered phase
          do 80 i=0,ichain-1
          sb(1,i)=1.0d0
          sb(2,i)=0.0d0
 80       continue
          fret0=0.0d0
          do 100 ii=1,3000
```

```
          fret=func(sb,0)
          erff=abs(fret0/fret -1.0d0)
          if (erff .le. erf) go to 110
            fret0=fret
           do 90 i=0,ichain-1
           do 90 j1=1,2
           sb(j1,i)=nsb(j1,0)
 90       continue
 100       continue
c         above gives the free energy of ordered phase
 110      if(fretf .le. fret) then
           tpdis=tpt
          else
           tpord=tpt
          endif
 180      continue
          ipf=0
c          if(itdta .eq. iper) then
c          write(2,500) temp,dta
c          write(2,500) fretf, fret
c          write(2,500)((sb(j1,i),j1=1,2),i=0,ichain-1)
c          endif
c         above calculates either ordered or disordered phase
c         following calculates the free energy of modulated phases
          s(0)=0
          fretf0=0.0d0
          it0=0
          do 170 its=1,itl
```

```
        do 120 i=1,ichain-1
        s(i)=mod(s(i-1)+it(i,its), nps)
120      continue
        do 130 j=0,ichain-1
        sb(1,j) = COS(pie*dble(s(j)))
        sb(2,j) = SIN(pie*dble(s(j)))
130     continue
        fret0=0.0d0
        do 150 ii=1,3000
        fret=func(sb,it(0,its))
        erff=abs(fret0/fret-1.0d0)
        if (erff .le. erf) go to 160
          fret0=fret
         do 140 i=0,ichain-1
         do 140 j1=1,2
         sb(j1,i)=nsb(j1,i)
140      continue
150      continue
160     if(fret .le. fretf0) then
        fretf0=fret
        it0=it(0,its)
        do 165 i=0,ichain-1
        do 165 j1=1,2
        sb0(j1,i)=sb(j1,i)
165     continue
        end if
        if (fretf0 .lt. fretf .and. abs(fretf0/fretf-1.0d0)
    c    .gt. 10.0d0*erf) then
```

```
          ipf=1
          go to 175
         end if
 170    CONTINUE
c       above give the calculation of free energy of modulate phase
 175    if(ipf .eq.1) then
          dmax=dta
        else
          dmin=dta
        endif
         if(itdta .eq. iper) then
         write(2,501) temp,dta, it0
         write(2,500) fretf, fretf0
         write(2,500)((sb0(j1,i),j1=1,2),i=0,ichain-1)
         endif
 190    continue
 500    format(1x,2d22.14)
 501    format(1x,2d22.14, i3)
        stop
         end



         double precision function func(sb,its)
C THIS IS A SUBROUTINE TO CACULATE FREE ENERGY
c   ichain is period length of strip and mult is width of strip
c   nps is number of Potts states. pie is math parameter,
c   temp is inverse of temperature and dta means chiral phase
         parameter(ichain=9,mult=1)
```

```
          parameter(nps=3,mnps=nps**mult)
          integer intrix
         double precision tdum1
         double precision so,pie,temp,dta
         double precision nsb,erf
          common so(mnps,2),pie
c     above first class
          common temp,dta
c     above second class
          common nsb(2,0:ichain-1)
          common tdum1(mnps,mnps)
          common erf,ipmt(2,mnps),intrix(mnps,mult)
c     above third class
          double precision tt,st, rnorm
          double precision sb,t1,sum,bt,scl
          dimension sb(2,0:ichain-1)
          dimension t1(mnps)
          dimension st(mnps,0:ichain), bt(mnps,0:(ichain-1))
          dimension tt(mnps,0:ichain), scl(2)
          integer its
c     following produces part of transfer matrix due to mean field
          do 10 i1=1,mnps
          DO 10 ii = 0,ichain-1
          sum=temp*(sb(1,ii)*
     z    (cos(intrix(i1,mult)*pie)+
     z    cos(intrix(i1,1)*pie))
     z    + sb(2,ii)*(sin(intrix(i1,mult)*pie)+
     z    sin(intrix(i1,1)*pie)))
```

```
        bt(i1,ii) =exp(sum)
  10    CONTINUE
c    above produces part of transfer matrix due to mean field
c    following calculates eigenvalue and left eigenvector
        do 20 i1=1, mnps
        tt(i1, ichain)=1.0d0
  20    continue
 1000   do 30 i1=1,mnps
        tt(i1,0)=tt(i1,ichain)
  30    continue
        scl(1)=1.0d0
        do 90 ii2=1, ichain
        do 40 i1=1,mnps
        t1(i1)=tt(i1, ii2-1)*bt(i1,ii2-1)
  40    continue
        do 60 i2=1,mnps
        sum =0.0d0
        do 50 i1=1,mnps
        sum=sum+t1(i1)*tdum1(i1,i2)
  50    continue
        tt(i2,ii2)=sum
  60    continue
        sum=0.0d0
        do 70 i2=1,mnps
        sum=sum+tt(i2,ii2)*tt(i2,ii2)
  70    continue
        scl(2)=sqrt(sum/dble(mnps))
        do 80 i2=1,mnps
```

```
        tt(i2,ii2)=tt(i2,ii2)/scl(2)
 80     continue
        scl(1)=scl(1)*scl(2)
 90     continue
        if(its.ne.0) then
            if (its .eq. 1) then
        do 140 ii2=1, ichain
         do 100 i1=1,mnps
        t1(i1)=tt(i1, ichain)*bt(ipmt(2,i1),ii2-1)
100     continue
        do 120 i2=1,mnps
        sum =0.0d0
        do 110 i1=1,mnps
        sum=sum+t1(i1)*tdum1(i1,i2)
110     continue
        tt(i2,ichain)=sum
120     continue
        sum=0.0d0
        do 130 i2=1,mnps
        sum=sum+tt(i2,ichain)*tt(i2,ichain)
130     continue
        scl(2)=sqrt(sum/dble(mnps))
        do 135 i2=1,mnps
        tt(i2,ichain)=tt(i2,ichain)/scl(2)
135     continue
        scl(1)=scl(1)*scl(2)
140     continue
        do 200 ii2=1, ichain
```

```
         do 150 i1=1,mnps
        t1(i1)=tt(i1, ichain)*bt(ipmt(1,i1),ii2-1)
150     continue
        do 170 i2=1,mnps
        sum =0.0d0
        do 160 i1=1,mnps
        sum=sum+t1(i1)*tdum1(i1,i2)
160     continue
        tt(i2,ichain)=sum
170     continue
        sum=0.0d0
        do 180 i2=1,mnps
        sum=sum+tt(i2,ichain)*tt(i2,ichain)
180     continue
        scl(2)=sqrt(sum/dble(mnps))
        do 190 i2=1,mnps
        tt(i2,ichain)=tt(i2,ichain)/scl(2)
190     continue
        scl(1)=scl(1)*scl(2)
200     continue
         else
        do 260 ii2=1, ichain
         do 210 i1=1,mnps
        t1(i1)=tt(i1, ichain)*bt(ipmt(1,i1),ii2-1)
210     continue
        do 230 i2=1,mnps
        sum =0.0d0
        do 220 i1=1,mnps
```

```
        sum=sum+t1(i1)*tdum1(i1,i2)
220     continue
        tt(i2,ichain)=sum
230     continue
        sum=0.0d0
        do 240 i2=1,mnps
        sum=sum+tt(i2,ichain)*tt(i2,ichain)
240     continue
        scl(2)=sqrt(sum/dble(mnps))
        do 250 i2=1,mnps
        tt(i2,ichain)=tt(i2,ichain)/scl(2)
250     continue
        scl(1)=scl(1)*scl(2)
260     continue
        do 320 ii2=1, ichain
         do 270 i1=1,mnps
        t1(i1)=tt(i1, ichain)*bt(ipmt(2,i1),ii2-1)
270     continue
        do 290 i2=1,mnps
        sum =0.0d0
        do 280 i1=1,mnps
        sum=sum+t1(i1)*tdum1(i1,i2)
280     continue
        tt(i2,ichain)=sum
290     continue
        sum=0.0d0
        do 300 i2=1,mnps
        sum=sum+tt(i2,ichain)*tt(i2,ichain)
```

```
 300     continue
         scl(2)=sqrt(sum/dble(mnps))
         do 310 i2=1,mnps
         tt(i2,ichain)=tt(i2,ichain)/scl(2)
 310     continue
         scl(1)=scl(1)*scl(2)
 320     continue
           end if
         end if
         sum=0.0d0
         do 330 i1=1,mnps
         sum=sum+(tt(i1,ichain)-tt(i1,0))**2
 330     continue
         sum=sqrt(sum/dble(mnps))
         if (sum .gt. erf) goto 1000
c       above calculates the left eigenvector
c       following calculates right eigenvector
         do 335 i1=1, mnps
         st(i1,0)=1.0d0
 335     continue
 2000    do 340 i1=1,mnps
         tt(i1,ichain)=st(i1,0)
         st(i1,ichain)=st(i1,0)
 340     continue
          scl(1)=1.0d0
         if(its.ne.0) then
             if (its .eq. 1) then
         do 400 ii2=ichain-1, 0, -1
```

```
        do 360 i2=1,mnps
        sum =0.0d0
        do 350 i1=1,mnps
        sum=sum+ tdum1(i2,i1)*st(i1, ii2+1)
350     continue
        t1(i2)=sum
360     continue
        do 370 i1=1,mnps
        st(i1,ii2)=bt(ipmt(1,i1),ii2)*t1(i1)
370     continue
        sum=0.0d0
        do 380 i2=1,mnps
        sum=sum+st(i2,ii2)*st(i2,ii2)
380     continue
        scl(2)=sqrt(sum/dble(mnps))
        do 390 i2=1,mnps
        st(i2,ii2)=st(i2,ii2)/scl(2)
390     continue
        scl(1)=scl(1)*scl(2)
400     continue
        do 405 i1=1,mnps
        st(i1,ichain)=st(i1,0)
405     continue
        do 460 ii2=ichain-1, 0, -1
        do 420 i2=1,mnps
        sum =0.0d0
        do 410 i1=1,mnps
        sum=sum+ tdum1(i2,i1)*st(i1, ii2+1)
```

```
410     continue
        t1(i2)=sum
420     continue
        do 430 i1=1,mnps
        st(i1,ii2)=bt(ipmt(2,i1),ii2)*t1(i1)
430     continue
        sum=0.0d0
        do 440 i2=1,mnps
        sum=sum+st(i2,ii2)*st(i2,ii2)
440     continue
        scl(2)=sqrt(sum/dble(mnps))
        do 450 i2=1,mnps
        st(i2,ii2)=st(i2,ii2)/scl(2)
450     continue
        scl(1)=scl(1)*scl(2)
460     continue
        do 465 i1=1,mnps
        st(i1,ichain)=st(i1,0)
465     continue
         else
        do 520 ii2=ichain-1, 0, -1
        do 480 i2=1,mnps
        sum =0.0d0
        do 470 i1=1,mnps
        sum=sum+ tdum1(i2,i1)*st(i1, ii2+1)
470     continue
        t1(i2)=sum
480     continue
```

```
        do 490 i1=1,mnps
        st(i1,ii2)=bt(ipmt(2,i1),ii2)*t1(i1)
490     continue
        sum=0.0d0
        do 500 i2=1,mnps
        sum=sum+st(i2,ii2)*st(i2,ii2)
500     continue
        scl(2)=sqrt(sum/dble(mnps))
        do 510 i2=1,mnps
        st(i2,ii2)=st(i2,ii2)/scl(2)
510     continue
        scl(1)=scl(1)*scl(2)
520     continue
        do 525 i1=1,mnps
        st(i1,ichain)=st(i1,0)
525     continue
        do 580 ii2=ichain-1, 0, -1
        do 540 i2=1,mnps
        sum =0.0d0
        do 530 i1=1,mnps
        sum=sum+ tdum1(i2,i1)*st(i1, ii2+1)
530     continue
        t1(i2)=sum
540     continue
        do 550 i1=1,mnps
        st(i1,ii2)=bt(ipmt(1,i1),ii2)*t1(i1)
550     continue
        sum=0.0d0
```

```
        do 560 i2=1,mnps
        sum=sum+st(i2,ii2)*st(i2,ii2)
560     continue
        scl(2)=sqrt(sum/dble(mnps))
        do 570 i2=1,mnps
        st(i2,ii2)=st(i2,ii2)/scl(2)
570     continue
        scl(1)=scl(1)*scl(2)
580     continue
        do 585 i1=1,mnps
        st(i1,ichain)=st(i1,0)
585     continue
          endif
        endif
        do 640 ii2=ichain-1, 0, -1
        do 600 i2=1,mnps
        sum =0.0d0
        do 590 i1=1,mnps
        sum=sum+ tdum1(i2,i1)*st(i1, ii2+1)
590     continue
        t1(i2)=sum
600     continue
        do 610 i1=1,mnps
        st(i1,ii2)=bt(i1,ii2)*t1(i1)
610     continue
        sum=0.0d0
        do 620 i2=1,mnps
        sum=sum+st(i2,ii2)*st(i2,ii2)
```

```
 620     continue
         scl(2)=sqrt(sum/dble(mnps))
         do 630 i2=1,mnps
         st(i2,ii2)=st(i2,ii2)/scl(2)
 630     continue
         scl(1)=scl(1)*scl(2)
 640     continue
         sum=0.0d0
         do 650 i1=1,mnps
         sum=sum+(tt(i1,ichain)-st(i1,0))**2
 650     continue
         sum=sqrt(sum/dble(mnps))
         if (sum .gt. erf) goto 2000
c        above calculates the right eigenvector
         do 690 ii2=0, ichain-1
         SUM = 0.d0
         DO 680 MM = 1, mnps
         SUM=SUM+tt(mm, ii2)*st(mm,ii2)
  680    CONTINUE
         rnorm = SUM
         do 670 iii = 1,2
         SUM = 0.d0
         DO 660 MM = 1, mnps
         SUM=SUM+tt(mm, ii2)*So(MM,iii)*st(mm,ii2)
  660    CONTINUE
         Nsb(iii,ii2) = SUM/rnorm
  670    CONTINUE
  690    continue
```

```
       sum = 0.d0
       DO 700 II = 0,ichain -1
       DO 700 JJ = 1, 2
       sum = sum +temp*Nsb(JJ,II)* Nsb(jj,II)
700    CONTINUE
       DO 710 II = 0, ichain - 1
       DO 710 MM =1, 2
       sum = sum-2.0d0*temp*sb(MM,II)*Nsb(MM,II)
710    CONTINUE
       if (its .eq. 0) then
       func = (- log(scl(1)) - sum)
     z  /(dble(ichain)*temp*dble(mult))
       else
       func = (- (log(scl(1)))/3.0d0 - sum)
     z  /(dble(ichain)*temp*dble(mult))
       endif
      return
      end
```

APPENDIX D

MAIN FORTRAN PROCEDURE FOR CHAPTER 3

```
c        This is the procedure to find critical point,
c        wavevector at critical point and coherent
c        coefficient. "mult" is parameter to denote the
c        width of strip in mean field calculation.
c        This procedure includes main, one subroutine
c        printed here and three standard routines
c        called "rg.f" (which is for diagonalization
c        of real matrix), "cg.f" (which is for diagonalization
c        of complex matrix) and "cvert.f" (which is for
c        inversion of complex matrix).
         parameter(mult=7)
         parameter(nps=3,mnps=nps**(mult-1))
        double precision pie,temp,dta,phl
        double precision st1,eng1
        double complex csb,css,cm,czero,st2,eng2
         common pie
         common csb(mnps)
         common css(mnps)
         common cm(mnps),czero
c    above first class
         common temp,dta,phl
c    above second class
```

```
          common st1(mnps,mnps)
          common st2(mnps,mnps)
          common eng1(mnps,mnps)
          common eng2(mnps,mnps)
c    above third class
          integer intrix(mnps,mult)
          double precision sum,sum0,sum1,sum2,rat
          double complex suc,suc0,suc1,suc2
          double precision errb, ddta(5,11)
          double precision fmin,rnom,rdem,theta
          double complex omega
          double precision tpt,tpv,kxy
          character*6 ppout,ppin
          character*2 cwidth,cpotts
          if (mult .le. 9) cwidth='w'//char(mult+48)
          if (mult .gt. 9) cwidth='w'//char(mult+55)
          if (nps .le. 9) cpotts='a'//char(nps+48)
          if (nps .gt. 9) cpotts='a'//char(nps+55)
          ppin=cpotts//cwidth//'.o'
          ppout=cpotts//cwidth//'.b'
          open (unit=3, file= ppin, status='old')
          open (unit=2,file=ppout,status='new')
          read(3, *) ((ddta(i,j),i=1,5),j=1,11)
ccccccccccccccccccccccccccccccccccccccccccccccc
c         when rat=0.0d0 give weiss result
c         when rat=1.0d0 give bethe result
c         kxy is the ratio of interactions between
c         chiral direction and non-chiral direction
```

```
          rat=1.0d0
          kxy=100.0d0
ccccccccccccccccccccccccccccccccccccccccccccccccc
          pie =2.0d0*3.14159265358979323846264338328d0
     z    /dble(nps)
          czero=cmplx(0.0d0,0.0d0)
          omega=cmplx(cos(pie),sin(pie))
          do 10 irow=1,mnps
          do 10 icol=1,mult
          intrix(irow,icol)=mod(int((irow-1)/(nps**(icol-1))),nps)
 10       continue
c         following defines quantities such as boundary spin, central
c         spin and one column magnetic operator in Z3 invariant base
          do 15 i1=1,mnps
          csb(i1)=cmplx((cos(pie*dble(intrix(i1,mult)))
     c    +cos(pie*dble(intrix(i1,1))))/2.0d0
     c     ,(sin(pie*dble(intrix(i1,mult)))
     c     +sin(pie*dble(intrix(i1,1))))/2.0d0)
 15      continue
         do 20 i1=1,mnps
         if (mod(mult,2) .eq. 0) then
         css(i1)=cmplx((cos(pie*dble(intrix(i1,mult/2)))+
     c   cos(pie*dble(intrix(i1,mult/2+1))))/2.0d0,
     c   -(sin(pie*dble(
     c intrix(i1,mult/2)))+sin(pie*dble(intrix(i1,mult/2+1))
     c   ))/2.0d0)
         else
         css(i1)=cmplx(cos(pie*dble(intrix(i1,(mult+1)/2))),
```

```
     c  -sin(pie*dble(intrix(i1,(mult+1)/2))) )
        endif
 20     continue
         do 30 i1=1,mnps
         cm(i1)=czero
         do 25 i2=1,mult
         cm(i1)=cm(i1)+cmplx(cos(pie*dble(intrix(i1,i2))),
     c   sin(pie*dble(intrix(i1,i2))))
 25      continue
 30      continue
c        above defines quantities such as boundary spin, central
c        spin and one column magnetic operator in Z3 invariant base
         do 700 itdta=1,6
         dta=ddta(1, itdta)
         tpt=ddta(2, itdta)
         phl=ddta(3,itdta)
         nit=0
 600     temp=tpt
c        following gives the column transfer matrix
c        and one column energy operator in Z3 bases
         do 50 i1=1,mnps
         do 50 i2=1,mnps
        sum=0.0d0
        do 35 im=1,mult-1
        sum=sum+kxy*cos((dble(intrix(i1,im)-
     z  intrix(i2,im))+dta)*pie)
     z  +cos(dble((intrix(i1,im)-intrix(i1,im+1)))*pie)
 35     continue
```

```
      sum=sum+kxy*cos(dble((intrix(i1,mult)-
     z   intrix(i2,mult))+dta)*pie)
      sum0=sum
       sum=0.0d0
      do 40 im=1,mult-1
      sum=sum+kxy*cos((dble(intrix(i1,im)-
     z   intrix(i2,im)-1)+dta)*pie)
     z  +cos(dble(intrix(i1,im)-intrix(i1,im+1))*pie)
40    continue
      sum=sum+kxy*cos(dble((intrix(i1,mult)-
     z    intrix(i2,mult)-1)+dta)*pie)
      sum1=sum
       sum=0.0d0
      do 45 im=1,mult-1
      sum=sum+kxy*cos(dble((intrix(i1,im)-
     z   intrix(i2,im)-2)+dta)*pie)
     z  +cos(dble((intrix(i1,im)-intrix(i1,im+1)))*pie)
45    continue
      sum=sum+kxy*cos(dble((intrix(i1,mult)-
     z   intrix(i2,mult)-2)+dta)*pie)
      sum2=sum
       sum=exp(temp*(sum0-kxy*mult*cos(dta*pie)))
     z   +exp(temp*(sum1-kxy*mult*cos(dta*pie)))
     z    +exp(temp*(sum2-kxy*mult*cos(dta*pie)))
       suc=exp(temp*(sum0-kxy*mult*cos(dta*pie)))+omega*
     z  exp(temp*(sum1-kxy*mult*cos(dta*pie)))+
     z   omega*omega*exp(temp*(sum2-kxy*mult*cos(dta*pie)))
       st1(i1,i2)=sum
```

```
          st2(i1,i2)=suc
          sum=temp*(sum0*exp(temp*(sum0-kxy*mult*cos(dta*pie)))
     z    +sum1*exp(temp*(sum1-kxy*mult*cos(dta*pie)))
     z     +sum2*exp(temp*(sum2-kxy*mult*cos(dta*pie))))
          suc=temp*(sum0*exp(temp*(sum0-kxy*mult*cos(dta*pie)))
     z    +omega*sum1*exp(temp*(sum1-kxy*mult*cos(dta*pie)))
     z    +omega*omega*sum2*exp(temp*(sum2-kxy*mult*cos(dta*pie))))
          eng1(i1,i2)=sum
          eng2(i1,i2)=suc
 50      continue
c         following gives the column transfer matrix
c         and one column energy operator in Z3 bases
         call auxdia(theta,fmin,errb,rnom,rdem,rat)
         tpv=tpt-errb/rdem
         nit=nit+1
         if (abs(tpv/tpt-1.0d0) .gt. 1.0d-6 ) then
         tpt=tpv
         go to 600
         endif
         if (dta .ne. 0.0d0) then
         theta=theta/(dta*pie)
         end if
         write(2,502) dta,temp,theta,fmin,idd
 700     continue
 502     format(1x,d10.2,3d14.6,i3)
         stop
          end
```

```
          subroutine auxdia(xmin,fmin,errb,rnom,rdem,rat)
          parameter(mult=7)
          parameter(nps=3,mnps=nps**(mult-1))
         double precision pie,temp,dta,phl
         double precision st1,eng1
         double complex csb,css,cm,czero,st2,eng2
          common pie
          common csb(mnps)
          common css(mnps)
          common cm(mnps),czero
c     above first class
          common temp,dta,phl
c     above second class
          common st1(mnps,mnps)
          common st2(mnps,mnps)
          common eng1(mnps,mnps)
          common eng2(mnps,mnps)
c     above third class, ss31(mnps,mnps-1) sub by eng2(mnps,mnps)
          double precision sum
          double complex suc,suc1
          double complex ssl0(mnps),ssr0(mnps),sbl0(mnps)
     c    ,sbr0(mnps),csb31(mnps,mnps-1)
     c    ,ss12(mnps-1,mnps),b021(mnps,mnps-1),b013(mnps-1,mnps),
     c    hl0(mnps-1),hr0(mnps-1),csb12(mnps-1,mnps),
     c    h022(mnps,mnps),
     c    magl0(mnps),wri2(mnps),wri1(mnps-1),
     c    magr0(mnps)
          double complex vlf1(mnps,mnps-1),vrf1(mnps,mnps-1)
```

```
      double complex vlf2(mnps,mnps),vrf2(mnps,mnps)
      double precision emaxx,test,xmin,zr(mnps,mnps)
      double complex vl0(mnps),vr0(mnps),root
      double precision wr(mnps),wi(mnps)
      double precision vr(mnps,mnps),fv2(mnps),fv3(mnps)
      double precision errb,fmin,fv1(mnps),zi(mnps,mnps)
      double precision errb1,errb2,rdem1,rdem2,test1,test2
      double precision rat
      equivalence (zr,csb31),(zi,ss12),(vr,b021)
      integer iv1(mnps)
      integer iv2(mnps)
      double complex df,f,eav
      double precision rnom,rdem,ax,bx,rnom1,rnom2
c     following gives the diagonalization of real block
c     we use index 1 to denote this block
      call rg(mnps,mnps,st1,wr,wi,1,vr,iv1,fv1,info)
      emaxx=sqrt(wr(1)*wr(1)+wi(1)*wi(1))
      maxid=1
      do 10 ii=2,mnps
      test=sqrt(wr(ii)*wr(ii)+wi(ii)*wi(ii))
      if (emaxx .le. test) then
      maxid=ii
      emaxx=test
      endif
 10   continue
      do 15 ii=1,mnps
      vr0(ii)=cmplx(vr(ii,maxid)/sqrt(emaxx),0.0d0)
 15   continue
```

```
        ii=1
1000    if (ii .lt. maxid) then
        if (wi(ii) .eq. 0.0d0 ) then
        wri1(ii)=cmplx(wr(ii)/emaxx,wi(ii)/emaxx)
        do 20 jj=1,mnps
        vrf1(jj,ii)=cmplx(vr(jj,ii)/sqrt(emaxx),0.0d0)
20      continue
        ii=ii+1
        else
        wri1(ii)=cmplx(wr(ii)/emaxx,wi(ii)/emaxx)
        wri1(ii+1)=cmplx(wr(ii)/emaxx,-wi(ii)/emaxx)
       do 25 jj=1,mnps
        vrf1(jj,ii)=cmplx(vr(jj,ii)/sqrt(emaxx),
    c   vr(jj,ii+1)/sqrt(emaxx))
        vrf1(jj,ii+1)=cmplx(vr(jj,ii)/sqrt(emaxx),
    c   -vr(jj,ii+1))
25      continue
        ii=ii+2
        endif
       go to 1000
       endif
        ii=maxid+1
1200     if (ii .le. mnps) then
        if (wi(ii) .eq. 0.0d0 ) then
        wri1(ii-1)=cmplx(wr(ii)/emaxx,wi(ii)/emaxx)
        do 35 jj=1,mnps
        vrf1(jj,ii-1)=cmplx(vr(jj,ii)/sqrt(emaxx),0.0d0)
35      continue
```

```
         ii=ii+1
         else
         wri1(ii-1)=cmplx(wr(ii)/emaxx,wi(ii)/emaxx)
         wri1(ii)=cmplx(wr(ii)/emaxx,-wi(ii)/emaxx)
        do 40 jj=1,mnps
         vrf1(jj,ii-1)=cmplx(vr(jj,ii)/sqrt(emaxx),
    c     vr(jj,ii+1)/sqrt(emaxx))
         vrf1(jj,ii)=cmplx(vr(jj,ii)/sqrt(emaxx),
    c    -vr(jj,ii+1)/sqrt(emaxx))
40      continue
         ii=ii+2
         endif
        go to 1200
        endif
        do 45 ii=1,mnps
        do 45 jj=1,mnps-1
        vrf2(ii,jj)=vrf1(ii,jj)
45      continue
        do 50 ii=1,mnps
        vrf2(ii,mnps)=vr0(ii)
50      continue
        call CVERT(vrf2,mnps,mnps,iv2)
        do 55 ii=1,mnps-1
        do 55 jj=1,mnps
        vlf1(jj,ii)=vrf2(ii,jj)
55      continue
       do 60 ii=1,mnps
       vl0(ii)=vrf2(mnps,ii)
```

```
 60    continue
       do 65 ii=1,mnps
       do 65 jj=1,mnps
       st1(ii,jj)=dble(st2(ii,jj))
       vr(ii,jj)=aimag(st2(ii,jj))
 65    continue
c     above gives diagonalization of real block
c     following gives diagonalization of complex block (2)
c     there are two, one(2) is the conjugate of the other(3)
       call cg(mnps,mnps,st1,vr,wr,wi,1,zr,zi,fv1,fv2,fv3,info)
       do 70 ii=1,mnps
       wri2(ii)=cmplx(wr(ii)/emaxx,wi(ii)/emaxx)
 70    continue
        do 75 ii=1,mnps
        do 75 jj=1,mnps
        vrf2(ii,jj)=cmplx(zr(ii,jj)/sqrt(emaxx),zi(ii,jj)/sqrt(emaxx))
 75    continue
        do 80 ii=1,mnps
        do 80 jj=1,mnps
        vlf2(jj,ii)=vrf2(ii,jj)
 80    continue
        call cvert(vlf2,mnps,mnps,iv2)
c     above gives diagonalization of complex block (2)
c      following gives all the related matrix elements
c      which will be used in calculation of correlation
       do 90 mm=1,mnps
       suc=czero
       suc1=czero
```

```
      do 85 nn=1,mnps
      suc=suc+eng1(mm,nn)*vr0(nn)
      suc1=suc1+vl0(nn)*eng1(nn,mm)
85    continue
      st2(mm,1)=suc
      st2(mm,2)=suc1
90    continue
      do 100 jj=1,mnps-1
      suc=czero
      suc1=czero
      do 95 mm=1,mnps
      suc=suc+vlf1(mm,jj)*st2(mm,1)
      suc1=suc1+st2(mm,2)*vrf1(mm,jj)
95    continue
      hl0(jj)=suc/emaxx
      hr0(jj)=suc1/emaxx
100   continue
      suc=czero
      do 105 mm=1,mnps
      suc=suc+vl0(mm)*st2(mm,1)
105   continue
      eav=suc/emaxx
      do 115 ii=1,mnps
      do 115 mm=1,mnps
      suc=czero
      do 110 nn=1,mnps
      suc=suc+vlf2(nn,ii)*eng2(nn,mm)
110   continue
```

```
      st2(ii,mm)=suc
115   continue
      do 125 ii=1,mnps
      do 125 jj=1,mnps
      suc=czero
      do 120 mm=1,mnps
      suc=suc+st2(ii,mm)*vrf2(mm,jj)
120   continue
      h022(ii,jj)=suc/emaxx
125   continue
      do 135 jj=1,mnps
      suc=czero
      suc1=czero
      do 130 kk=1,mnps
      suc=suc+conjg(vlf2(kk,jj))*css(kk)*vr0(kk)
      suc1=suc1+vl0(kk)*css(kk)*vrf2(kk,jj)
130   continue
      ssl0(jj)=suc
      ssr0(jj)=suc1
135   continue
      do 145 jj=1,mnps
      suc=czero
      suc1=czero
      do 140 kk=1,mnps
      suc=suc+vlf2(kk,jj)*csb(kk)*vr0(kk)
      suc1=suc1+vl0(kk)*csb(kk)*conjg(vrf2(kk,jj))
140   continue
      sbl0(jj)=suc
```

```
      sbr0(jj)=suc1
145   continue
      do 150 ii=1,mnps
      do 150 kk=1,mnps
      st2(kk,ii)=conjg(vlf2(kk,ii))*css(kk)
150   continue
      do 160 ii=1,mnps
      do 160 jj=1,mnps-1
      suc=czero
      do 155 kk=1,mnps
      suc=suc+st2(kk,ii)*vrf1(kk,jj)
155   continue
      eng2(ii,jj)=suc
160   continue
      do 165 ii=1,mnps
      do 165 kk=1,mnps
      st2(kk,ii)=conjg(vlf2(kk,ii))*conjg(csb(kk))
165   continue
      do 175 ii=1,mnps
      do 175 jj=1,mnps-1
      suc=czero
      do 170 kk=1,mnps
      suc=suc+st2(kk,ii)*vrf1(kk,jj)
170   continue
      csb31(ii,jj)=suc
175   continue
      do 180 ii=1,mnps-1
      do 180 kk=1,mnps
```

```
      st2(kk,ii)=vlf1(kk,ii)*conjg(csb(kk))
180   continue
      do 190 ii=1,mnps-1
      do 190 jj=1,mnps
      suc=czero
      do 185 kk=1,mnps
      suc=suc+st2(kk,ii)*vrf2(kk,jj)
185   continue
      csb12(ii,jj)=suc
190   continue
      do 195 ii=1,mnps-1
      do 195 kk=1,mnps
      st2(kk,ii)=vlf1(kk,ii)*css(kk)
195   continue
      do 210 ii=1,mnps-1
      do 210 jj=1,mnps
      suc=czero
      do 200 kk=1,mnps
      suc=suc+st2(kk,ii)*vrf2(kk,jj)
200   continue
      ss12(ii,jj)=suc
210   continue
      do 215 ii=1,mnps-1
      do 215 kk=1,mnps
      st2(kk,ii)=vlf1(kk,ii)*csb(kk)
215   continue
      do 225 ii=1,mnps-1
      do 225 jj=1,mnps
```

```
      suc=czero
      do 220 kk=1,mnps
      suc=suc+st2(kk,ii)*conjg(vrf2(kk,jj))
220   continue
      b013(ii,jj)=suc
225  continue
      do 230 ii=1,mnps
      do 230 kk=1,mnps
      st2(kk,ii)=vlf2(kk,ii)*csb(kk)
230   continue
      do 240 ii=1,mnps
      do 240 jj=1,mnps-1
      suc=czero
      do 235 kk=1,mnps
      suc=suc+st2(kk,ii)*vrf1(kk,jj)
235   continue
      b021(ii,jj)=suc
240   continue
      do 250 jj=1,mnps
      suc=cmplx(0.0d0,0.0d0)
      suc1=cmplx(0.0d0,0.0d0)
      do 245 kk=1,mnps
      suc=suc+vlf2(kk,jj)*cm(kk)*vr0(kk)
      suc1=suc1+vl0(kk)*cm(kk)*conjg(vrf2(kk,jj))
245   continue
      magl0(jj)=suc
      magr0(jj)=suc1
250  continue
```

```
c      above gives all of the matrix elements
c      following searches for corresponding qmin
c      for fixed dta and temp
        ax=0.0d0
        bx=phl*dta*pie
        do 310 it=1,60
        xmin=(ax+bx)/2.0d0
        root=cmplx(cos(xmin),sin(xmin))
        suc=czero
        do 255 mm=1,mnps
        suc=suc+ssr0(mm)*sbl0(mm)/(1.0d0-wri2(mm)/root)
 255    continue
        df=suc
        suc=czero
        do 260 mm=1,mnps
        suc=suc+sbr0(mm)*ssl0(mm)*root*conjg(wri2(mm))/
     c   (1.0d0-root*conjg(wri2(mm)))
 260    continue
        df=df+suc
        errb1=dble(df)
        suc=czero
        do 265 mm=1,mnps
        suc=suc+conjg(sbr0(mm))*sbl0(mm)/(1.0d0-wri2(mm)/root)
 265    continue
        df=suc
        suc=czero
        do 270 mm=1,mnps
        suc=suc+sbr0(mm)*conjg(sbl0(mm))*root*conjg(wri2(mm))/
```

```
     c   (1.0d0-root*conjg(wri2(mm)))
270     continue
        df=df+suc
        errb2=dble(df)
        errb=errb1-rat*errb2-(1.0d0-rat)/temp
        suc=czero
        do 275 mm=1,mnps
        suc=suc+ssr0(mm)*sbl0(mm)*cmplx(0.0d0,-1.0d0)*
     c  (wri2(mm)/root)/((1.0d0-wri2(mm)/root)*
     c  (1.0d0-wri2(mm)/root))
275     continue
        df=suc
        suc=czero
        do 280 mm=1,mnps
        suc=suc+sbr0(mm)*ssl0(mm)*cmplx(0.0d0,1.0d0)*
     c   root*conjg(wri2(mm))/((1.0d0-root*conjg(wri2(mm)))*
     c   (1.0d0-root*conjg(wri2(mm))))
280     continue
        df=df+suc
        test1=dble(df)
        suc=czero
        do 285 mm=1,mnps
        suc=suc+conjg(sbr0(mm))*sbl0(mm)*cmplx(0.0d0,-1.0d0)*
     c  (wri2(mm)/root)/((1.0d0-wri2(mm)/root)*
     c  (1.0d0-wri2(mm)/root))
285     continue
        df=suc
        suc=czero
```

```
        do 290 mm=1,mnps
        suc=suc+sbr0(mm)*conjg(sbl0(mm))*cmplx(0.0d0,1.0d0)*
     c   root*conjg(wri2(mm))/((1.0d0-root*conjg(wri2(mm)))*
     c   (1.0d0-root*conjg(wri2(mm))))
 290    continue
        df=df+suc
        test2=dble(df)
        test=test1-rat*test2
        if (test .gt. 0.0d0) then
        ax =xmin
        endif
        if (test .lt. 0.0d0) then
        bx =xmin
        endif
        if (test .eq. 0.0d0) then
        go to 3000
        endif
 310    continue
 3000    root=cmplx(cos(xmin),sin(xmin))
c       above gives the right qmin and errb
c       which at critical temperature is zero
c       following calculates related correlation and their
c       summation and the k derivative of errb called rdem
        do 320 mm=1,mnps
        st2(mm,1)=ssr0(mm)/(1.0d0-wri2(mm)/root)
 320    continue
        do 325 mm=1,mnps-1
        st2(mm,2)=hl0(mm)/(1.0d0-wri1(mm))
```

```
325     continue
        do 335 mm=1,mnps
        suc=czero
        do 330 nn=1,mnps-1
        suc=suc+b021(mm,nn)*st2(nn,2)
330     continue
        vr0(mm)=suc
335     continue
        suc=czero
        do 340 mm=1,mnps
        suc=suc+st2(mm,1)*vr0(mm)
340     continue
        f=suc
        do 345 mm=1,mnps-1
        st2(mm,1)=hr0(mm)/(1.0d0-wri1(mm))
345     continue
        do 350 mm=1,mnps
        st2(mm,2)=sbl0(mm)/(1.0d0-wri2(mm)/root)
350     continue
        do 360 mm=1,mnps-1
        suc=czero
        do 355 nn=1,mnps
        suc=suc+ss12(mm,nn)*st2(nn,2)
355     continue
        vr0(mm)=suc
360     continue
        suc=czero
        do 365 mm=1,mnps-1
```

```
      suc=suc+st2(mm,1)*vr0(mm)
365   continue
      f=f+suc
      do 370 mm=1,mnps
      st2(mm,1)=root*conjg(wri2(mm))*sbr0(mm)
     c  /(1-root*conjg(wri2(mm)))
370   continue
      do 375 mm=1,mnps-1
      st2(mm,2)=hl0(mm)/(1.0d0-wri1(mm))
375   continue
      do 385 mm=1,mnps
      suc=czero
      do 380 nn=1,mnps-1
      suc=suc+eng2(mm,nn)*st2(nn,2)
380   continue
      vr0(mm)=suc
385   continue
      suc=czero
      do 390 mm=1,mnps
      suc=suc+st2(mm,1)*vr0(mm)
390   continue
      f=f+suc
      do 395 mm=1,mnps-1
      st2(mm,1)=hr0(mm)/(1.0d0-wri1(mm))
395   continue
      do 400 mm=1,mnps
      st2(mm,2)=ssl0(mm)*root*conjg(wri2(mm))
     c /(1.0d0-root*conjg(wri2(mm)))
```

```
400    continue
       do 410 mm=1,mnps-1
       suc=czero
       do 405 nn=1,mnps
       suc=suc+b013(mm,nn)*st2(nn,2)
405    continue
       vr0(mm)=suc
410    continue
       suc=czero
       do 415 mm=1,mnps-1
       suc=suc+st2(mm,1)*vr0(mm)
415    continue
       f=f+suc
       do 420 mm=1,mnps
       st2(mm,1)=ssr0(mm)/(root-wri2(mm))
420    continue
      do 425 mm=1,mnps
       st2(mm,2)=sbl0(mm)/
    z  (1.0d0-wri2(mm)/root)
425   continue
       do 435 mm=1,mnps
       suc=czero
       do 430 nn=1,mnps
       suc=suc+h022(mm,nn)*st2(nn,2)
430    continue
       vr0(mm)=suc
435    continue
       suc=czero
```

```
      do 440 mm=1,mnps
      suc=suc+st2(mm,1)*vr0(mm)
440   continue
      f=f+suc
      do 445 mm=1,mnps
      st2(mm,1)=sbr0(mm)*root/
     c (1.0d0-root*conjg(wri2(mm)))
445   continue
      do 450 mm=1,mnps
      st2(mm,2)=ssl0(mm)/(1.0d0-root*conjg(wri2(mm)))
450   continue
      do 460 mm=1,mnps
      suc=czero
      do 455 nn=1,mnps
      suc=suc+conjg(h022(mm,nn))*st2(nn,2)
455   continue
      vr0(mm)=suc
460   continue
      suc=czero
      do 465 mm=1,mnps
      suc=suc+st2(mm,1)*vr0(mm)
465   continue
      f=f+suc
      do 470 mm=1,mnps
      st2(mm,1)=-root*wri2(mm)/((root-wri2(mm))*(root-wri2(mm)))
470   continue
      suc=czero
      do 475 mm=1,mnps
```

```
      suc=suc+ssr0(mm)*sbl0(mm)*st2(mm,1)
475   continue
      f=f+suc*eav
      suc=czero
      do 480 mm=1,mnps
      suc=suc+sbr0(mm)*ssl0(mm)*conjg(st2(mm,1))
480   continue
      f=f+suc*eav
      rdem1=dble(f/temp)
      do 485 mm=1,mnps
      st2(mm,1)=conjg(sbr0(mm))/(1.0d0-wri2(mm)/root)
485   continue
      do 490 mm=1,mnps-1
      st2(mm,2)=hl0(mm)/(1.0d0-wri1(mm))
490   continue
      do 510 mm=1,mnps
      suc=czero
      do 500 nn=1,mnps-1
      suc=suc+b021(mm,nn)*st2(nn,2)
500   continue
      vr0(mm)=suc
510   continue
      suc=czero
      do 515 mm=1,mnps
      suc=suc+st2(mm,1)*vr0(mm)
515   continue
      f=suc
      do 520 mm=1,mnps-1
```

```
      st2(mm,1)=hr0(mm)/(1.0d0-wri1(mm))
520   continue
      do 525 mm=1,mnps
      st2(mm,2)=sbl0(mm)/(1.0d0-wri2(mm)/root)
525   continue
      do 535 mm=1,mnps-1
      suc=czero
      do 530 nn=1,mnps
      suc=suc+csb12(mm,nn)*st2(nn,2)
530   continue
      vr0(mm)=suc
535   continue
      suc=czero
      do 540 mm=1,mnps-1
      suc=suc+st2(mm,1)*vr0(mm)
540   continue
      f=f+suc
      do 545 mm=1,mnps
      st2(mm,1)=root*conjg(wri2(mm))*sbr0(mm)
    c   /(1-root*conjg(wri2(mm)))
545   continue
      do 550 mm=1,mnps-1
      st2(mm,2)=hl0(mm)/(1.0d0-wri1(mm))
550   continue
      do 560 mm=1,mnps
      suc=czero
      do 555 nn=1,mnps-1
      suc=suc+csb31(mm,nn)*st2(nn,2)
```

```
555     continue
        vr0(mm)=suc
560     continue
        suc=czero
        do 565 mm=1,mnps
        suc=suc+st2(mm,1)*vr0(mm)
565     continue
        f=f+suc
        do 570 mm=1,mnps-1
        st2(mm,1)=hr0(mm)/(1.0d0-wri1(mm))
570     continue
        do 575 mm=1,mnps
        st2(mm,2)=conjg(sbl0(mm))*root*conjg(wri2(mm))
    c  /(1.0d0-root*conjg(wri2(mm)))
575     continue
        do 590 mm=1,mnps-1
        suc=czero
        do 580 nn=1,mnps
        suc=suc+b013(mm,nn)*st2(nn,2)
580     continue
        vr0(mm)=suc
590     continue
        suc=czero
        do 595 mm=1,mnps-1
        suc=suc+st2(mm,1)*vr0(mm)
595     continue
        f=f+suc
        do 600 mm=1,mnps
```

```
       st2(mm,1)=conjg(sbr0(mm))/(root-wri2(mm))
600    continue
      do 605 mm=1,mnps
       st2(mm,2)=sbl0(mm)/
    z  (1.0d0-wri2(mm)/root)
605   continue
       do 615 mm=1,mnps
       suc=czero
       do 610 nn=1,mnps
       suc=suc+h022(mm,nn)*st2(nn,2)
610    continue
       vr0(mm)=suc
615    continue
       suc=czero
       do 620 mm=1,mnps
       suc=suc+st2(mm,1)*vr0(mm)
620    continue
       f=f+suc
       do 625 mm=1,mnps
       st2(mm,1)=sbr0(mm)*root/
    c  (1.0d0-root*conjg(wri2(mm)))
625    continue
       do 630 mm=1,mnps
       st2(mm,2)=conjg(sbl0(mm))/(1.0d0-root*conjg(wri2(mm)))
630    continue
       do 640 mm=1,mnps
       suc=czero
       do 635 nn=1,mnps
```

```
      suc=suc+conjg(h022(mm,nn))*st2(nn,2)
635   continue
      vr0(mm)=suc
640   continue
      suc=czero
      do 645 mm=1,mnps
      suc=suc+st2(mm,1)*vr0(mm)
645   continue
      f=f+suc
      do 650 mm=1,mnps
      st2(mm,1)=-root*wri2(mm)/((root-wri2(mm))*(root-wri2(mm)))
650   continue
      suc=czero
      do 655 mm=1,mnps
      suc=suc+conjg(sbr0(mm))*sbl0(mm)*st2(mm,1)
655   continue
      f=f+suc*eav
      suc=czero
      do 660 mm=1,mnps
      suc=suc+sbr0(mm)*conjg(sbl0(mm))*conjg(st2(mm,1))
660   continue
      f=f+suc*eav
      rdem2=dble(f/temp)
      rdem=rdem1-rat*rdem2+(1.0d0-rat)/(temp*temp)
      suc=czero
      do 665 mm=1,mnps
      suc=suc+ssr0(mm)*magl0(mm)/(1.0d0-wri2(mm)/root)
665   continue
```

```
        df=suc
        suc=czero
        do 670 mm=1,mnps
        suc=suc+magr0(mm)*ssl0(mm)*root*conjg(wri2(mm))/
     c  (1.0d0-root*conjg(wri2(mm)))
 670    continue
         df=df+suc
         rnom1=dble(df)
        suc=czero
        do 675 mm=1,mnps
        suc=suc+conjg(sbr0(mm))*magl0(mm)/(1.0d0-wri2(mm)/root)
 675    continue
        df=suc
        suc=czero
        do 680 mm=1,mnps
        suc=suc+magr0(mm)*conjg(sbl0(mm))*root*conjg(wri2(mm))/
     c  (1.0d0-root*conjg(wri2(mm)))
 680    continue
         df=df+suc
         rnom2=dble(df)
        rnom=(1.0d0-rat+rat*temp*errb1)*(rnom1-rat*rnom2)/temp
        fmin=rnom/rdem
c       above calculates related correlation and their summation
c       and the k derivative of errb called rdem
        return
        end
```

VITA

Bai-Qi Jin

Candidate for the Degree of

Doctor of Philosophy

Thesis: SOME ASPECTS OF THE CHIRAL POTTS MODEL AND THE ISING MODEL

Major Field: Physics

Biographical:

Personal Data: Born in Wenzhou, Zhejiang, P. R. China on March 12, 1969.

Education: Received Bachelor of Science degree in Physics from Zhejiang University, Hangzhou, Zhejiang in July 1990; received Master of Science degree in Physics from Institute of High Energy Physics, Chinese Academy of Sciences, Beijing, P. R. China in February 1996. Completed the requirements for the Doctor of Philosophy degree with a major in Physics at Oklahoma State University in August 2001.

Name: Bai-Qi Jin Date of Degree: August, 2001

Institution: Oklahoma State University Location: Stillwater, Oklahoma

Title of Study: SOME ASPECTS OF THE CHIRAL POTTS MODEL AND THE ISING MODEL

Pages in Study: 176 Candidate for the Degree of Doctor of Philosophy

Major Field: Physics

Scope and Method of Study: In this thesis, we study two-dimensional statistical physics models. In the first three chapters, the 3-state chiral Potts model is used to study the question of the existence of a Lifshitz point and its related phase transitions. After an introduction in Chapter 1, the mean-field transfer matrix method with effective field determined by Bogoliubov's variational inequality is used to explore the phase diagram of this model in Chapter 2. In Chapter 3, we study this problem by the mean-field transfer matrix method with Weiss- and Bethe-type mean-field approximations respectively, and analyze the nature of the phase transition with the coherent anomaly method. Chapters 4 and 5 are contributions to the study of the Z-invariant Ising model and the quasi-periodic Ising model. In Chapter 6, functional relations are used for the calculation of the exact free energy of the integrable chiral Potts model.

Findings and Conclusions: Our numerical studies indicate that possibly no Lifshitz point exists at finite chirality in the 3-state chiral Potts model. This result is in contrast with many other numerical studies. Furthermore, the coherent anomaly behaviors are examined in these mean-field transfer matrix approximations. Although the coherent anomaly method does give some interesting indications, we find that either much larger systems or some exact information are necessary for us to make a definite conclusion about the nature of the phase transitions in this model. In Chapter 4, the scaling form of the correlation function in the inhomogeneous Z-invariant Ising model is presented and it is applied to the study of quasi-periodic Ising models in Chapter 5. The results provide evidence that the ferromagnetic quasi-periodic Ising model with different strengths of interactions is not much different from the regular Ising model but significantly different—in its wavevector-dependent susceptibility pattern—from the case with both ferro- and antiferromagnetic interactions. Finally, an extension to Baxter's formula of the exact free energy is obtained in Chapter 6.

ADVISOR'S APPROVAL: _____